European Journal of Taxonomy 1055: 1–57
https://doi.org/10.5852/ejt.2026.1055.3277
europeanjournaloftaxonomy.eu
ISSN 2118-9773
2026 · Stec D.

Received: 3 January 2026 • *Accepted: 3 April 2026* • *Published: 18 May 2026*

Topic editor: Magalie Castelin • *Section editor: Martin Vinther Sørensen* • *Desk editor: Pepe Fernández*

Monograph

urn:lsid:zoobank.org:pub:FCD61E9D-7FF9-40B2-8A03-E05BCF667B8B

Integrative taxonomy reveals four new species in the superdiverse genus *Macrobiotus* (Tardigrada: Eutardigrada: Macrobiotidae)

Daniel STEC

Institute of Systematics and Evolution of Animals, Polish Academy of Sciences,
Sławkowska 17, 31-016 Kraków, Poland.
Email: daniel_stec@interia.eu

Abstract. Four new species of the genus *Macrobiotus* are described from Asia and Africa: *Macrobiotus witalinskii* sp. nov., *M. dalaticus* sp. nov., *M. surmaczi* sp. nov., and *M. hoianicus* sp. nov. Species delimitation is based on detailed morphological and morphometric analyses using phase-contrast light microscopy and scanning electron microscopy, complemented by molecular data from four commonly used genetic markers. Phylogenetic analyses consistently place all four species within *Macrobiotus* clade C, each forming a distinct, well-supported monophyletic lineage. The newly described taxa expand the known morphological and ecological diversity of clade C and show that egg and body coloration characters previously considered diagnostic for this lineage are not evolutionarily conserved. These results further emphasize the value of integrative taxonomy for documenting hidden diversity and for supporting future biodiversity assessments, including large-scale DNA barcoding and metabarcoding surveys of tardigrades.

Keywords. Egg ornamentation, morphology, species complex, systematics, tardigrade, water bears.

Stec D. 2026. Integrative taxonomy reveals four new species in the superdiverse genus *Macrobiotus* (Tardigrada: Eutardigrada: Macrobiotidae). *European Journal of Taxonomy* 1055: 1–57.
https://doi.org/10.5852/ejt.2026.1055.3277

Introduction

Species are the fundamental units of biodiversity. Properly named and delimited species are crucial for studying and conserving life on our planet, particularly at a time when global environments are rapidly changing due to human activities (Raposo *et al.* 2021; Hatfield *et al.* 2025; Saban & Wiens 2025; Shi *et al.* 2025). Biodiversity loss is accelerating, and it is likely that biological entities (lineages and taxa) are disappearing before they are ever observed or formally recognized (Cowie *et al.* 2022). The scientific discipline responsible for the recognition, naming, and cataloguing of species is taxonomy. However, taxonomy is currently facing serious challenges, including chronic underfunding and a shortage of expert knowledge resulting from a declining number of trained taxonomists (Engel *et al.* 2021; Páll-Gergely *et al.* 2024). Although recent studies have shown that the rate of species descriptions has accelerated in recent years (Li *et al.* 2025) (largely due to the widespread adoption of modern molecular methods) this trend is not uniform across all organismal groups (Cerretti *et al.* 2025). The so-

called 'taxonomic impediment' is particularly pronounced in neglected groups and phyla, among which meiofauna represents a prominent example. Meiofauna comprises metazoan organisms that are typically smaller than 1 mm and are most commonly associated with aquatic environments, although many species require only a thin film of water to remain active. This assemblage includes a wide range of biologically fascinating taxa, such as kinorhynchs, loriciferans, nematodes, platyhelminths, gastrotrichs, rotifers, tardigrades, and others (Martínez *et al.* 2025). Across these groups, taxonomic impediments vary in magnitude but are generally driven by: (i) a shortage of taxonomic expertise, (ii) a lack of stable funding schemes for natural history research, (iii) methodological and logistical challenges inherent to working with microscopic organisms, and (iv) extensive and often cryptic species diversity.

The present contribution aims to add a further piece to our knowledge of tardigrade biodiversity. Tardigrades are a phylum of microscopic metazoans, best known to the general public for their ability to survive extreme environmental conditions through entry into cryptobiosis (Schill 2018). They inhabit marine, freshwater, and terrestrial environments; in the latter, they are typically associated with at least temporarily moist microhabitats such as cryptogams, rock pools, cryoconite, leaf litter, and similar substrates (Schill 2018). To date, more than 1500 tardigrade species have been formally described, the majority of which have been recorded from mosses and lichens (McFatter *et al.* 2007; Garey *et al.* 2008; Degma & Guidetti 2025). Tardigrade diversity is currently classified into 36 families and 164 genera (Degma & Guidetti 2025). Among these, the family Macrobiotidae Thulin, 1928 (comprising more than 370 species – and subspecies – level taxa) is the most species-rich and represents a dominant component of the terrestrial tardigrade fauna (Surmacz *et al.* 2025b). Although several large genus-level taxa, such as *Mesobiotus* Vecchi, Cesari, Bertolani, Jönsson, Rebecchi & Guidetti, 2016 (84 species) and *Paramacrobiotus* Guidetti, Schill, Bertolani, Dandekar & Wolf, 2009 (48 species), have been separated from *Macrobiotus* C.A.S. Schultze, 1834 (Guidetti *et al.* 2009; Vecchi *et al.* 2016), the latter remains the most species-rich genus, currently including 133 species – and subspecies – level taxa (Degma & Guidetti 2025). The genus *Macrobiotus* is morphologically and genetically highly diverse, encompassing deeply divergent phylogenetic lineages that nevertheless remain difficult to subdivide further into additional genera (Stec *et al.* 2021a, 2022; Stec 2024).

This study describes four new species of the genus *Macrobiotus* from Vietnam and Madagascar. The species descriptions are based on detailed morphological and morphometric analyses conducted using phase-contrast light microscopy and scanning electron microscopy. In addition, all examined species were sequenced for four DNA fragments commonly employed in tardigrade taxonomy and phylogenetic studies. These molecular data also enabled the elucidation of the phylogenetic positions of the investigated taxa among their congeners.

Material and methods

Sample processing

Moss and lichen samples containing three new species were collected in Vietnam by Daniel Stec and Krzysztof Miler in August 2018. A moss sample, containing the fourth new species, was collected in Madagascar, by Wojciech Witaliński in December 2022. Samples were examined for terrestrial tardigrades using standard methods as described in Stec *et al.* (2015). In order to perform taxonomic descriptions, isolated animals and eggs extracted from the samples were split into three groups for specific analyses: morphological analysis with phase contrast light microscopy, morphological analysis with scanning electron microscopy, and DNA sequencing (for details please see sections Material examined provided below for each species description).

Microscopy and imaging

Specimens for light microscopy were mounted on microscope slides in a small drop of Hoyer's medium and secured with a cover slip, following the protocol by Morek *et al.* (2016). Slides were then dried for five days at 60°C. Dried slides were sealed with a transparent nail polish and examined under a ZEISS Axio A1 light microscope with phase contrast (PCM), associated with a digital camera (DLT-Cam PRO). Immediately after mounting the specimens in the medium, slides were also checked under PCM for the presence of males and females in the studied population, as the spermatozoa in testis and vas deferens are visible only for a few hours after mounting (Coughlan & Stec 2019; Coughlan *et al.* 2019). In order to obtain well extended animals and clean eggs for SEM, the specimens were processed according to the protocol by Stec *et al.* (2015). In short, eggs were first subjected to a water/ethanol and an ethanol/acetone series, then to CO_2 critical point drying and finally sputter coated with a thin layer of gold. Specimens were examined under high vacuum in a Versa 3D DualBeam Scanning Electron Microscope at the ATOMIN facility of the Jagiellonian University, Kraków, Poland. All figures were assembled in Corel Photo-Paint X6. For structures that could not be satisfactorily focused in a single photograph, a stack of 2–6 images were taken with an equidistance of ca 0.2 µm and assembled manually into a single deep-focus image.

Morphometrics and morphological nomenclature

All measurements are given in micrometres (µm). Sample size was adjusted following recommendations by Stec *et al.* (2016). Structures were measured only if their orientation was suitable. Body length was measured from the anterior extremity to the end of the body, excluding the hind legs. The buccal apparatus and claws were classified according to Pilato & Binda (2010). The terminology used to describe oral cavity armature and egg shell morphology follows Kaczmarek & Michalczyk (2017). Macroplacoid length sequence is given according to (Kaczmarek *et al.* 2014) whereas morphological states of cuticular bars on legs follow Kiosya *et al.* (2021). Buccal tube length and the level of the stylet support insertion point were measured according to Pilato (1981). The *pt* index is the ratio of the length of a given structure to the length of the buccal tube expressed as a percentage (Pilato 1981). All other measurements and nomenclature follow Kaczmarek & Michalczyk (2017). Buccal tube width was measured as the external and internal diameter at the level of the stylet support insertion point. Lengths of the claw branches were measured from the base of the claw (i.e., excluding the lunula) to the top of the branch, including accessory points. Distance between egg processes was measured as the shortest distance between the base edges of the two closest processes. Morphometric data were handled using the "Parachela" ver. 1.8 template available from the Tardigrada Register (Michalczyk & Kaczmarek 2013) and are given in Supp. files (Supp. file 1, Supp. file 2, Supp. file 3, Supp. file 4). Tardigrade taxonomy follows Bertolani *et al.* (2014) and Stec *et al.* (2021a).

DNA sequencing

The DNA was extracted from individual animals following a Chelex® 100 resin (Bio-Rad) extraction method by Casquet *et al.* (2012) with modifications described in detail in Stec *et al.* (2020a). Before the DNA extraction each specimen was mounted on slides with water and check under light microscope. Four DNA fragments differing in mutation rates were sequenced. Namely: the small ribosome subunit (18S rRNA, nDNA), the large ribosome subunit (28S rRNA, nDNA), the internal transcribed spacer (ITS-2, nDNA), and the cytochrome oxidase subunit I (COI, mtDNA). All fragments were amplified and sequenced according to the protocols described in Stec *et al.* (2020a); primers are listed in Table 1. Sequencing products were read with the ABI 3130xl sequencer at the Genomed company (Warsaw, Poland). Sequences were processed in BioEdit ver. 7.2.5 (Hall 1999) and submitted to GenBank. Prior submission all obtained COI sequences were translated into protein sequences in MEGA12 (Kumar *et al.* 2024) to check against pseudogenes.

Table 1. Primers with their original references used for amplification of the four DNA fragments sequenced in the study.

DNA marker	Primer name	Primer direction	Primer sequence (5′–3′)	Primer source
18S rRNA	18S_Tar_Ff1	forward	AGGCGAAACCGCGAATGGCTC	Stec *et al.* 2017a
	18S_Tar_Rr1	reverse	GCCGCAGGCTCCACTCCTGG	
28S rRNA	28SF0002	forward	GRCRAGAKTACCCGCTGAAC	Stec 2022b
	28SR0990	reverse	CCTTGGTCCGTGTTTCAAGAC	Mironov *et al.* 2012
ITS-2	ITS2_Eutar_Ff	forward	CGTAACGTGAATTGCAGGAC	Stec *et al.* 2018c
	ITS2_Eutar_Rr	reverse	TCCTCCGCTTATTGATATGC	
COI	LCO1490-JJ	forward	CHACWAAYCATAAAGATATYGG	Astrin & Stüben 2008
	HCO2198-JJ	reverse	AWACTTCVGGRTGVCCAAARAATCA	

Phylogenetic analysis and molecular species delimitation

To establish phyletic positions of four new species a phylogenetic tree of Macrobiotidae super clade I sensu Stec *et al.* (2021a) was constructed. For this purpose a data set from Stec (2024) was used with additional sequences of *Macrobiotus* taxa for which DNA sequences were published in the meanwhile (Appendix 1). The DNA sequences of three species that represents Macrobiotidae super clade II sensu Stec *et al.* (2021a) were used as outgroup (Appendix 1). The sequences were aligned using the AUTO method (for COI and ITS-2) and the Q-INS-I method (for ribosomal markers: 18S rRNA and 28S rRNA) of MAFFT ver. 7 (Katoh *et al.* 2002; Katoh & Toh 2008) and manually checked against non-conservative alignments in BioEdit. The aligned sequences were trimmed to: 1020 (18S rRNA), 780 (28S rRNA), 658 (COI) bp. The ITS-2 alignment was processed using GBlocks ver. 0.91b (Castresana 2000); to remove ambiguously aligned regions, using the default 'less stringent' settings and its final length was 227 bp. The sequences were then concatenated using SequenceMatrix (Vaidya *et al.* 2011). Before partitioning, the concatenated alignment was divided into 6 data blocks constituting three separate blocks of ribosomal markers and three separate blocks of three codon positions in COI data set. Using PartitionFinder (Lanfear *et al.* 2017) under the Akaike Information Criterion (AIC), the best scheme of partitioning and substitution models were chosen for Bayesian phylogenetic analysis. Bayesian inference (BI) marginal posterior probabilities were calculated for the concatenated (18S rRNA+28S rRNA+ITS-2+COI) data set using MrBayes ver. 3.2 (Ronquist & Huelsenbeck 2003). Random starting trees were used and the analysis was run for fifteen million generations, sampling the Markov chain every 1000 generations. An average standard deviation of split frequencies of < 0.01 was used as a guide to ensure the two independent analyses had converged. The program Tracer ver. 1.7 (Rambaut *et al.* 2018) was then used to ensure Markov chains had reached stationarity, and to determine the correct 'burn-in' for the analysis which was the first 10% of generations. The ESS values were greater than 200 and the consensus tree was obtained after summarising the resulting topologies and discarding the 'burn-in'. ModelFinder (Kalyaanamoorthy *et al.* 2017) was used to choose the best-fit models according to the AIC for Maximum Likelihood (ML) analysis. Then ML reconstruction was conducted using W-IQ-TREE (Nguyen *et al.* 2015; Trifinopoulos *et al.* 2016). One thousand ultrafast bootstrap (UFBoot) replicates were applied to provide support values for branches (Hoang *et al.* 2018). The consensus trees were viewed and visualized by FigTree ver. 1.4.3 available from http://tree.bio.ed.ac.uk/software/figtree. The best evolutionary models of sequence evolution selected for BI and ML analyses, as well as respective raw trees, are given in Supp. file 5.

Abbreviations

ISEA PAS = Institute of Systematics and Evolution of Animals, Polish Academy of Sciences, Sławkowska 17, 31-016 Kraków, Poland

OCA = oral cavity armature
PCM = phase contrast light microscopy
SEM = scanning electron microscopy

Results

Taxonomic treatment

Phylum Tardigrada Doyère, 1840
Class Eutardigrada Richters, 1926
Order Parachela Schuster, Nelson, Grigarick & Christenberry, 1980
Superfamily Macrobiotoidea Thulin, 1928
Family Macrobiotidae Thulin, 1928
Genus *Macrobiotus* C.A.S. Schultze, 1834

Macrobiotus witalinskii sp. nov.
urn:lsid:zoobank.org:act:AE970A08-77A7-4BE0-BC6C-3FE4A74951FF
Figs 1–7; Tables 2–3

Etymology

The species name *witalinskii* is a patronym honouring Prof. Wojciech Witaliński, a distinguished Polish acarologist from Jagiellonian University. The species is named in recognition of his contributions to the taxonomy of Acari and his supervision of the author's bachelor thesis.

Material examined

107 animals, 20 eggs mounted on microscope slides in Hoyer's medium, 5 animals and 4 eggs examined under SEM and two animals processed for DNA sequencing.

Type material

Holotype

MADAGASCAR • Amber Mountain, road from Joffreville; 12°30′49″ S, 49°10′56″ E; 993 m a.s.l.; Dec. 2018; W. Witaliński leg.; moss collected from tree branch; primary tropical forest; ISEA PAS, slide MG.001.06.

Paratypes

MADAGASCAR • 106 specs; same data as for holotype; ISEA PAS, slides MG.001.02 to MG.001.09 • 20 eggs; same data as for holotype; ISEA PAS, slides MG.001.01, MG.001.10, MG.001.11.

Description

Animals

Body transparent in juveniles and whitish in adults; after fixation in Hoyer's medium, the body becomes transparent (Fig. 1). Eyes present in alive and Hoyer-fixed specimens. Cuticular pores are scattered randomly over the entire body surface (Figs 1–2), being more sparsely distributed on the ventral side. Two pore morphotypes can be distinguished: larger oval pores (1.2–1.7 μm in diameter) and smaller, roundish pores (0.5–0.9 μm in diameter). Granulation is present over the entire body cuticle, being denser in the dorso-caudal region; however, it is clearly visible only under SEM, and its density increases from

head to caudal part of the dorsal cuticle (Fig. 2). Under PCM, body granulation is discernible only in the dorso-caudal part of the body (Fig. 1). Extremely fine granulation patches are present on the external surfaces of legs I–III, but are visible exclusively under SEM (Fig. 3), whereas granulation is absent from the internal surfaces of legs I–III (Fig. 3). Dense granulation is present on the lateral and dorsal surfaces of leg IV and is clearly visible under both PCM and SEM (Fig. 3). A pulvinus-shaped cuticular bulge is centrally located on the internal surface of all legs I–III (Fig. 3) and is observable only when the legs are fully extended and properly oriented.

Claws are small and slender, of the *hufelandi* type (Fig. 4). Primary branches bear distinct accessory points, a common tract, and a well-developed stalk connecting the claw to the lunula (Fig. 4). Lunulae on legs I–IV are smooth (Fig. 4). A divided cuticular bar and double muscle attachments occur above claws I–III but are very poorly visible (Fig. 4). Shadowed extensions originating from the lunulae of claws IV are present and are faintly visible only under PCM (Fig. 4).

Mouth antero-ventral. Bucco-pharyngeal apparatus of the *Macrobiotus* type (Fig. 5), with a ventral lamina and ten small peribuccal lamellae followed by six buccal sensory lobes. Under PCM, the OCA

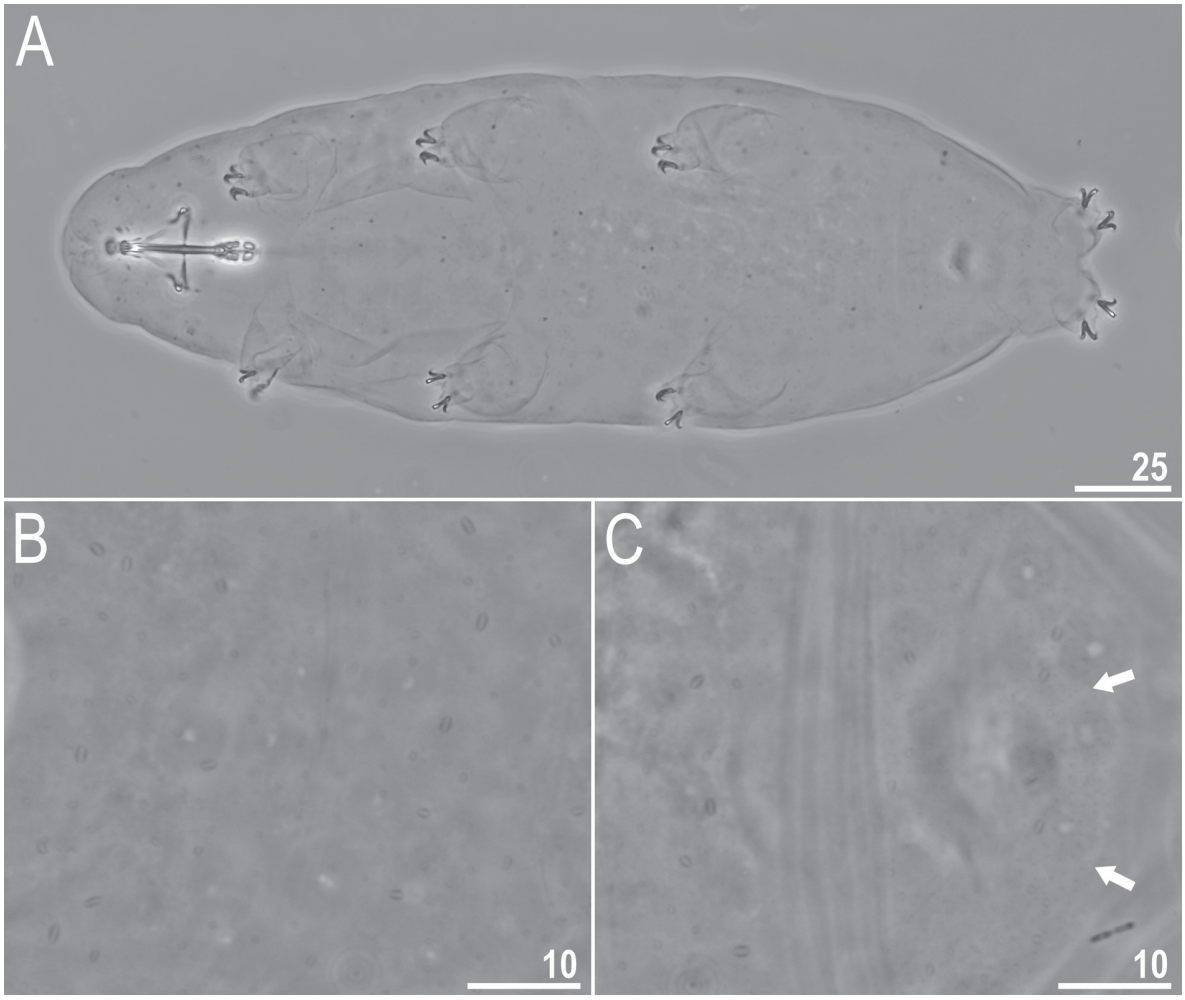

Fig. 1. *Macrobiotus witalinskii* sp. nov., holotype (ISEA PAS), habitus, body granulation, and cuticular pores, PCM. **A**. Dorso-ventral projection. **B**. Pores in the central part of the dorsal body cuticle. **C**. Granulation and pores in the caudal part of the dorsal body cuticle (holotype, PCM). Arrows indicate granulation faintly visible under PCM. Scale bars in μm.

is of the *maculatus* type, with the first and second bands of teeth not visible (Fig. 5); however, all three bands are clearly discernible under SEM (Fig. 5). The first band of teeth consists of numerous extremely small cones arranged in several rows, located anteriorly in the oral cavity on the bases of the peribuccal lamellae and immediately posterior to them (Fig. 5). The second band of teeth is situated between the ring fold and the third band and is composed of several rows of small cones, larger than those of the first band (Fig. 5). The third band of teeth is located in the posterior portion of the oral cavity, between the second band and the opening of the buccal tube (Fig. 5); it is discontinuous and divided into dorsal and ventral portions. Under PCM, these dorsal and ventral teeth appear as a single transverse ridges, each with two dark thickenings (Fig. 5). Under SEM the dorsal and ventral portions are also clearly distinguishable and form continuous ridges, each bearing two peaks, with the dorsal teeth being larger and more distinct than the ventral ones (Fig. 5). The pharyngeal bulb is spherical, with triangular apophyses, two rod-shaped macroplacoids, and a small granular microplacoid (Fig. 5). The macroplacoid length sequence is 2 < 1, with the first and second macroplacoids constricted centrally and subterminally, respectively (Fig. 5). Measurements and morphometric statistics of the animals are provided in Table 2.

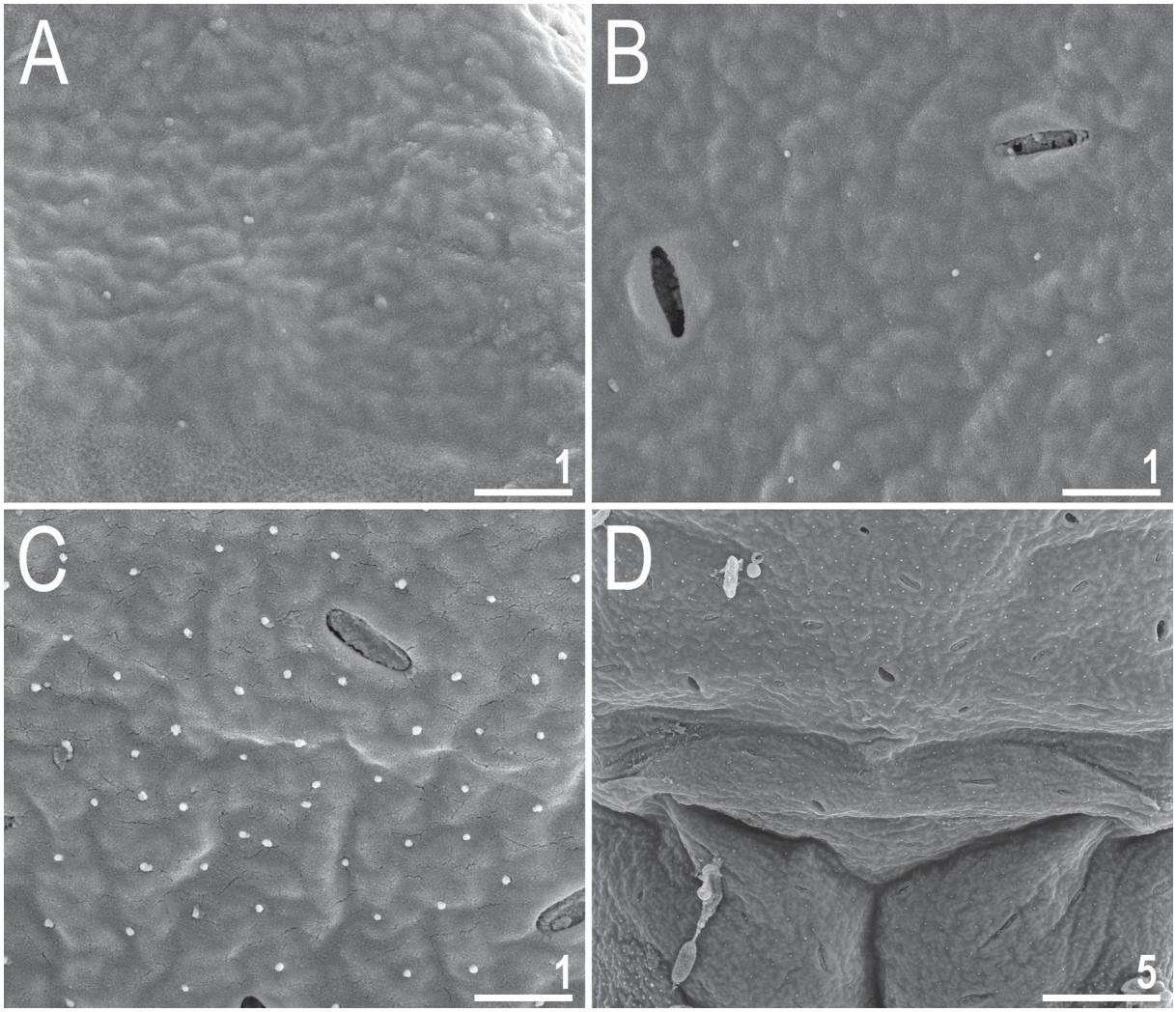

Fig. 2. *Macrobiotus witalinskii* sp. nov., paratypes (ISEA PAS), body granulation and cuticular pores, SEM. **A**. Body granulation in the head region of the dorsal body cuticle. **B**. Body granulation in the central part of the dorsal body cuticle. **C–D**. Body granulation in the caudal part of the dorsal body cuticle. Scale bars in μm.

Eggs

Eggs laid freely, white, spherical, and ornamented (Figs 6–7). The surface between egg processes is of the *hufelandi* type, with the eggshell between processes covered by a reticulum (Figs 6–7). The reticulum and egg processes are attached to the egg surface by multiple pillar-like structures that are visible only under SEM (Fig. 7). The reticular mesh is composed of distinct pores (0.5–0.9 μm in diameter), the diameter of which is larger than the width of the nodes and bars forming the mesh, giving the reticulum a very distinct and delicate appearance (Figs 6–7). The pores are generally uniform in size and shape, which gives an initial impression of uniform distribution. However, closer examination reveals a single ring of peribasal meshes surrounding each egg process and, occasionally, one to two additional interbasal meshes between them, usually smaller than the peribasal meshes (Figs 6–7). Under PCM, dark thickenings can be distinguished around the bases of the egg processes, which under SEM correspond to the portions linking the reticulum with the walls of the egg processes (Figs 6–7). Egg processes are conical, with a wider proximal portion near the egg surface and a distinctly narrower distal portion (Figs 6–7). Walls of the proximal portion are smooth, whereas the distal portion is rough, being covered by granules that are clearly visible under SEM and very faintly visible under PCM (Figs 6–7). The wider proximal and narrower distal portions of the egg processes are approximately similar in length (Figs 6–7). Measurements and morphometric statistics of the eggs are provided in Table 3.

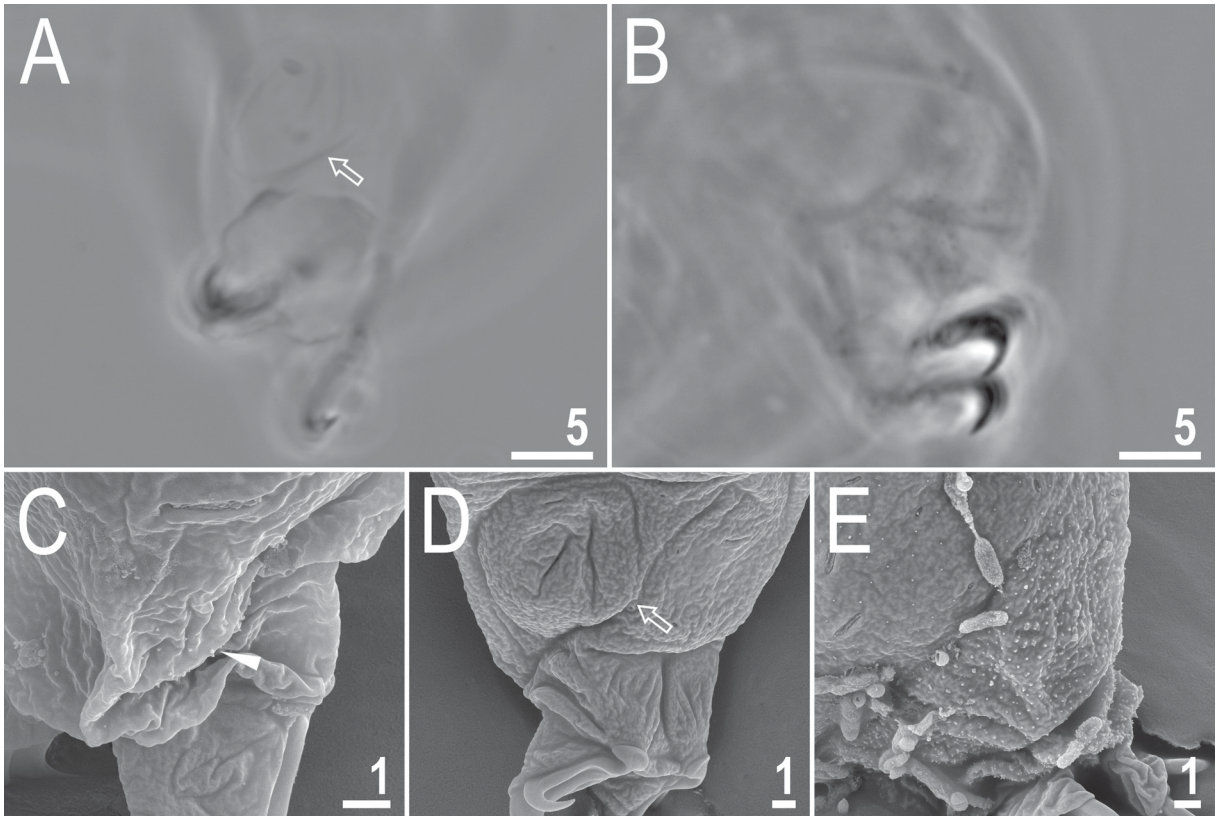

Fig. 3. *Macrobiotus witalinskii* sp. nov., paratypes (ISEA PAS), leg cuticle. **A–B**. PCM. **C–E**. SEM. **A**. Internal surface of leg II. **B**. Granulation on the hind legs. **C**. Granulation on the external surface of leg III. **D**. Internal surface of leg II. **E**. Granulation on the hind leg. Empty arrows indicate a pulvinus-shaped cuticular bulge, and the filled arrowhead indicates delicate granulation on the external leg surface. Scale bars in μm.

Table 2. Measurements [in µm] and *pt* values [in %] of selected morphological structures of individuals of *Macrobiotus witalinskii* sp. nov.; specimens mounted in Hoyer's medium; N: number of specimens/ structures measured; range: refers to the smallest and the largest structure among all measured specimens; SD: standard deviation.

Character	N	Range		Mean		SD		Holotype	
		µm	*pt*	µm	*pt*	µm	*pt*	µm	*pt*
Body length	24	207–300	*900–1176*	258	*1039*	23	*74*	271	*1075*
Buccal tube									
Buccal tube length	24	20.3–27.8	–	24.8	–	1.4	–	25.2	–
Stylet support insertion point	24	13.5–18.5	*64.4–66.5*	16.3	*65.6*	1.0	*0.7*	16.4	*65.1*
Buccal tube external width	24	1.8–2.6	*8.0–9.9*	2.2	*8.9*	0.2	*0.4*	2.3	*9.1*
Buccal tube internal width	24	0.8–1.4	*3.5–5.6*	1.1	*4.6*	0.2	*0.6*	1.4	*5.6*
Ventral lamina length	23	11.2–13.9	*46.5–52.2*	12.4	*49.6*	0.7	*1.6*	12.6	*50.0*
Placoid lengths									
Macroplacoid 1	24	3.5–5.5	*17.1–21.1*	4.7	*19.1*	0.4	*1.2*	5.0	*19.8*
Macroplacoid 2	24	2.2–3.4	*9.5–13.1*	2.9	*11.5*	0.3	*0.8*	3.0	*11.9*
Microplacoid	24	0.7–1.5	*3.4–6.2*	1.1	*4.6*	0.2	*0.6*	0.9	*3.6*
Macroplacoid row	24	6.4–9.6	*30.2–37.6*	8.4	*33.8*	0.7	*1.9*	8.9	*35.3*
Placoid row	24	7.5–11.5	*36.3–44.7*	10.1	*40.6*	0.9	*2.2*	10.2	*40.5*
Claw 1 heights									
External primary branch	23	3.7–6.3	*15.0–23.9*	5.4	*21.7*	0.6	*1.8*	5.4	*21.4*
External secondary branch	22	3.4–5.2	*15.2–20.4*	4.5	*18.0*	0.4	*1.2*	4.7	*18.7*
Internal primary branch	23	4.2–6.0	*18.8–22.8*	5.3	*21.2*	0.4	*1.0*	5.2	*20.6*
Internal secondary branch	18	3.1–4.8	*13.9–18.3*	4.2	*16.9*	0.4	*1.1*	4.4	*17.5*
Claw 2 heights									
External primary branch	23	4.7–6.3	*20.8–24.3*	5.6	*22.7*	0.4	*1.0*	5.6	*22.2*
External secondary branch	20	3.9–5.2	*16.5–20.4*	4.5	*18.1*	0.3	*1.0*	4.4	*17.5*
Internal primary branch	23	4.6–6.1	*20.4–24.3*	5.4	*22.0*	0.4	*1.0*	5.4	*21.4*
Internal secondary branch	18	3.6–5.1	*15.8–19.2*	4.4	*17.5*	0.4	*1.0*	4.2	*16.7*
Claw 3 heights									
External primary branch	22	4.6–6.4	*21.2–24.7*	5.7	*23.0*	0.4	*0.9*	5.7	*22.6*
External secondary branch	18	3.8–5.3	*16.9–20.6*	4.7	*18.9*	0.3	*1.1*	4.9	*19.4*
Internal primary branch	23	4.0–6.1	*19.7–23.9*	5.5	*22.1*	0.5	*1.0*	5.4	*21.4*
Internal secondary branch	21	3.6–5.2	*15.6–19.6*	4.4	*17.6*	0.4	*1.0*	4.4	*17.5*
Claw 4 heights									
Anterior primary branch	20	5.2–7.5	*23.2–29.0*	6.3	*25.5*	0.6	*1.7*	6.0	*23.8*
Anterior secondary branch	17	4.2–5.8	*18.8–22.4*	5.1	*20.7*	0.5	*1.2*	4.9	*19.4*
Posterior primary branch	20	5.4–7.7	*24.6–29.4*	6.6	*26.6*	0.6	*1.5*	6.2	*24.6*
Posterior secondary branch	17	4.7–6.3	*19.2–24.3*	5.4	*21.7*	0.4	*1.4*	5.2	*20.6*

Table 3. Measurements [in µm] of selected morphological structures of the eggs of *Macrobiotus witalinskii* sp. nov.; eggs mounted in Hoyer's medium; process base/height ratio is expressed as percentage; N: number of eggs/structures measured; range: refers to the smallest and the largest structure among all measured specimens; SD: standard deviation.

Character	N	Range	Mean	SD
Egg bare diameter	15	44.9 – 54.0	48.9	2.7
Egg full diameter	15	56.8 – 67.0	61.4	3.1
Process height	45	5.0 – 8.4	6.5	0.7
Process base width	45	1.8 – 3.1	2.5	0.3
Process base/height ratio	45	28% – 50%	38%	6%
Inter-process distance	45	1.5 – 3.2	2.4	0.4
Number of processes on the egg circumference	15	31 – 34	32.7	1.1

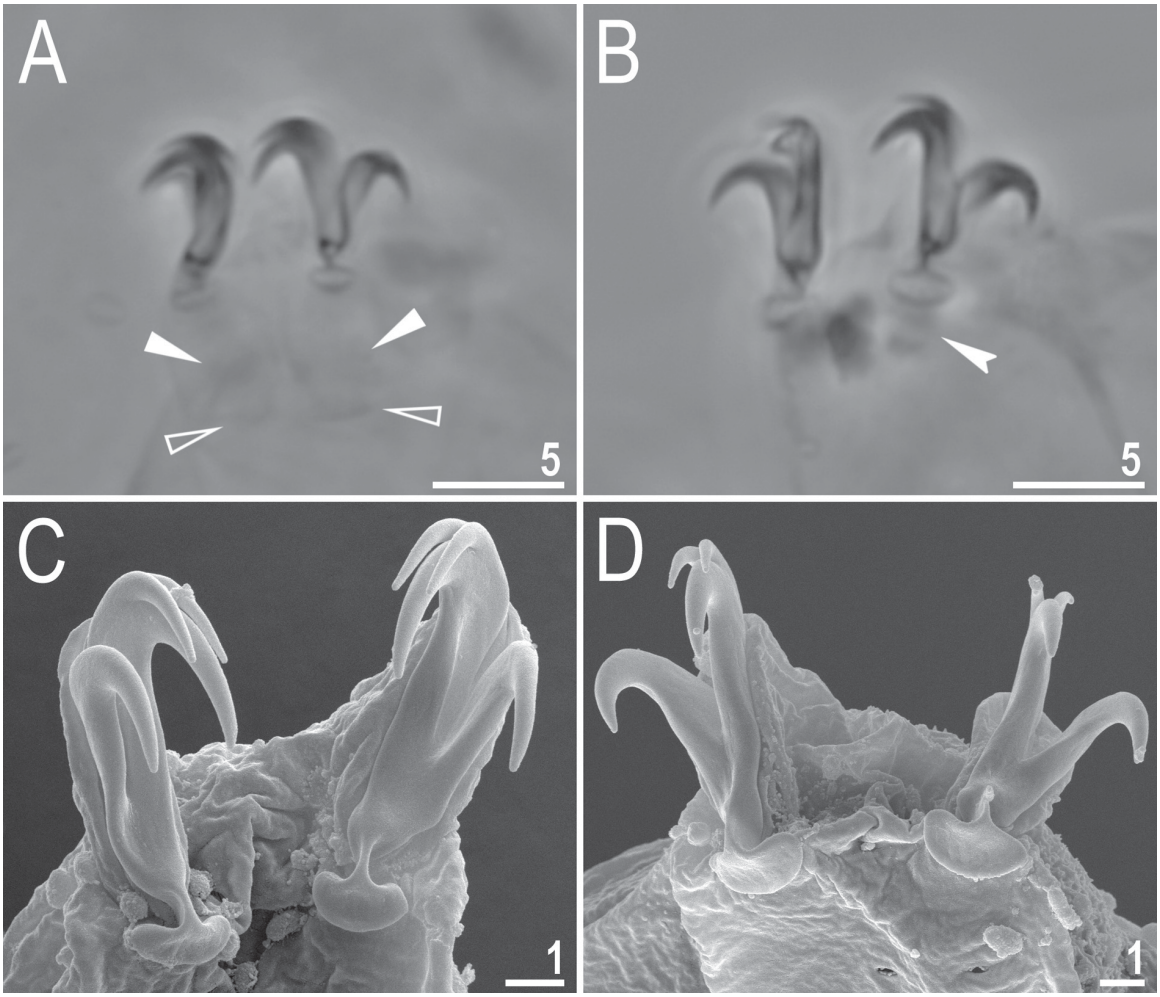

Fig. 4. *Macrobiotus witalinskii* sp. nov., paratypes (ISEA PAS), claws. **A–B**. PCM, **C–D**. SEM. **A**. Claws III. **B**. Claws IV. **C**. Claws II. **D**. Claws IV. The filled indented arrowhead indicates shadowed extensions extending from the lunulae (visible under PCM), empty flat arrowheads indicate paired muscle attachments, and filled flat arrowheads indicate faintly visible cuticular bars. Scale bars in µm.

Reproduction

The type population of *M. witalinskii* sp. nov. is dioecious. Both males with testes filled with sperm and females with ovaries containing oocytes were observed in specimens freshly mounted in Hoyer's medium.

Differential diagnosis

By having (i) only the third band of teeth in the oral cavity armature clearly visible under light microscopy, (ii) eggs with conical processes bearing sharp apices, lacking terminal discs or a flattened distal portion, and (iii) reticulation present on the egg surface between processes, the new species is similar to only one species of *Macrobiotus*: *Macrobiotus drakensbergi* Dastych, 1993, known

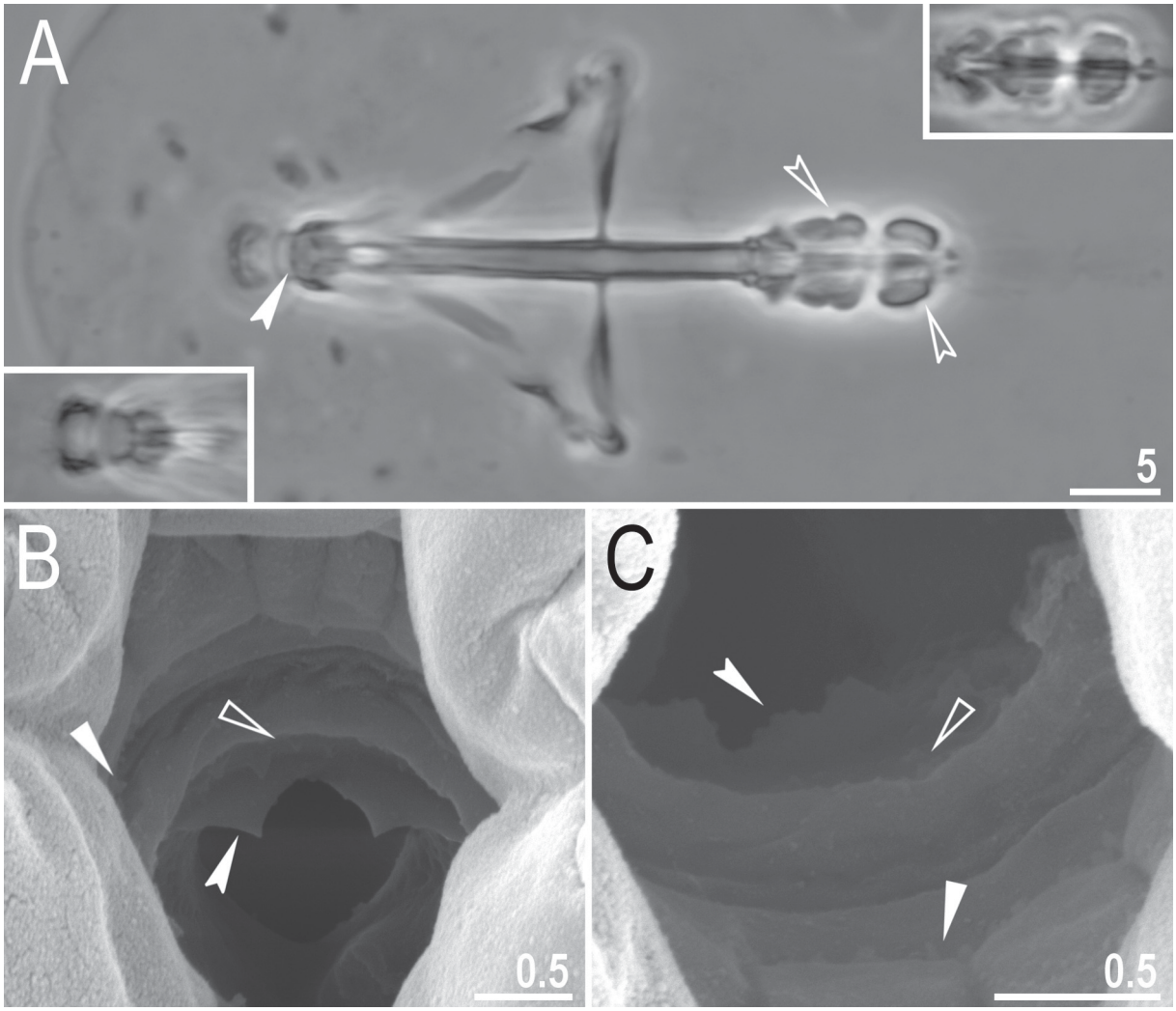

Fig. 5. *Macrobiotus witalinskii* sp. nov., buccal apparatus and oral cavity armature. **A–B**. PCM, holotype (ISEA PAS). **B–C**. SEM, paratypes (ISEA PAS). **A**. Buccal apparatus in dorsal view. The lower left inset shows the ventral view of the. **B–C**. Oral cavity armature observed under SEM from different angles, dorsal (**B**) and ventral (**C**) views. Filled flat arrowheads indicate the first band of teeth, empty flat arrowheads indicate the second band of teeth, filled indented arrowheads indicate the third band of teeth, and empty indented arrowheads indicate the central and subterminal constrictions in the first and second macroplacoids, respectively. Scale bars in μm.

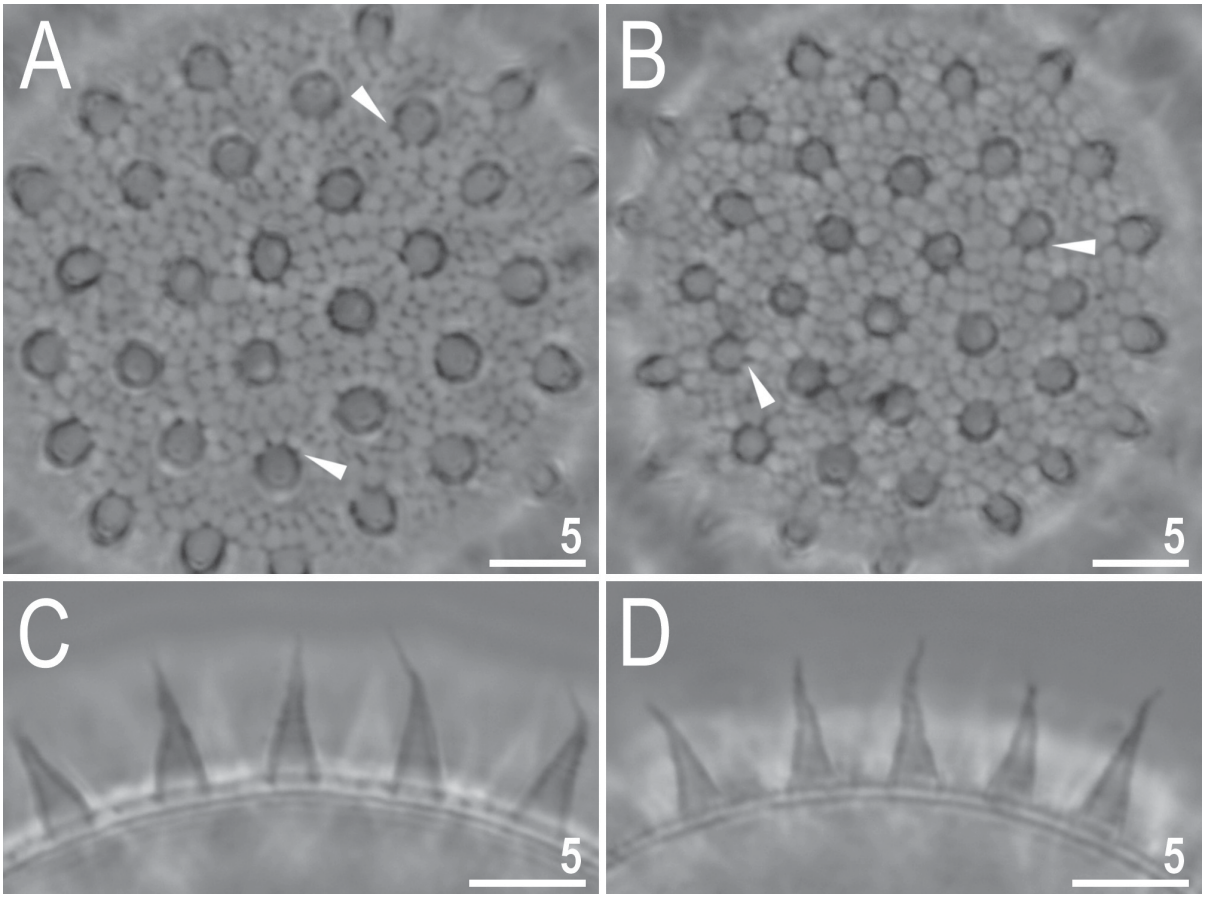

Fig. 6. *Macrobiotus witalinskii* sp. nov., PCM images of the egg at ×1000 magnification. **A–B**. Egg surface. **C–D**. Midsections of egg processes. Filled flat arrowheads indicate dark thickenings around the bases of the egg processes. Scale bars in μm.

exclusively from South Africa (Dastych 1993). However, *Macrobiotus witalinskii* sp. nov. differs from *M. drakensbergi* in several diagnostic characters: (i) the presence of leg granulation (granulation absent in *M. drakensbergi*), (ii) normally developed hind legs (hind legs reduced in *M. drakensbergi*), (iii) the morphology of the ventral portion of the third band of teeth in the OCA, which in the new species forms a single continuous transverse ridge bearing two peaks (teeth), whereas in *M. drakensbergi* it consists of three separate teeth, (iv) a different shape of claws (claws stout with straight basal portion in the new species vs claws dumpy with rounded basal portion in *M. drakensbergi*, (v) the presence of smooth lunulae on legs I–IV (all lunulae dentate in *M. drakensbergi*), and (vi) the shape of the egg processes, which in the new species are conical with a wider proximal portion and a distinctly narrower distal portion of approximately similar length and clearly separated, whereas in *M. drakensbergi* the processes are short, wide, cone-shaped, with short sharp apices and positioned close to one another.

Macrobiotus dalaticus sp. nov.
urn:lsid:zoobank.org:act:A569A718-CF23-49F5-A73A-7E24D14FACFB
Figs 8–15; Tables 4–5

Etymology

The species name *dalaticus* refers to Đà Lạt, the region in the Central Highlands of Vietnam where the species was collected. The adjective is formed in reference to the type locality.

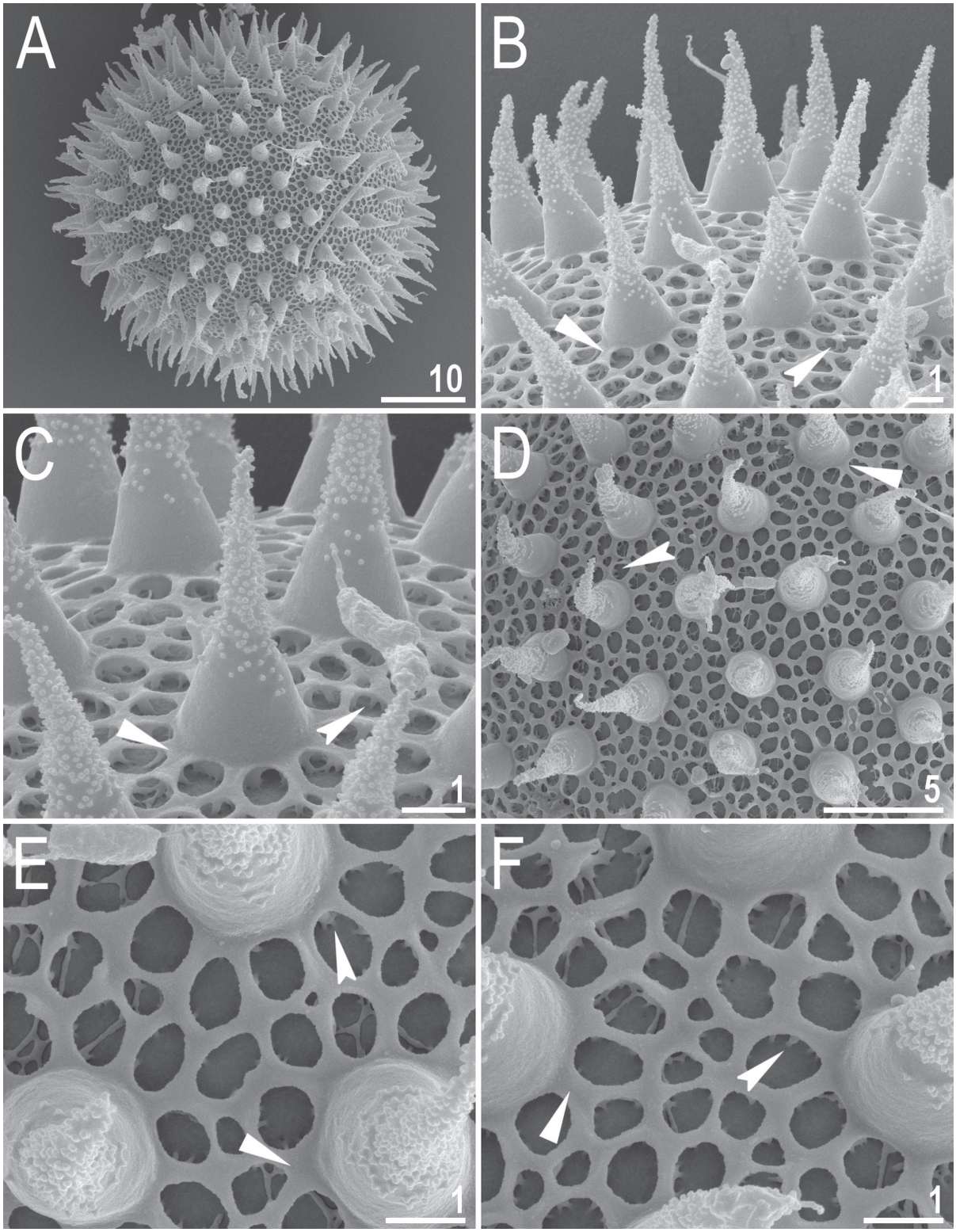

Fig. 7. *Macrobiotus witalinskii* sp. nov., SEM images of the eggs. **A**. Entire egg. **B–F**. Details of egg processes and the surface between them. Filled flat arrowheads indicate thickenings (corresponding to dark thickenings visible under PCM) around the bases of the egg processes, and filled indented arrowheads indicate pillar-like structures connecting the reticulum and egg processes to the egg surface. Scale bars in μm.

Material examined

51 animals, 50 eggs mounted on microscope slides in Hoyer's medium, 8 animals and 6 eggs examined under SEM and two animals processed for DNA sequencing.

Type material

Holotype

VIETNAM • Central Highlands, Đà Lạt region, Datanla Waterfall area (Xe Trượt Ống Datanla); 11°53′56″ N, 108°26′56″ E; 1290 m a.s.l.; Aug. 2018; D. Stec and K. Miler leg.; lichen collected from rock in mountain forest; ISEA PAS, slide VN.002.02.

Paratypes

VIETNAM • 50 specs; same data as for holotype; ISEA PAS, slides VN.002.02, VN.002.03, VN.002.05 to VN.002.11 • 50 eggs; same data as for holotype; ISEA PAS, slides VN.002.01, VN.002.04, VN.002.12 to VN.002.14.

Description

Animals

Body transparent in juveniles and yellowish in adults; after fixation in Hoyer's medium, the body becomes transparent (Fig. 8). Eyes present in alive and Hoyer-fixed specimens. Cuticular pores are

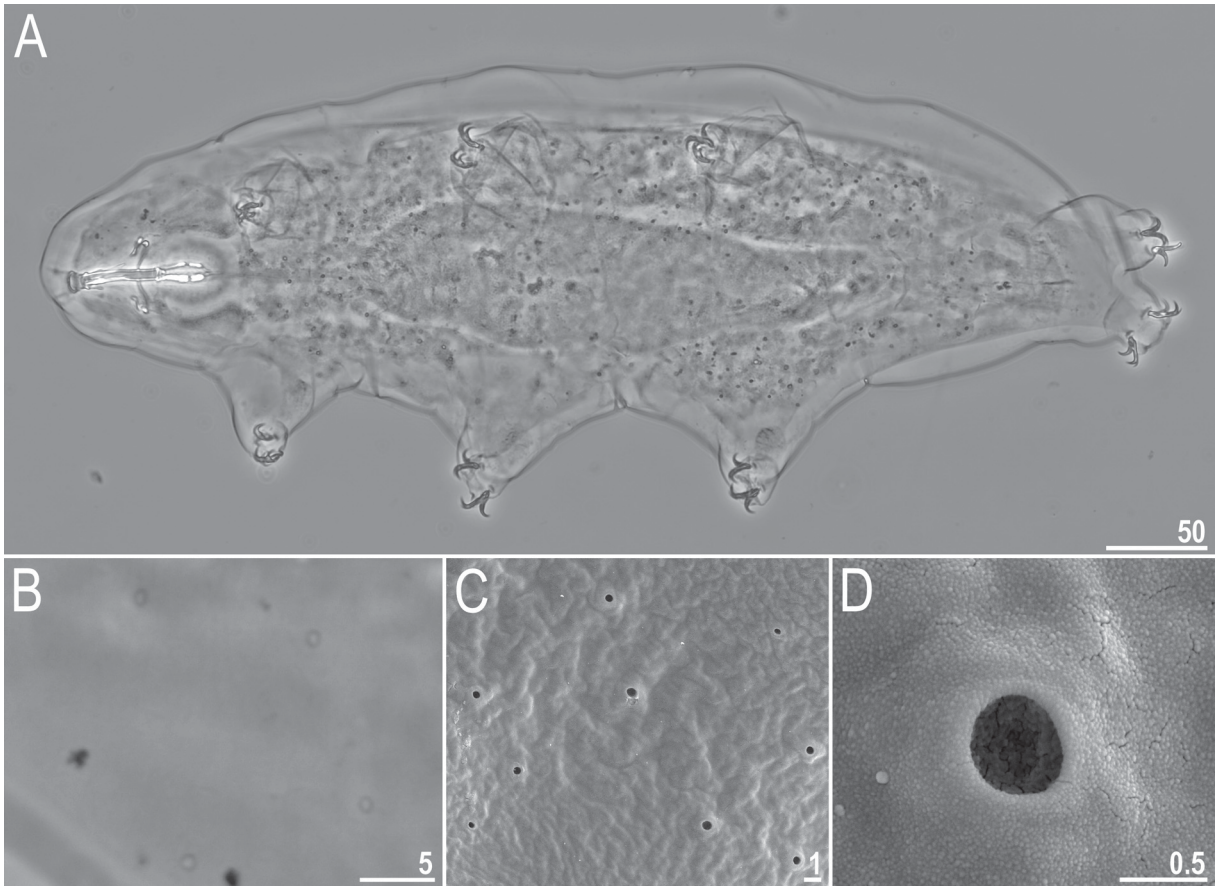

Fig. 8. *Macrobiotus dalaticus* sp. nov., habitus and cuticular pores. **A–B**. PCM, holotype (ISEA PAS). **A**. Dorso-ventral projection. **B**. Pores in the body cuticle. **C–D**. SEM, paratype (ISEA PAS), pores in the body cuticle. Scale bars in μm.

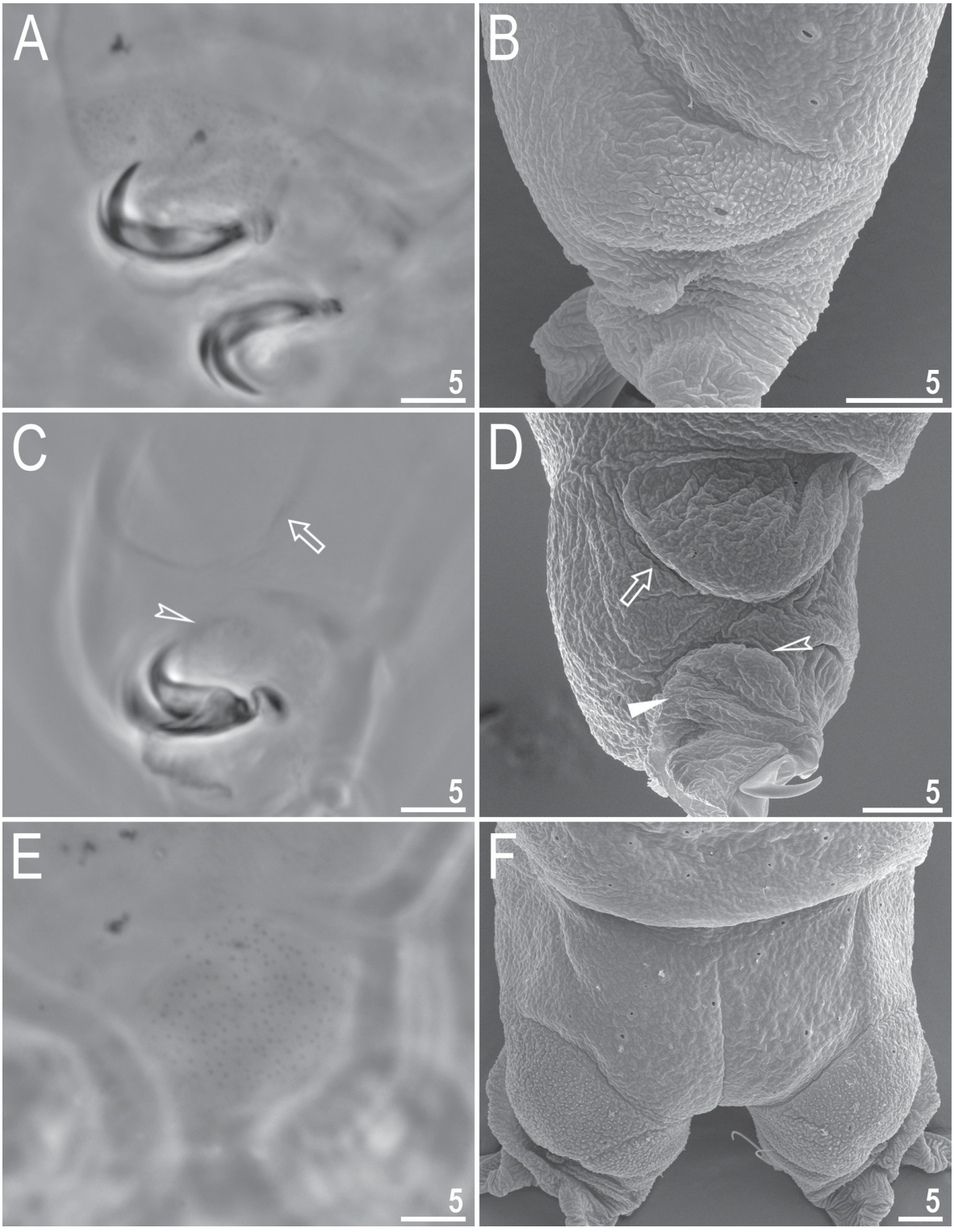

Fig. 9. *Macrobiotus dalaticus* sp. nov., leg cuticle. **A–D, F**. Paratypes (ISEA PAS). **E**. Holotype (ISEA PAS). **A–B**. Granulation on the external surface of leg III (PCM and SEM, respectively). **C–D**. Internal surface of leg III (PCM and SEM, respectively). **E–F**. Granulation on the hind legs (PCM and SEM, respectively). Empty arrows indicate a pulvinus-shaped cuticular bulge, empty indented arrowheads indicate a cuticular fold in the distal leg portion, and filled flat arrowheads indicate delicate granulation on the internal leg surface. Scale bars in μm.

scattered randomly over the entire body surface (Fig. 8), being more sparsely distributed on the ventral side. Pores are circular and uniform in size and shape (0.4–0.6 μm in diameter). Body granulation is absent except on the legs. Fine granulation patches are present on the external surfaces of legs I–III and are clearly visible under both PCM and SEM (Fig. 9), whereas granulation is absent from the internal surfaces of legs I–III; only occasionally can extremely sparse minute granules be observed under SEM on the fronto-internal surface of the distal leg portions (Fig. 9). Distinct granulation is also present on the lateral and dorsal surfaces of leg IV and is clearly visible under both PCM and SEM (Fig. 9). On the internal surface of legs I–III, a pulvinus-shaped cuticular bulge is centrally located, and a faint cuticular fold occurs in the distal portion of the legs just above the claws (Fig. 9). Both structures are visible only when the legs are fully extended and properly oriented on the slide.

Claws slender, of the *hufelandi* type (Figs 10–11). Primary branches bear distinct accessory points, a common tract, and a well-developed stalk connecting the claw to the lunula (Figs 10–11). Lunulae on legs I–III are smooth, whereas those on hind legs are clearly dentate (Figs 10–11). A divided cuticular

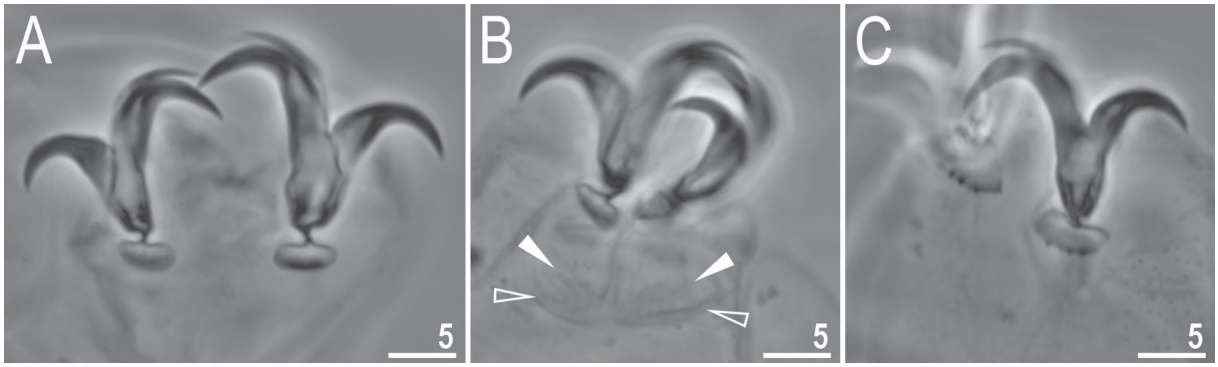

Fig. 10. *Macrobiotus dalaticus* sp. nov., claws, PCM. **A, C**. Holotype (ISEA PAS). **B**.Paratype (ISEA PAS). **A**. Claws III. **B**. Claws II. **C**. Claws IV. Empty flat arrowheads indicate paired muscle attachments, and filled flat arrowheads indicate faintly visible cuticular bars. Scale bars in μm.

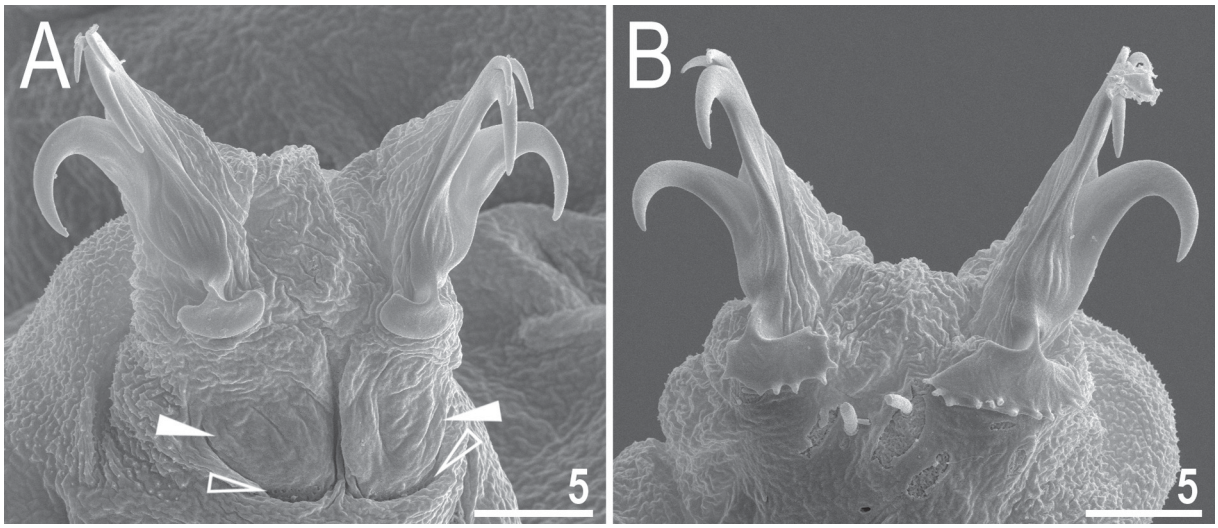

Fig. 11. *Macrobiotus dalaticus* sp. nov., paratypes (ISEA PAS), claws; SEM. **A**. Claws II. **B**. Claws IV. Empty flat arrowheads indicate paired muscle attachments, and filled flat arrowheads indicate cuticular bars. Scale bars in μm.

Table 4. Measurements [in µm] and *pt* values [in %] of selected morphological structures of individuals of *Macrobiotus dalaticus* sp. nov.; specimens mounted in Hoyer's medium; N: number of specimens/ structures measured; range: refers to the smallest and the largest structure among all measured specimens; SD: standard deviation.

Character	N	Range		Mean		SD		Holotype	
		µm	*pt*	µm	*pt*	µm	*pt*	µm	*pt*
Body length	30	314 –578	*1121–1498*	434	*1319*	69	*118*	535	*1471*
Buccal tube									
Buccal tube length	30	27.1 –40.1	–	32.8	–	3.0	–	36.4	–
Stylet support insertion point	30	19.8 –28.6	*71.0–73.9*	23.8	*72.6*	2.2	*0.8*	26.9	*73.9*
Buccal tube external width	30	3.5 –5.7	*11.6–15.7*	4.5	*13.8*	0.6	*1.1*	5.7	*15.7*
Buccal tube internal width	30	2.0 –4.3	*6.6–11.1*	2.9	*8.8*	0.5	*1.1*	3.8	*10.4*
Ventral lamina length	30	15.5 –23.9	*53.1–62.7*	18.9	*57.8*	1.9	*2.7*	22.0	*60.4*
Placoid lengths									
Macroplacoid 1	30	7.2 –12.9	*23.6–33.3*	9.4	*28.5*	1.5	*2.6*	11.8	*32.4*
Macroplacoid 2	30	3.6 –7.4	*12.3–21.4*	5.3	*16.1*	1.0	*1.9*	6.7	*18.4*
Microplacoid	30	1.6 –3.8	*5.9–10.5*	2.6	*7.8*	0.5	*1.1*	2.8	*7.7*
Macroplacoid row	30	12.6 –22.5	*39.6–57.8*	16.0	*48.6*	2.5	*4.1*	19.6	*53.8*
Placoid row	30	15.5 –26.3	*50.6–67.1*	19.5	*59.2*	2.8	*4.2*	23.4	*64.3*
Claw 1 heights									
External primary branch	29	8.8 –13.5	*29.4–39.7*	11.4	*34.9*	1.3	*2.5*	13.4	*36.8*
External secondary branch	27	7.2 –11.9	*24.1–35.5*	9.1	*28.1*	1.2	*2.9*	9.8	*26.9*
Internal primary branch	28	8.7 –12.0	*27.4–35.2*	10.2	*31.2*	1.0	*2.0*	11.4	*31.3*
Internal secondary branch	26	6.3 –10.5	*20.1–31.3*	8.2	*25.0*	1.0	*2.2*	9.5	*26.1*
Claw 2 heights									
External primary branch	29	9.0 –15.5	*30.1–46.3*	12.4	*38.0*	1.6	*3.4*	15.2	*41.8*
External secondary branch	27	7.9 –12.2	*24.9–36.4*	9.9	*30.1*	1.2	*2.7*	12.1	*33.2*
Internal primary branch	29	8.9 –12.6	*27.9–39.3*	10.7	*32.6*	1.1	*2.6*	12.6	*34.6*
Internal secondary branch	26	7.3 –10.4	*20.7–31.0*	8.7	*26.4*	0.9	*2.5*	10.2	*28.0*
Claw 3 heights									
External primary branch	30	9.3 –15.2	*31.1–45.4*	12.5	*38.1*	1.4	*3.4*	14.4	*39.6*
External secondary branch	26	7.9 –11.9	*25.6–35.8*	10.1	*30.5*	1.3	*2.8*	11.9	*32.7*
Internal primary branch	30	8.5 –12.4	*27.6–37.0*	10.6	*32.5*	1.1	*2.5*	12.3	*33.8*
Internal secondary branch	24	7.0 –10.5	*21.6–30.7*	8.5	*26.1*	1.0	*2.2*	9.7	*26.6*
Claw 4 heights									
Anterior primary branch	30	9.8 –15.1	*29.7–45.1*	12.0	*36.7*	1.4	*2.8*	14.4	*39.6*
Anterior secondary branch	27	7.5 –11.8	*24.2–35.2*	9.3	*28.1*	1.2	*2.5*	11.2	*30.8*
Posterior primary branch	29	11.3 –17.1	*36.9–47.8*	13.7	*41.7*	1.4	*2.6*	17.1	*47.0*
Posterior secondary branch	11	8.6 –11.3	*28.2–35.8*	10.3	*30.7*	0.8	*2.4*	?	*?*

bar and double muscle attachments occur above claws I–III and are very poorly visible under PCM, but distinct under SEM (Figs 10–11).

Mouth antero-ventral. Bucco-pharyngeal apparatus of the *Macrobiotus* type (Fig. 12), with a ventral lamina and ten small peribuccal lamellae followed by six buccal sensory lobes. Under PCM, the OCA is of the *patagonicus* type, with only the first band of teeth not visible (Fig. 12); however, all three bands

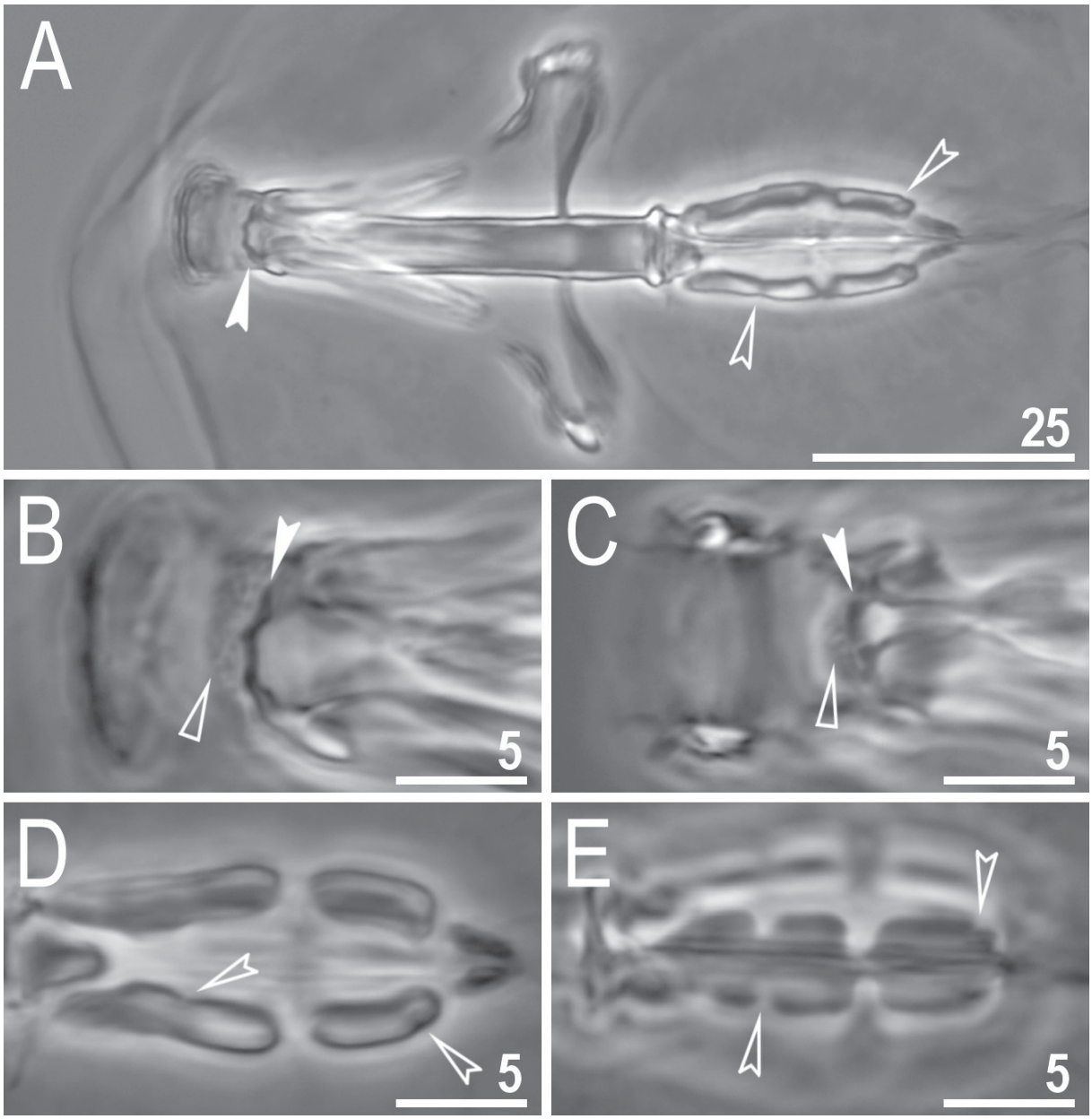

Fig. 12. *Macrobiotus dalaticus* sp. nov., paratypes (ISEA PAS), PCM images of the buccal apparatus. **A**. Entire buccal apparatus. **B–C**. Oral cavity armature, dorsal (B) and ventral (C) teeth, respectively. **D–E**. Placoid morphology, dorsal (D) and ventral (E) placoids, respectively. Empty flat arrowheads indicate the second band of teeth, filled indented arrowheads indicate the third band of teeth, and empty indented arrowheads indicate the central and subterminal constrictions in the first and second macroplacoids, respectively. Scale bars in μm.

Table 5. Measurements [in μm] of selected morphological structures of the eggs of *Macrobiotus dalaticus* sp. nov.; eggs mounted in Hoyer's medium; process base/height ratio is expressed as percentage; N: number of eggs/structures measured; range: refers to the smallest and the largest structure among all measured specimens; SD: standard deviation.

Character	N	Range	Mean	SD
Egg bare diameter	30	53.6–66.5	61.8	2.8
Egg full diameter	30	63.5–75.6	71.0	2.7
Process height	90	2.7–5.8	4.2	0.6
Process base width	90	2.1–4.2	3.2	0.5
Process base/height ratio	90	55%–109%	77%	13%
Terminal disc width	90	1.8–4.8	3.3	0.6
Inter-process distance	90	2.0–5.9	3.4	0.7
Number of processes on the egg circumference	30	28–34	32.4	1.3

are clearly discernible under SEM (Fig. 13). The first band of teeth consists of numerous extremely small cones arranged in several rows, located anteriorly in the oral cavity on the bases of the peribuccal lamellae and immediately posterior to them (Fig. 13). The second band of teeth is situated between the ring fold and the third band, and is composed of several rows of small cones, larger than those of the first band which under PCM are seen as dark dots (Figs 12–13). The third band of teeth is located in the posterior portion of the oral cavity, between the second band and the opening of the buccal tube (Figs 12–13); it is discontinuous and divided into dorsal and ventral portions. Under PCM, the dorsal teeth form a single transverse ridge with two distinct bends / thickenings, whereas the ventral teeth appear as two separate lateral transverse ridges with an elongated median tooth between them (Fig. 12). Under SEM, the dorsal teeth indeed form a single ridge with two larger lateral peaks and several smaller median peaks and indentations (Fig. 13), corresponding to the bends / thickenings observed under PCM (Fig. 12).

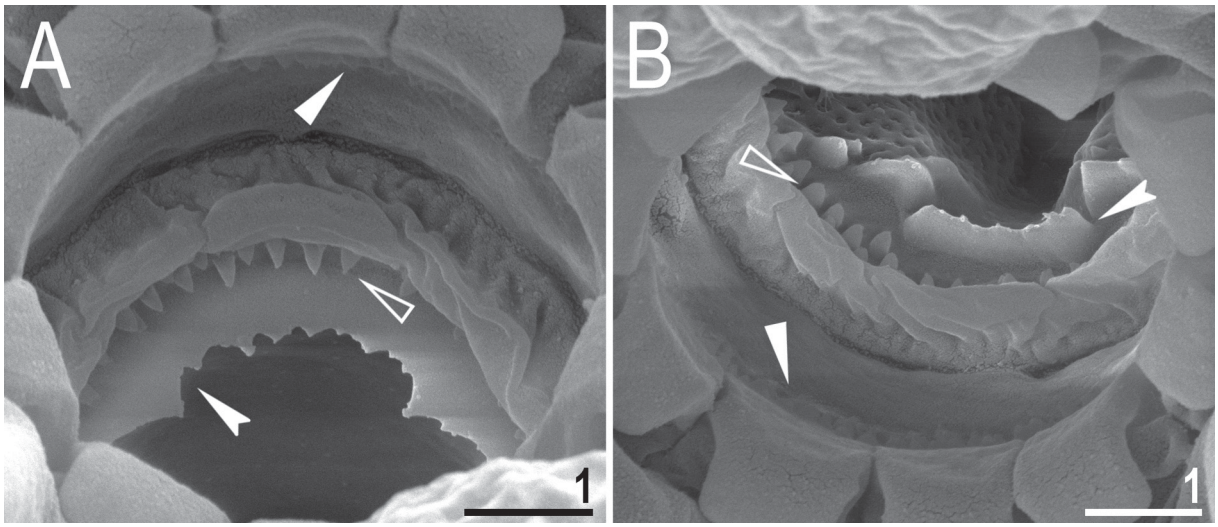

Fig. 13. *Macrobiotus dalaticus* sp. nov., paratypes (ISEA PAS). **A–B**. Oral cavity armature observed under SEM from different angles, dorsal and ventral views, respectively. Filled flat arrowheads indicate the first band of teeth, empty flat arrowheads indicate the second band of teeth, and filled indented arrowheads indicate the third band of teeth. Scale bars in μm.

Under SEM, the ventral teeth are also separated into one median and two lateral teeth, with the latter positioned more posteriorly relative to the median tooth (Fig. 13). The pharyngeal bulb is spherical, with triangular apophyses, two rod-shaped macroplacoids, and a distinct triangular microplacoid (Fig. 12). The macroplacoid length sequence is 2 < 1, with the first and second macroplacoids constricted centrally and subterminally, respectively (Fig. 12). Measurements and morphometric statistics are provided in Table 4.

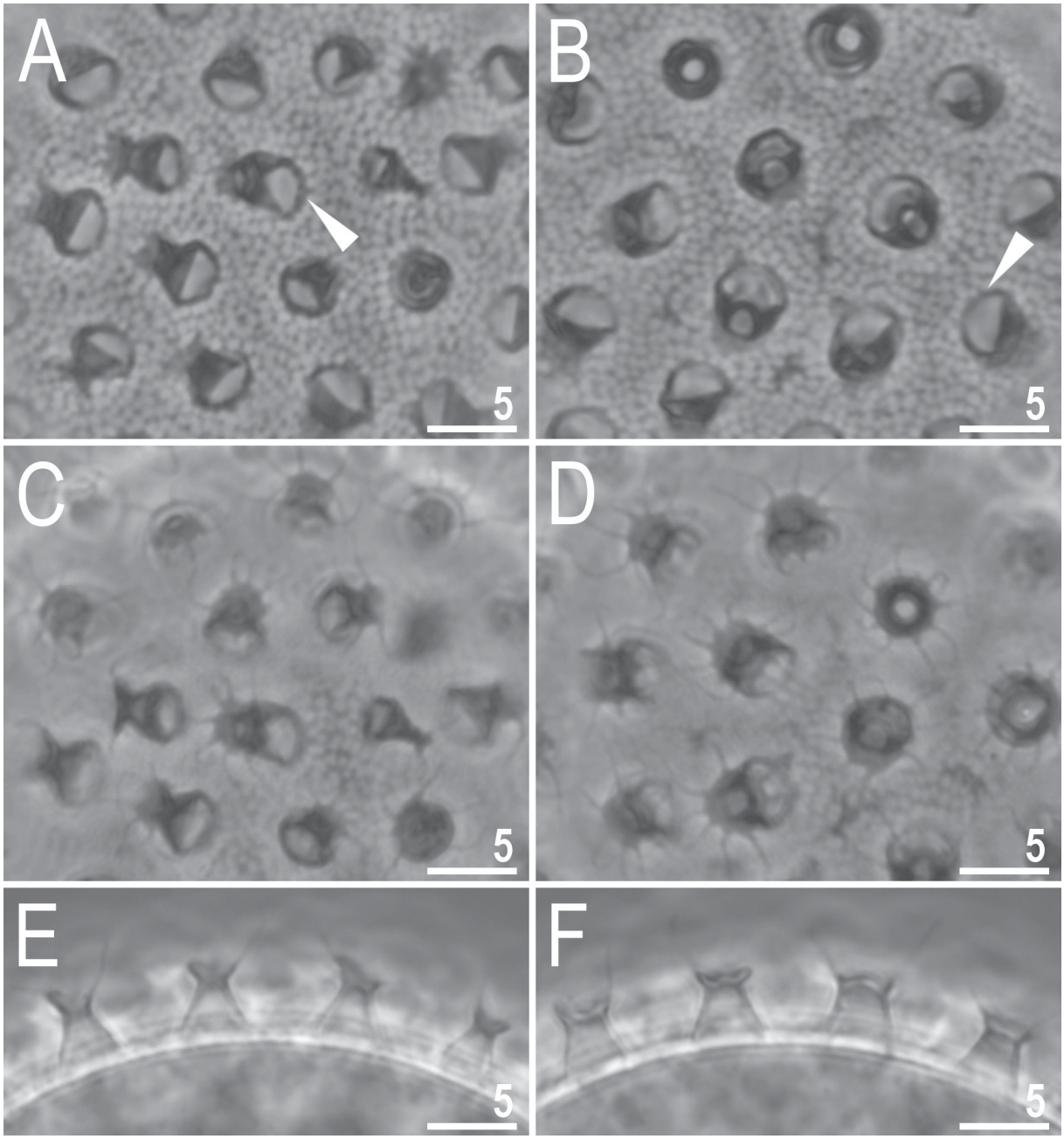

Fig. 14. *Macrobiotus dalaticus* sp. nov., PCM images of the egg at ×1000 magnification. **A–B**. Egg surface, focused on the surface between processes. **C–D**. Egg surface focused on egg processes and terminal discs. **E–F**. Midsections of egg processes. Filled flat arrowheads indicate thickenings around the bases of the egg processes. Scale bars in μm.

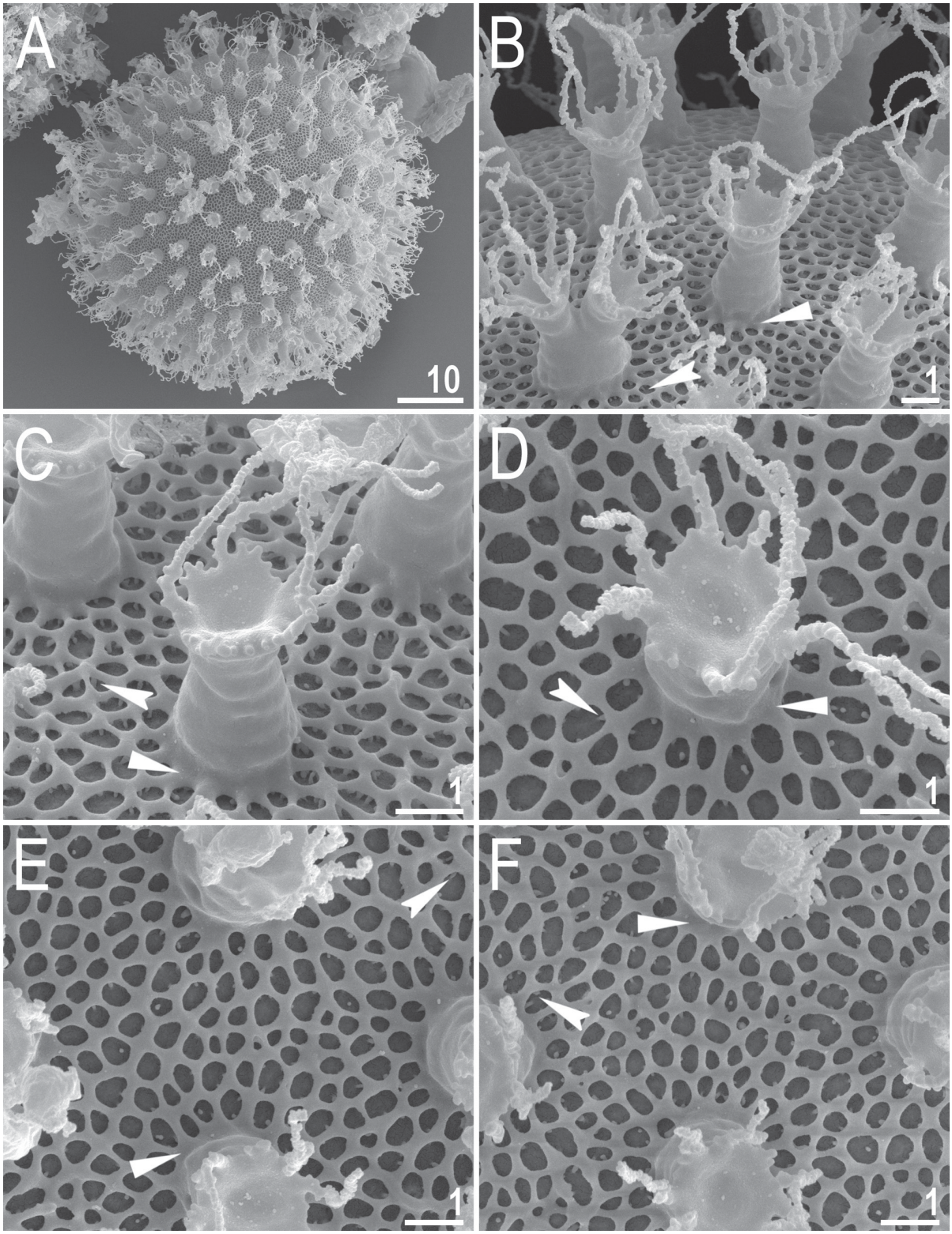

Fig. 15. *Macrobiotus dalaticus* sp. nov., SEM images of the eggs. **A**. Entire egg. **B–F**. Details of egg processes and the surface between them. Filled flat arrowheads indicate thickenings (corresponding to dark thickenings visible under PCM) around the bases of the egg processes, and filled indented arrowheads indicate pillar-like structures connecting the reticulum and egg processes to the egg surface. Scale bars in μm.

Eggs

Eggs laid freely, whitish to light yellow, spherical (Figs 14–15). The surface between egg processes is of the *hufelandi* type, with the eggshell between processes covered by a reticulum (Figs 14–15). The reticulum and egg processes are attached to the egg surface by multiple pillar-like structures that are visible only under SEM (Fig. 15). The pores of the reticulum are similar in size and uniformly distributed over the entire egg surface; notably, no peribasal rings of elongated pores or enlarged meshes are present around the bases of the processes (Figs 14–15). Several rows of pores occur between adjacent processes, and the width of the mesh bars and nodes is smaller than the pore diameter (Figs 14–15). Pores are circular to oval (longer diameter 0.3–0.7 μm) (Figs 14–15). Under PCM, faint dark thickenings or darker rings can be distinguished around the bases of the egg processes, which under SEM correspond to the portions linking the reticulum with the walls of the egg processes (Figs 14–15). Egg processes are shaped like inverted goblets, with slightly concave conical trunks and well-defined terminal discs (Figs 14–15). Terminal discs are cog-shaped, with a smooth concave central area and serrated margins (Figs 14–15). Many serrations are elongated into 8–14 thin, flexible filaments, less than 0.3 μm in diameter and 4–7 μm in length (Figs 14–15). Under PCM, the filaments appear hair-like (Fig. 14), whereas under SEM they show a rough surface covered with fine granulation or digitations, while the surface of the terminal discs appears smooth (Fig. 15). Although clearly visible under PCM, the filaments are very thin and may be overlooked or misinterpreted as debris attached to the eggs if careful examination is not performed. Measurements and morphometric statistics of the eggs are provided in Table 5.

Reproduction

The type population of *M. dalaticus* sp. nov. is dioecious. Both males with testes filled with sperm and females with ovaries containing oocytes were observed in specimens freshly mounted in Hoyer's medium.

Differential diagnosis

By having (i) a smooth body cuticle lacking dense patches of body granulation, except for the typical granulation present on the distal portions of the legs, and (ii) eggs with a reticulated surface between processes and egg processes bearing terminal discs with long, flexible filaments, the new species is most similar to two other *Macrobiotus* taxa: *Macrobiotus polypiformis* Roszkowska, Ostrowska, Stec, Janko & Kaczmarek, 2017 and *Macrobiotus sharopovi* Polishchuk, Kayastha, Młodzianowska, Warguła & Kaczmarek, 2025, both known only from Ecuador (Roszkowska *et al.* 2017; Polishchuk *et al.* 2025).

The new species differs from *M. polypiformis* by: (i) a better-developed OCA, with the second and third bands of teeth clearly visible under light microscopy in the new species, whereas only the third band of teeth is clearly visible in *M. polypiformis*; (ii) the absence of granulation in the central area of the terminal discs of the egg processes (granulation present in *M. polypiformis*); (iii) a longer first macroplacoid (7.2–12.9 μm in the new species vs 5.2–6.8 μm in *M. polypiformis*); (iv) longer macroplacoid and placoid rows (12.6–22.5 μm and 15.5–26.3 μm in the new species vs 9.0–11.8 μm and 11.1–14.5 μm in *M. polypiformis*, respectively); and (v) a larger number of egg processes on the egg circumference (28–34 in the new species vs 19–23 in *M. polypiformis*).

The new species further differs from *M. sharopovi* by: (i) the size and shape of cuticular pores (roundish pores 0.4–0.6 μm in diameter in the new species vs elliptical pores with thicker edges and 0.8–1.8 μm in diameter in *M. sharopovi*); (ii) the morphology of the ventral portion of the third band of teeth in the OCA, in which the ventral teeth appear as three separate teeth in the new species, whereas they form a single transverse ridge in *M. sharopovi*; (iii) the presence of granulation on the flexible filaments extending from the terminal discs of the egg processes (filaments smooth in *M. sharopovi*); (iv) smaller eggs (bare diameter 53.6–66.5 μm and full diameter 63.5–75.6 μm in the new species vs 70.0–84.1 μm and 81.7–97.9 μm in *M. sharopovi*, respectively); and (v) a larger number of egg processes on the egg circumference (28–34 in the new species vs 20–24 in *M. sharopovi*).

Macrobiotus surmaczi sp. nov.
urn:lsid:zoobank.org:act:3F006251-3C6E-4D97-802E-99253C71C909
Figs 16–21; Tables 6–7

Etymology

The species name *surmaczi* is a patronym honouring Bartłomiej Surmacz, a close colleague and collaborator of the author, in recognition of his contributions to tardigrade research and his involvement in joint studies on tardigrade diversity and ecology. The species epithet *surmaczi* is a noun in the genitive case.

Material examined

68 animals, 28 eggs mounted on microscope slides in Hoyer's medium, 6 animals and 4 eggs examined under SEM and two animals processed for DNA sequencing.

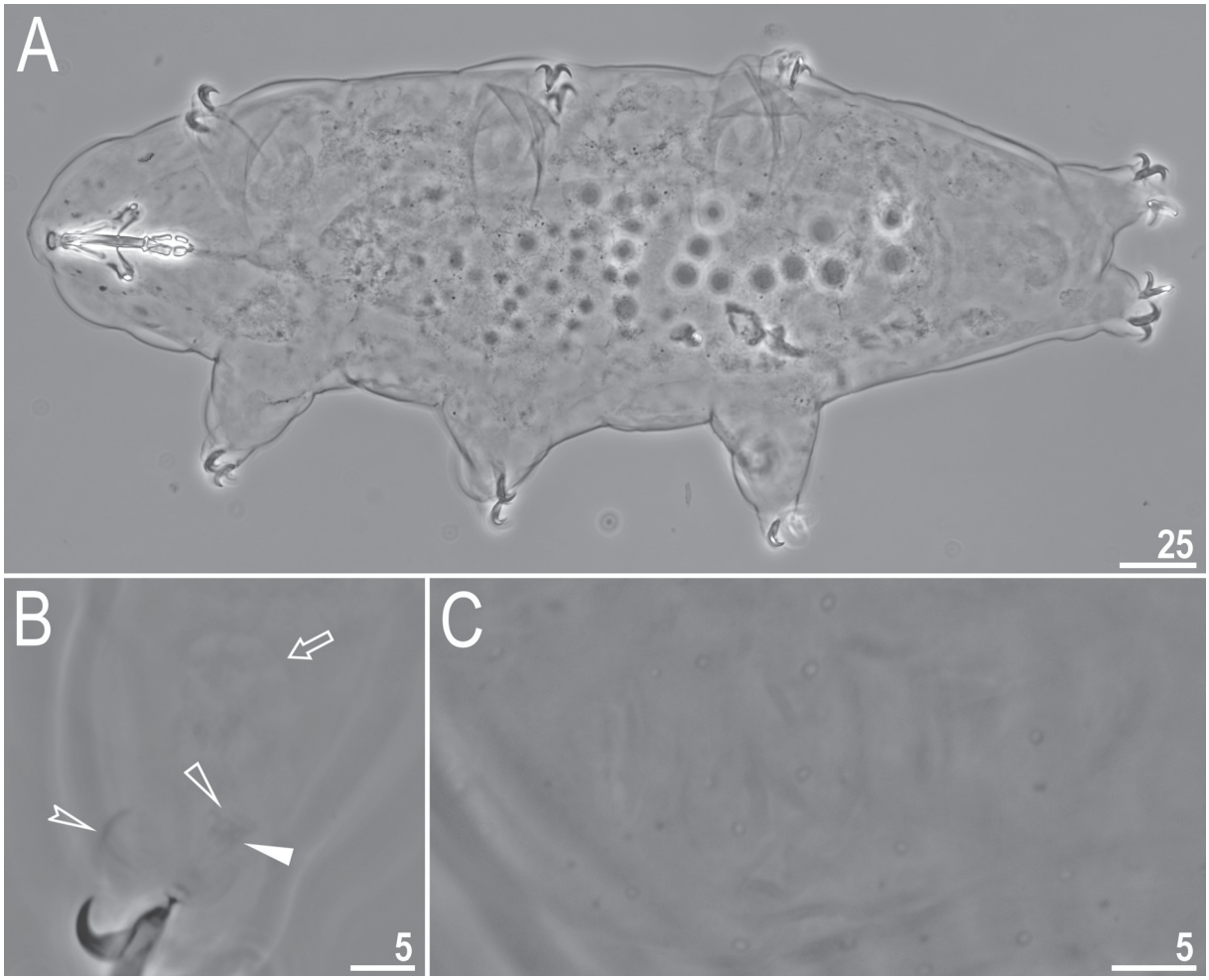

Fig. 16. *Macrobiotus surmaczi* sp. nov., habitus, internal leg surface, and cuticular pores, PCM. **A, C**. Holotype (ISEA PAS). **B**. Paratype (ISEA PAS). **A**. Dorso-ventral projection (PCM). **B**. Internal surface of leg II (PCM). **C**. Pores in the body cuticle (PCM). **D–E**. Empty arrow indicates a pulvinus-shaped cuticular bulge, empty indented arrowheads indicate a cuticular fold in the distal leg portion, empty flat arrowheads indicate muscle attachments, and filled flat arrowheads indicate faintly visible cuticular bars. Scale bars in μm.

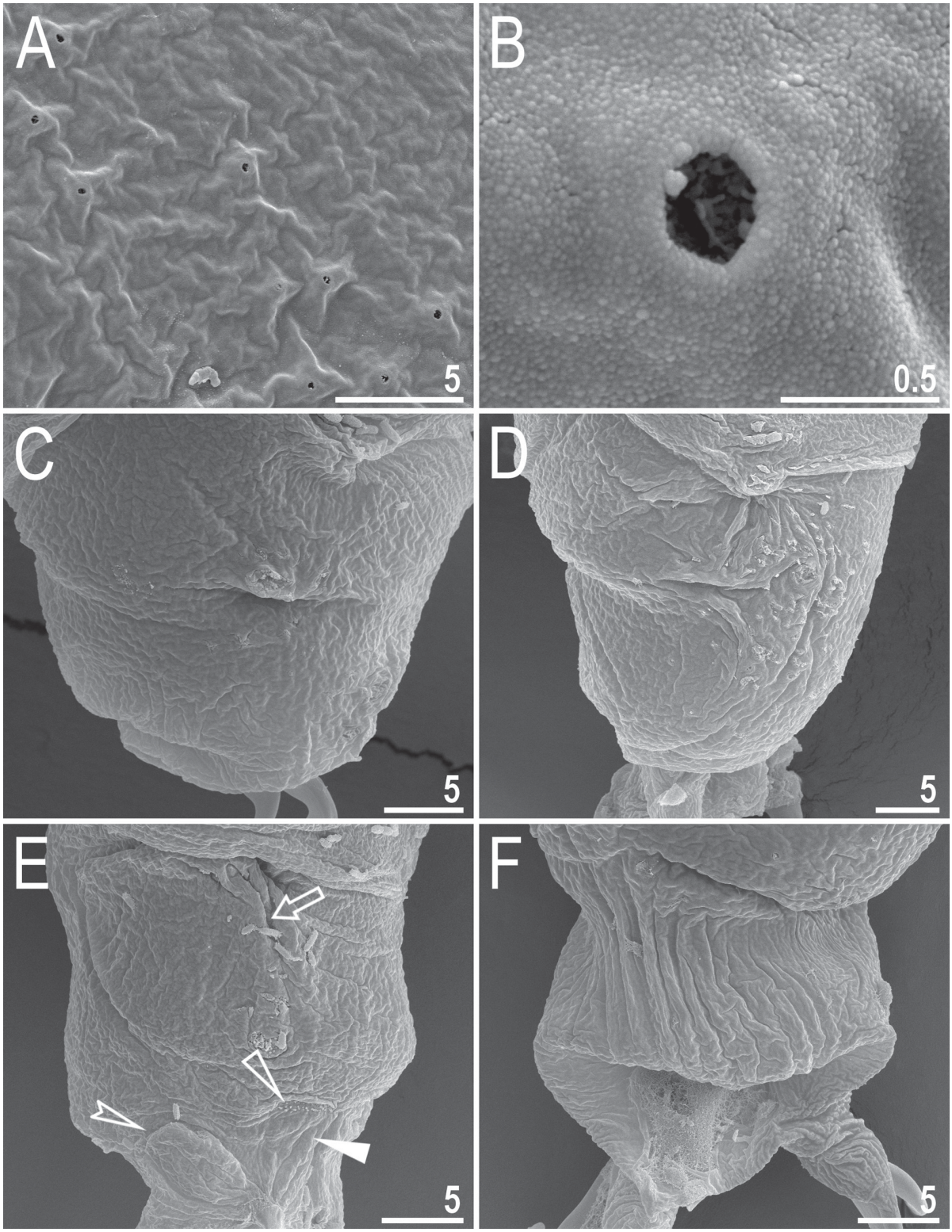

Fig. 17. *Macrobiotus surmaczi* sp. nov., paratypes (ISEA PAS), cuticular pores and leg cuticle; SEM. **A–B**. Cuticular pores in the body cuticle. **C–D**. External surface of legs I and III, respectively. **E**. Internal surface of leg III. **F**. Surface of the hind leg. Empty arrow indicates a pulvinus-shaped cuticular bulge, empty indented arrowhead indicates a cuticular fold in the distal leg portion, empty flat arrowhead indicates muscle attachments, and filled flat arrowhead indicates cuticular bars. Scale bars in μm.

Type material

Holotype

VIETNAM • Central Lâm Đồng Province, Đà Lạt, city park area ("Vườn Hoa"); 11°57′05″ N, 108°27′02″ E; 1491 m a.s.l.; Aug. 2018; D. Stec and K. Miler leg.; lichen collected from tree bark in urban environment; ISEA PAS, slide VN.003.07.

Paratypes

VIETNAM • 67 specs; same data as for holotype; ISEA PAS, slides VN.003.07 to VN.003.16 • 28 eggs; same data as for holotype; ISEA PAS, slides VN.003.01 to VN.003.06.

Description

Animals

Body transparent in juveniles and yellowish in adults; after fixation in Hoyer's medium, the body becomes transparent (Fig. 16). Eyes present in alive and Hoyer-fixed specimens. Cuticular pores are scattered randomly over the entire body surface (Figs 16–17), being more sparsely distributed on the

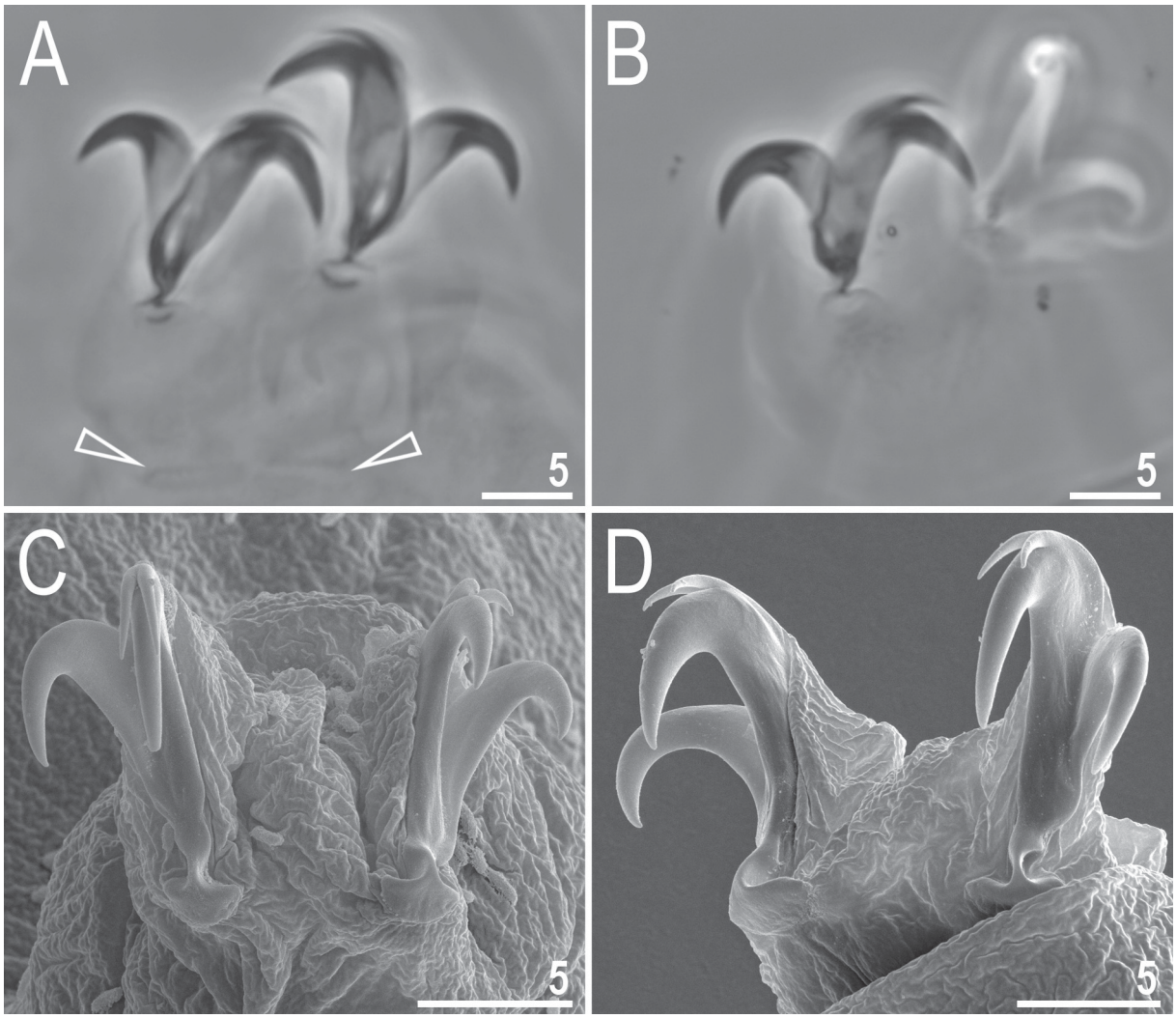

Fig. 18. *Macrobiotus surmaczi* sp. nov., claws. **A, C–D**. Paratypes (ISEA PAS). **B**. Holotype (ISEA PAS). **A**. Claws II (PCM). **B**. Claws IV (PCM). **C**. Claws I (SEM). **D**. Claws IV (SEM). Empty flat arrowheads indicate paired muscle attachments. Scale bars in μm.

ventral side. Pores are circular and uniform in size and shape (0.7–0.9 μm in diameter). Body and leg granulation are absent. On the internal surface of legs I–III, a pulvinus-shaped cuticular bulge is centrally located, and a faint cuticular fold occurs in the distal portion of the legs just above the claws (Figs 16–17). Both structures are visible only when the legs are fully extended and properly oriented on the slide.

Claws small and slender, of the *hufelandi* type (Fig. 18). Primary branches bear distinct accessory points, a common tract, and a well-developed stalk connecting the claw to the lunula (Fig. 18). Lunulae on legs I–IV are smooth (Fig. 18). A divided cuticular bar and double muscle attachments occur above claws I–III but are very poorly visible (Figs 16–18).

Mouth antero-ventral. Bucco-pharyngeal apparatus of the *Macrobiotus* type (Fig. 19), with a ventral lamina and ten small peribuccal lamellae followed by six buccal sensory lobes. Under PCM, the OCA is of the *maculatus* type, with the first and second bands of teeth not visible (Fig. 19); however, all three

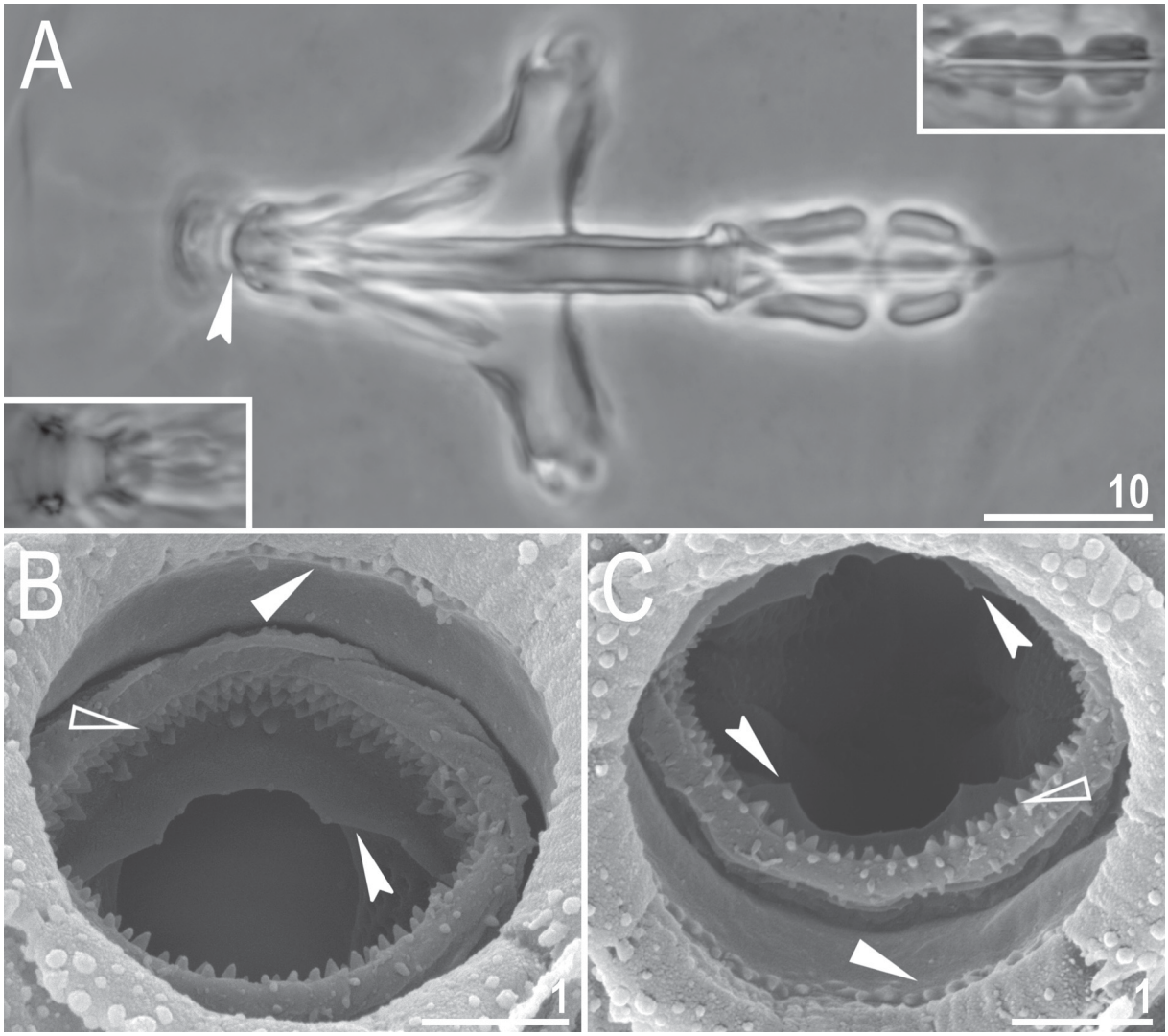

Fig. 19. *Macrobiotus surmaczi* sp. nov., paratypes (ISEA PAS), buccal apparatus and oral cavity armature; PCM. **A**. Buccal apparatus in dorsal view. The lower left inset shows the ventral view of the OCA, and the upper right inset shows the placoids in ventral view. **B–C**. Oral cavity armature observed under SEM from different angles, dorsal (B) and ventral (C) views, respectively. Filled flat arrowheads indicate the first band of teeth. Scale bars in μm.

Table 6. Measurements [in µm] and *pt* values [in %] of selected morphological structures of individuals of *Macrobiotus surmaczi* sp. nov.; specimens mounted in Hoyer's medium; N: number of specimens/ structures measured; range: refers to the smallest and the largest structure among all measured specimens; SD: standard deviation.

Character	N	Range		Mean		SD		Holotype	
		µm	*pt*	µm	*pt*	µm	*pt*	µm	*pt*
Body length	24	235 – 365	*909 – 1436*	313	*1137*	33	*133*	365	*1352*
Buccal tube									
Buccal tube length	24	24.5 – 31.6	–	27.6	–	2.1	–	27.0	–
Stylet support insertion point	24	16.1 – 21.3	*64.2 – 67.7*	18.3	*66.4*	1.6	*0.9*	17.7	*65.6*
Buccal tube external width	24	2.4 – 4.0	*9.8 – 15.6*	3.3	*12.0*	0.4	*1.2*	3.6	*13.3*
Buccal tube internal width	24	1.3 – 2.4	*5.3 – 9.0*	1.9	*7.0*	0.3	*0.9*	2.0	*7.4*
Ventral lamina length	24	12.8 – 17.4	*51.0 – 56.0*	14.8	*53.6*	1.4	*1.6*	14.1	*52.2*
Placoid lengths									
Macroplacoid 1	24	4.9 – 8.8	*19.5 – 27.8*	6.6	*23.9*	0.9	*2.3*	6.7	*24.8*
Macroplacoid 2	24	3.1 – 5.1	*12.7 – 16.8*	4.0	*14.6*	0.5	*1.3*	4.3	*15.9*
Microplacoid	24	1.1 – 2.2	*4.0 – 7.6*	1.7	*6.0*	0.3	*1.0*	1.9	*7.0*
Macroplacoid row	24	8.6 – 14.7	*35.1 – 48.9*	11.6	*41.9*	1.3	*3.3*	11.7	*43.3*
Placoid row	24	10.8 – 17.5	*44.1 – 58.2*	13.8	*49.8*	1.6	*3.8*	14.0	*51.9*
Claw 1 heights									
External primary branch	20	8.3 – 12.1	*31.1 – 42.7*	9.8	*35.7*	0.9	*2.9*	10.0	*37.0*
External secondary branch	19	6.6 – 10.0	*24.4 – 33.6*	8.0	*29.2*	0.9	*2.6*	7.5	*27.8*
Internal primary branch	21	7.3 – 10.7	*28.8 – 38.3*	9.1	*33.3*	0.8	*2.7*	9.5	*35.2*
Internal secondary branch	20	6.3 – 8.5	*23.4 – 32.0*	7.3	*26.9*	0.6	*2.1*	7.1	*26.3*
Claw 2 heights									
External primary branch	21	8.7 – 12.4	*30.4 – 42.3*	10.1	*36.8*	1.0	*3.1*	10.6	*39.3*
External secondary branch	20	6.9 – 9.9	*25.4 – 36.1*	8.5	*30.8*	0.9	*3.0*	8.9	*33.0*
Internal primary branch	20	8.0 – 12.2	*26.8 – 40.0*	9.4	*34.5*	1.0	*3.2*	9.9	*36.7*
Internal secondary branch	20	6.6 – 9.4	*23.4 – 33.2*	7.6	*27.9*	0.8	*2.6*	7.0	*25.9*
Claw 3 heights									
External primary branch	20	8.7 – 12.5	*31.1 – 42.4*	10.3	*37.1*	1.0	*3.2*	?	*?*
External secondary branch	17	6.8 – 10.5	*25.4 – 37.6*	8.6	*31.4*	1.0	*3.2*	?	*?*
Internal primary branch	22	8.2 – 12.3	*30.1 – 41.2*	9.6	*35.0*	1.0	*2.8*	9.9	*36.7*
Internal secondary branch	21	6.8 – 9.6	*23.4 – 34.0*	7.8	*28.6*	0.8	*2.2*	7.8	*28.9*
Claw 4 heights									
Anterior primary branch	20	9.4 – 14.1	*35.5 – 46.4*	11.1	*40.9*	1.1	*3.5*	11.0	*40.7*
Anterior secondary branch	17	7.6 – 12.0	*28.6 – 38.7*	9.3	*34.2*	1.0	*3.3*	8.7	*32.2*
Posterior primary branch	12	9.7 – 12.9	*36.5 – 48.4*	11.6	*43.5*	1.1	*3.5*	11.8	*43.7*
Posterior secondary branch	8	8.4 – 11.1	*33.5 – 40.5*	9.6	*36.8*	0.8	*2.7*	9.6	*35.6*

bands are clearly discernible under SEM (Fig. 19). The first band of teeth consists of numerous extremely small cones arranged in a single row, located anteriorly in the oral cavity on the bases of the peribuccal lamellae and immediately posterior to them (Fig. 19). The second band of teeth is situated between the ring fold and the third band and is composed of several rows of small cones, larger than those of the first band (Fig. 19). The third band of teeth is located in the posterior portion of the oral cavity, between the second band and the opening of the buccal tube (Fig. 19); it is discontinuous and divided into dorsal and ventral portions. Under PCM, the dorsal and ventral teeth appear as a single transverse ridge, with the ventral portion bearing two dark thickenings (Fig. 19). Under SEM, the dorsal and ventral portions

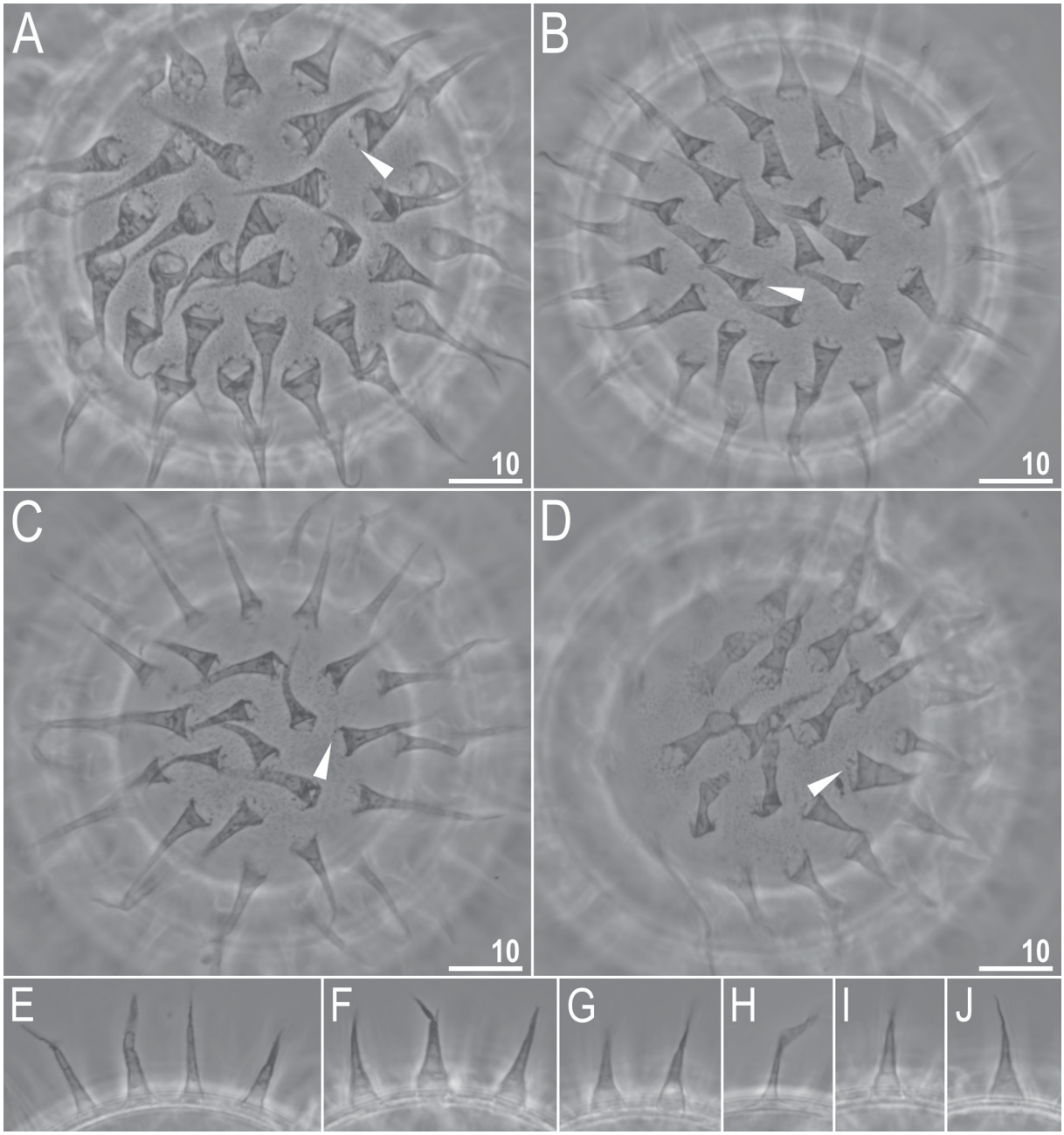

Fig. 20. *Macrobiotus surmaczi* sp. nov., PCM images of the egg at ×1000 magnification. **A–D**. Egg surface. **E–J**. Midsections of egg processes. Filled flat arrowheads indicate dark thickenings around the bases of the egg processes. Scale bars in μm.

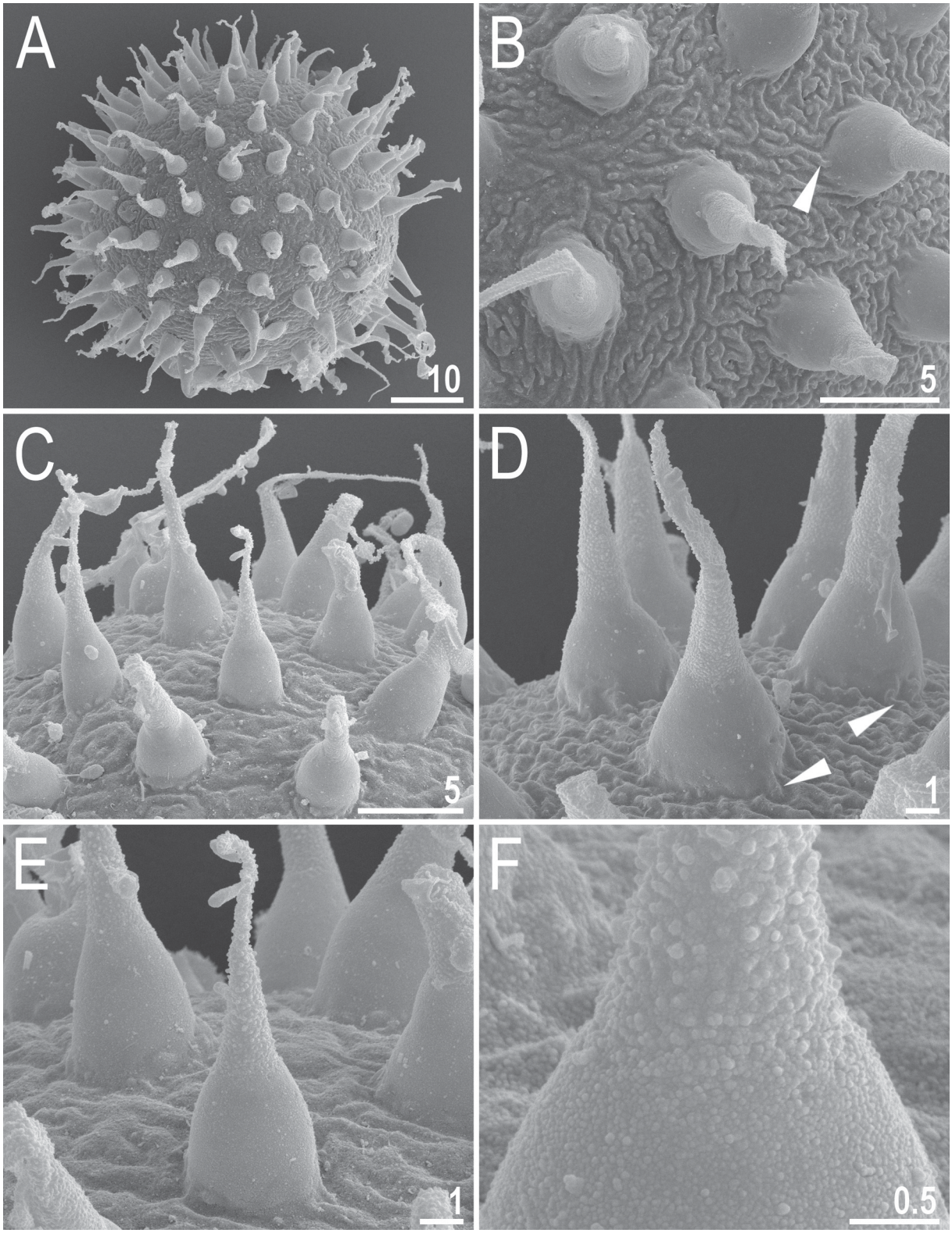

Fig. 21. *Macrobiotus surmaczi* sp. nov., SEM images of the eggs. **A**. Entire egg. **B–F**. Details of egg processes and the surface between them. Filled flat arrowheads indicate thickenings (corresponding to dark thickenings visible under PCM) around the bases of the egg processes. Scale bars in μm.

Table 7. Measurements [in µm] of selected morphological structures of the eggs of *Macrobiotus surmaczi* sp. nov.; eggs mounted in Hoyer's medium; process base/height ratio is expressed as percentage; N: number of eggs/structures measured; range: refers to the smallest and the largest structure among all measured specimens; SD: standard deviation.

Character	N	Range	Mean	SD
Egg bare diameter	23	52.3–66.5	58.4	3.7
Egg full diameter	23	71.0–95.3	82.8	7.4
Process height	69	8.0–17.8	13.3	2.4
Process base width	69	2.6–5.8	4.0	0.7
Process base/height ratio	69	16%–48%	31%	6%
Inter-process distance	69	2.2–7.8	3.9	0.8
Number of processes on the egg circumference	17	20–25	22.1	1.5

are clearly distinguishable and form continuous ridges, each bearing two peaks, with the ventral peaks being larger and more distinct than the dorsal ones (Fig. 19). The pharyngeal bulb is spherical, with triangular apophyses, two rod-shaped macroplacoids, and a small triangular microplacoid (Fig. 19). The macroplacoid length sequence is 2 < 1, with the first and second macroplacoids constricted centrally and subterminally, respectively (Fig. 19). Measurements and morphometric statistics are provided in Table 6.

Eggs

Eggs laid freely, yellowish, spherical, and ornamented (Figs 20–21). The surface between egg processes is of the *persimilis* type, with the eggshell between processes continuous, i.e. smooth or wrinkled but never forming pores or a reticulum (Figs 20–21). Under PCM, the egg surface appears generally smooth but covered with fine, scattered dark dots (Fig. 20). Observations under SEM confirm the continuous nature of the eggshell surface and the absence of reticulation; however, the surface is clearly wrinkled, forming a delicate sculpturing composed of fine grooves and folds (Fig. 21). These surface irregularities most probably correspond to the dark dots observed under PCM. Dark thickenings can be distinguished under PCM around the bases of the egg processes, which under SEM correspond to the thickened portions linking the egg surface with the walls of the egg processes (Figs 20–21). Egg processes are conical, with a wide proximal portion near the egg surface and a distinctly narrower distal portion (Figs 20–21). The walls of the proximal portion are smooth, whereas the distal portion is rough and flattened apically, being covered by granules that are clearly visible under SEM and occasionally very faintly visible under PCM (Figs 20–21). The apical flattening is usually poorly visible under PCM and can be observed only when the egg process is oriented with the flattened surface facing the observer. The wider proximal portion of the egg processes is usually shorter than the narrower distal portion (Figs 20–21). Measurements and morphometric statistics of the eggs are provided in Table 7.

Reproduction

The type population of *M. surmaczi* sp. nov. is dioecious. Both males with testes filled with sperm and females with ovaries containing oocytes were observed in specimens freshly mounted in Hoyer's medium.

Differential diagnosis

By having (i) a smooth, continuous body cuticle lacking dorsal gibbosities and (ii) eggs with conical, elongated processes bearing flattened apices and a smooth, continuous eggshell surface between processes, the new species is most similar to only one species of *Macrobiotus*: *Macrobiotus kristenseni*

Guidetti, Peluffo, Rocha, Cesari & Moly de Peluffo, 2013, known so far only from Argentina (Guidetti *et al.* 2013).

However, the new species differs from *M. kristenseni* in several diagnostic characters: (i) the absence of granulation on both the body and leg cuticle (typical granulation present on the distal portions of all legs in *M. kristenseni*); (ii) the morphology of the third band of teeth in the OCA, in which the dorsal and ventral portions appear as single, continuous transverse ridges in the new species, whereas in *M. kristenseni* both portions consist of three separate ridges; (iii) the presence of smooth lunulae on the hind legs (lunulae dentate in *M. kristenseni*); (iv) the morphology of the egg processes, which in the new species are conical with a wider proximal portion and a distinctly narrower distal portion that is flattened apically and covered with granules, whereas in *M. kristenseni* the processes are conical, rather spiky in shape, with a flattened distal portion lacking granulation; (v) the morphology of the egg surface between processes, which in the new species appears smooth and covered with fine, scattered dark dots under PCM and, under SEM, is confirmed to be continuous but distinctly wrinkled, forming a delicate sculpturing of fine grooves and folds, whereas in *M. kristenseni* the egg surface between processes shows light-refracting dots under PCM and is confirmed under SEM to be solid and smooth, without distinct sculpturing; and (vi) smaller eggs (bare diameter 52.3–66.5 μm and full diameter 71.0–95.3 μm in the new species vs 73.0–96.3 μm and 94.0–125.0 μm in *M. kristenseni*, respectively).

Macrobiotus hoianicus sp. nov.
urn:lsid:zoobank.org:act:4E0E4B5B-7E3B-43D2-82AE-C02244AAE4DF
Figs 22–29; Tables 8–9

Etymology

The species name *hoianicus* refers to Hội An, Vietnam, where the species was collected. The adjective is formed in reference to the type locality.

Material examined

77 animals, 48 eggs mounted on microscope slides in Hoyer's medium, 6 animals and 5 eggs examined under SEM and two animals processed for DNA sequencing.

Type material

Holotype

VIETNAM • Quảng Nam Province, Hội An, vicinity of Fukian Assembly Hall; 15°52′39″ N, 108°19′50″ E; 11 m a.s.l.; Aug. 2018; D. Stec and K. Miler leg.; moss collected from tree bark in urban environment; ISEA PAS, slide VN.004.13.

Paratypes

VIETNAM • 76 specs; same data as for holotype; ISEA PAS, slides VN.004.01 to VN.004.06, VN.004.13, VN.004.14 • 48 eggs; same data as for holotype; ISEA PAS, slides VN.004.07 to VN.004.12.

Description

Animals

Body transparent in juveniles and whitish in adults; after fixation in Hoyer's medium, the body becomes transparent (Fig. 22). Eyes present in alive and Hoyer-fixed specimens. Cuticular pores are scattered randomly over the entire body surface (Figs 22–23), being more sparsely distributed on the ventral side. Pores are roundish to oval and similar in size (0.6–0.1 μm in diameter). Granulation is present over the entire body cuticle, being denser in the dorso-caudal region; however, it is clearly visible only under SEM (Fig. 23). Under PCM, body granulation is discernible only in the dorso-caudal part of the

body (Fig. 22). In addition to the more or less evenly distributed body granulation, two dense patches of granulation are present on the left and right sides of the caudal body portion, between the main body trunk and the terminal body segment (Figs 22–23). Distinct granulation patches are also present on the external surfaces of legs I–III (Figs 24–25), whereas on the internal surfaces granulation occurs only on legs II–III (Figs 24–25). Dense and distinct granulation is also present on the lateral and dorsal surfaces of leg IV (Figs 24–25). On the internal surface of legs I–III, a pulvinus-shaped cuticular bulge is centrally located, and a faint cuticular fold occurs in the distal portion of the legs just above the claws (Figs 24–25). Both structures are visible only when the legs are fully extended and properly oriented on the slide.

Claws small and slender, of the *hufelandi* type (Fig. 26). Primary branches bear distinct accessory points, a common tract, and a well-developed stalk connecting the claw to the lunula (Fig. 26). Lunulae on legs I–IV are smooth (Fig. 26). A divided cuticular bar and double muscle attachments occur above claws I–III but are very poorly visible (Figs 24–26).

Mouth antero-ventral. Bucco-pharyngeal apparatus of the *Macrobiotus* type (Fig. 27), with a ventral lamina and ten small peribuccal lamellae followed by six buccal sensory lobes. Under PCM, the OCA

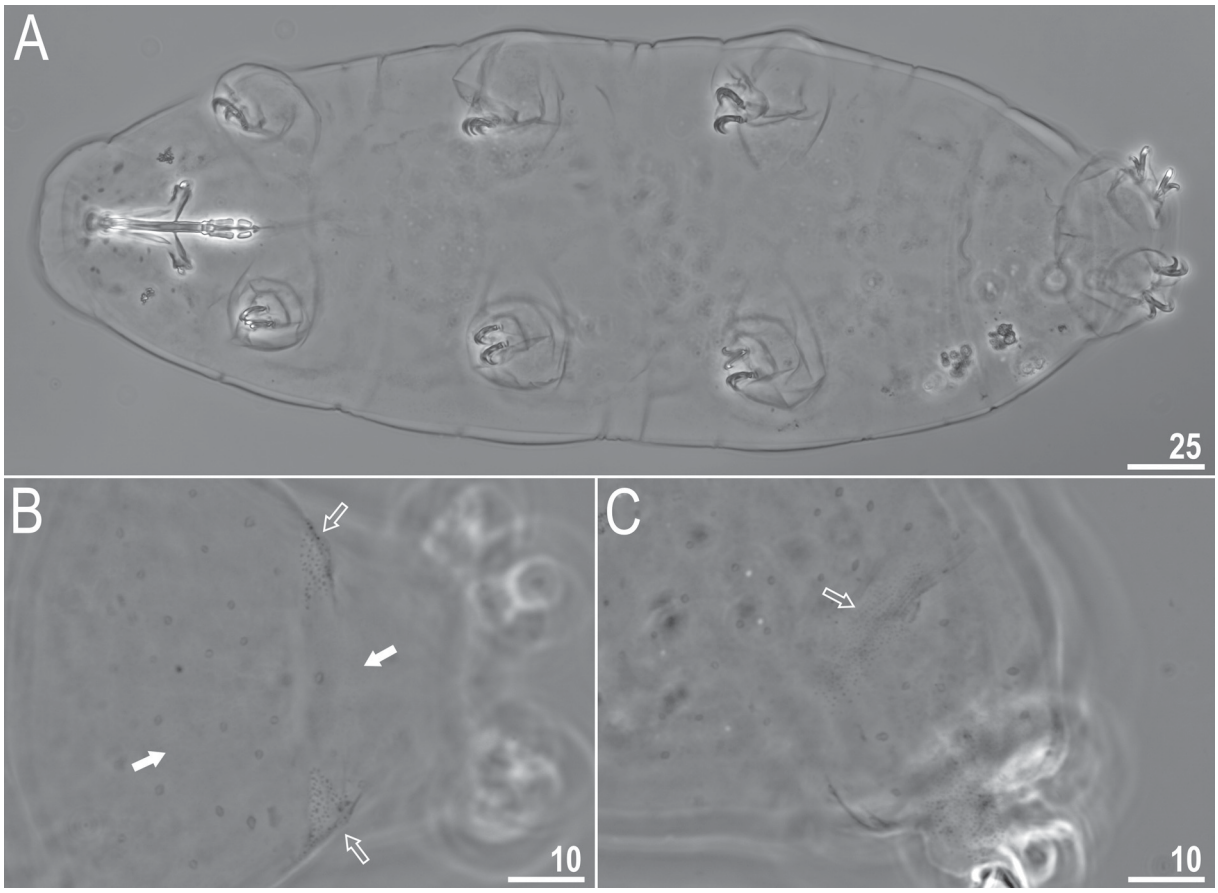

Fig. 22. *Macrobiotus hoianicus* sp. nov., habitus, body granulation, and cuticular pores; PCM. **A**. Holotype (ISEA PAS), dorso-ventral projection. **B–C**. Paratypes (ISEA PAS). **B**. Cuticular pores, faintly visible body granulation in the dorso-caudal body cuticle, and two patches of dense granulation on the lateral sides of the caudal body region (dorso-ventral projection). **C**. Dense patch of granulation on the lateral side of the caudal body region (lateral view). Filled arrows indicate body granulation faintly visible under PCM, and empty arrows indicate dense granulation patches on the lateral sides of the caudal body region. Scale bars in μm.

is of the *maculatus* type, with the first and second bands of teeth not visible (Fig. 27); however, all three bands are clearly discernible under SEM (Fig. 27). The first band of teeth consists of numerous extremely small cones arranged in a single row, located anteriorly in the oral cavity on the bases of the peribuccal lamellae and immediately posterior to them (Fig. 27). The second band of teeth is situated between the ring fold and the third band and is composed of several rows of small, sparsely distributed cones, larger than those of the first band (Fig. 27). The third band of teeth is located in the posterior portion of the oral cavity, between the second band and the opening of the buccal tube (Fig. 27); it is discontinuous and divided into dorsal and ventral portions. Under PCM, the dorsal and ventral teeth appear as a single transverse ridge, each with two dark thickenings (Fig. 27). Under SEM, the dorsal and ventral portions are clearly distinguishable: the dorsal portion forms a continuous ridge bearing two peaks (teeth), whereas the ventral portion is composed of two larger lateral teeth and one smaller median tooth (Fig. 27). The pharyngeal bulb is spherical, with triangular apophyses, two rod-shaped

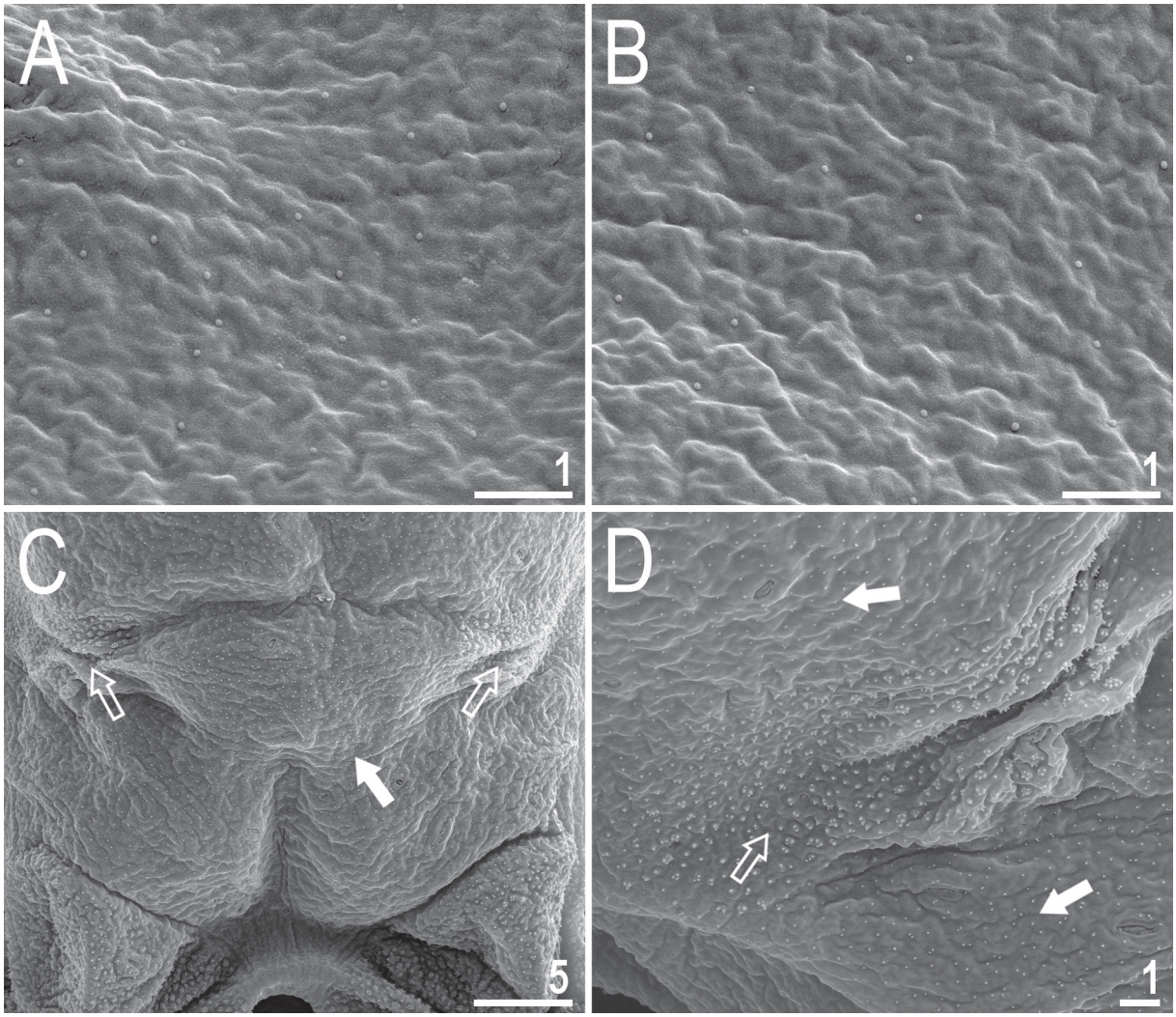

Fig. 23. *Macrobiotus hoianicus* sp. nov., paratypes (ISEA PAS), body granulation and cuticular pores; SEM. **A**. Body granulation in the head region of the dorsal body cuticle. **B**. Body granulation in the central part of the dorsal body cuticle. **C**. Body granulation in the caudal part of the dorsal body cuticle. **D**. Details of a dense granulation patch on the lateral side of the caudal body region. Filled arrows indicate regular body granulation faintly visible under PCM, and empty arrows indicate dense granulation patches on the lateral sides of the caudal body region. Scale bars in μm.

macroplacoids, and a small triangular microplacoid (Fig. 27). The macroplacoid length sequence is 2 < 1, with the first and second macroplacoids constricted centrally and subterminally, respectively, the latter constriction being extremely delicate (Fig. 27). Measurements and morphometric statistics of the animals are provided in Table 8.

Eggs

Eggs laid freely, white, spherical to slightly ovoid (Figs 28–29). The surface between egg processes is of the *hufelandi* type, i.e. covered with a reticulum (Figs 28–29). The reticular mesh is composed of distinct pores (0.4–0.6 μm in diameter), the diameter of which is usually similar to the width of the nodes and bars forming the mesh, giving the reticulum a robust appearance (Figs 28–29). Interbasal meshes are usually larger than peribasal meshes; however, the peribasal meshes do not form distinct rings around the bases of the egg processes (Figs 28–29). Under PCM, dark thickenings can be distinguished around

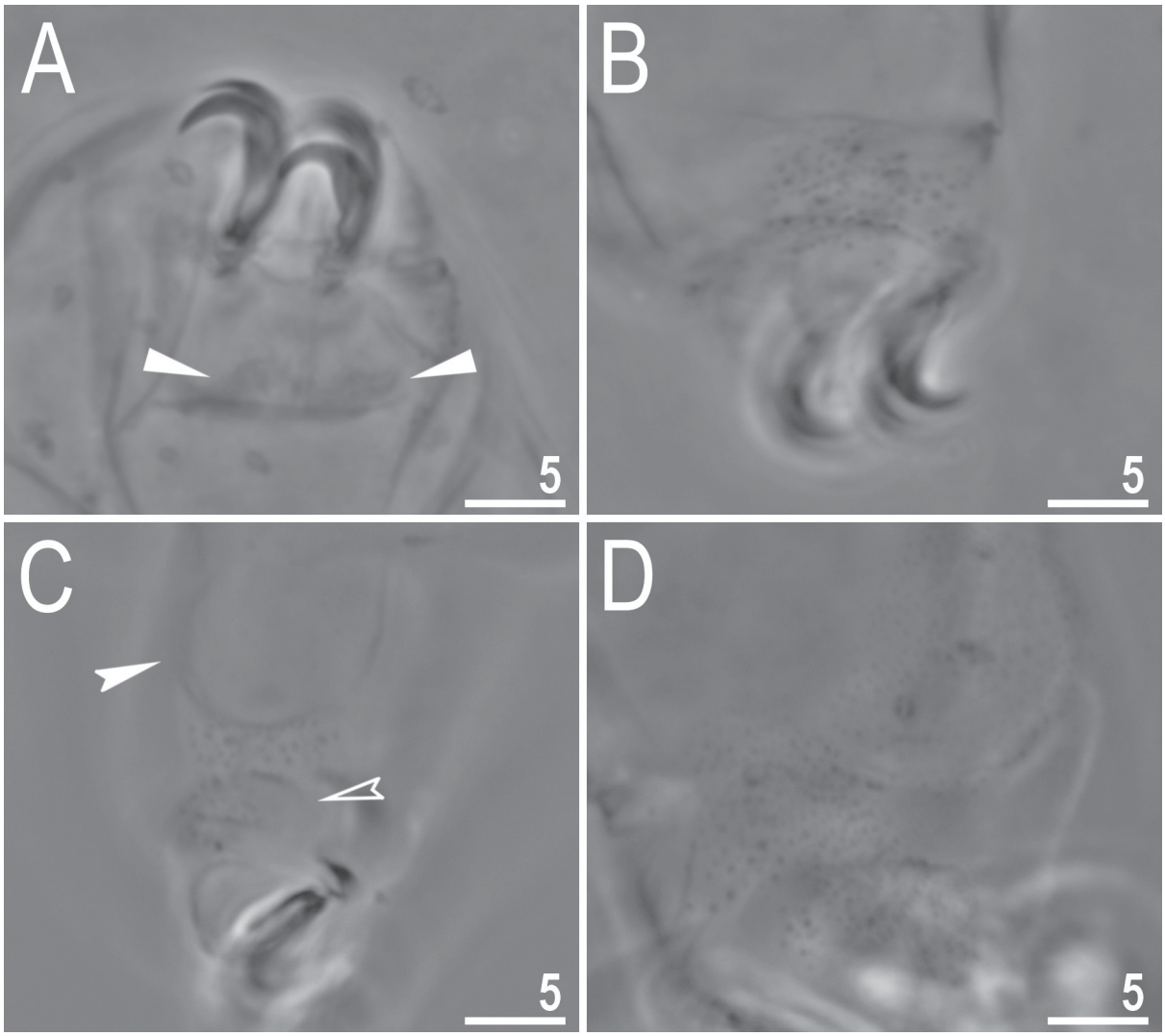

Fig. 24. *Macrobiotus hoianicus* sp. nov., paratypes (ISEA PAS), leg cuticle; PCM. **A**. Internal surface of leg III. **B**. Granulation on the external surface of leg II. **C**. Granulation on the internal surface of leg III. **D**. Granulation on the hind leg. Filled indented arrowhead indicates a pulvinus-shaped cuticular bulge, empty indented arrowhead indicates a cuticular fold in the distal leg portion, and filled flat arrowheads indicate a divided cuticular bar. Scale bars in μm.

Table 8. Measurements [in µm] and *pt* values [in %] of selected morphological structures of individuals of *Macrobiotus hoianicus* sp. nov.; specimens mounted in Hoyer's medium; N: number of specimens/ structures measured; range: refers to the smallest and the largest structure among all measured specimens; SD: standard deviation.

Character	N	Range		Mean		SD		Holotype	
		µm	*pt*	µm	*pt*	µm	*pt*	µm	*pt*
Body length	30	162–369	*827–1146*	316	*1021*	39	*73*	359	*1085*
Buccal tube									
Buccal tube length	30	19.6–33.7	–	30.9	–	2.9	–	33.1	–
Stylet support insertion point	30	13.9–23.8	*70.0–72.4*	21.9	*70.7*	2.1	*0.5*	23.4	*70.7*
Buccal tube external width	30	1.8–3.8	*8.8–11.3*	3.2	*10.2*	0.4	*0.6*	3.3	*10.0*
Buccal tube internal width	30	0.9–2.0	*3.4–6.7*	1.6	*5.3*	0.3	*0.7*	1.8	*5.4*
Ventral lamina length	30	10.5–18.7	*51.1–56.4*	16.7	*53.9*	1.8	*1.6*	18.3	*55.3*
Placoid lengths									
Macroplacoid 1	30	3.5–8.4	*17.9–25.6*	6.8	*21.8*	1.0	*1.9*	7.6	*23.0*
Macroplacoid 2	30	1.7–4.6	*8.7–13.9*	3.7	*12.0*	0.6	*1.2*	4.5	*13.6*
Microplacoid	30	0.8–2.4	*3.4–7.3*	1.8	*5.7*	0.4	*0.9*	2.1	*6.3*
Macroplacoid row	30	6.4–15.3	*32.7–47.4*	11.9	*38.4*	1.8	*3.0*	13.4	*40.5*
Placoid row	30	7.9–16.8	*39.0–51.9*	14.2	*45.8*	1.9	*3.0*	16.1	*48.6*
Claw 1 heights									
External primary branch	29	6.4–9.4	*25.4–32.7*	8.4	*27.2*	0.7	*1.5*	9.3	*28.1*
External secondary branch	15	4.7–8.0	*19.5–24.8*	6.8	*22.2*	0.8	*1.4*	7.4	*22.4*
Internal primary branch	30	6.0–9.1	*23.8–30.6*	8.1	*26.2*	0.7	*1.4*	9.1	*27.5*
Internal secondary branch	23	4.4–7.3	*18.3–22.5*	6.5	*21.0*	0.6	*1.1*	7.3	*22.1*
Claw 2 heights									
External primary branch	30	6.3–9.6	*25.6–32.1*	8.7	*28.3*	0.7	*1.4*	9.2	*27.8*
External secondary branch	24	4.9–8.5	*20.4–25.8*	7.2	*23.1*	0.7	*1.4*	7.3	*22.1*
Internal primary branch	29	6.0–9.4	*24.7–30.6*	8.3	*27.0*	0.7	*1.5*	8.8	*26.6*
Internal secondary branch	25	4.3–8.0	*19.0–24.7*	6.7	*21.3*	0.7	*1.5*	6.3	*19.0*
Claw 3 heights									
External primary branch	30	6.6–9.9	*26.0–33.7*	8.8	*28.6*	0.7	*1.7*	9.8	*29.6*
External secondary branch	21	6.4–8.5	*21.1–25.7*	7.3	*22.9*	0.5	*1.1*	8.5	*25.7*
Internal primary branch	30	6.3–9.5	*23.4–32.1*	8.3	*27.1*	0.7	*1.8*	9.5	*28.7*
Internal secondary branch	22	4.5–7.5	*18.3–23.0*	6.6	*21.4*	0.7	*1.2*	7.5	*22.7*
Claw 4 heights									
Anterior primary branch	29	6.8–11.2	*27.7–34.7*	9.6	*31.0*	0.8	*1.6*	11.2	*33.8*
Anterior secondary branch	22	6.4–8.8	*19.7–27.2*	7.6	*24.2*	0.6	*1.7*	8.2	*24.8*
Posterior primary branch	29	7.0–12.3	*28.5–37.2*	10.1	*32.7*	1.0	*2.0*	12.3	*37.2*
Posterior secondary branch	22	5.2–9.7	*22.7–29.3*	7.9	*25.6*	0.9	*1.6*	9.7	*29.3*

the bases of the egg processes, which under SEM correspond to the portions linking the reticulum with the walls of the egg processes (Figs 28–29). Egg processes are of inverted goblet shape, with slightly concave trunks and concave terminal discs (Figs 28–29). Terminal discs are round and strongly serrated to moderately dentate (Figs 28–29). Each terminal disc has a distinct concave central area, which may contain scattered granulation. Granulation is also consistently present on the serrated margins or teeth of the terminal discs (Figs 28–29). Measurements and morphometric statistics of the eggs are provided in Table 9.

Reproduction

The type population of *M. hoianicus* sp. nov. is dioecious. Both males with testes filled with sperm and females with ovaries containing oocytes were observed in specimens freshly mounted in Hoyer's medium.

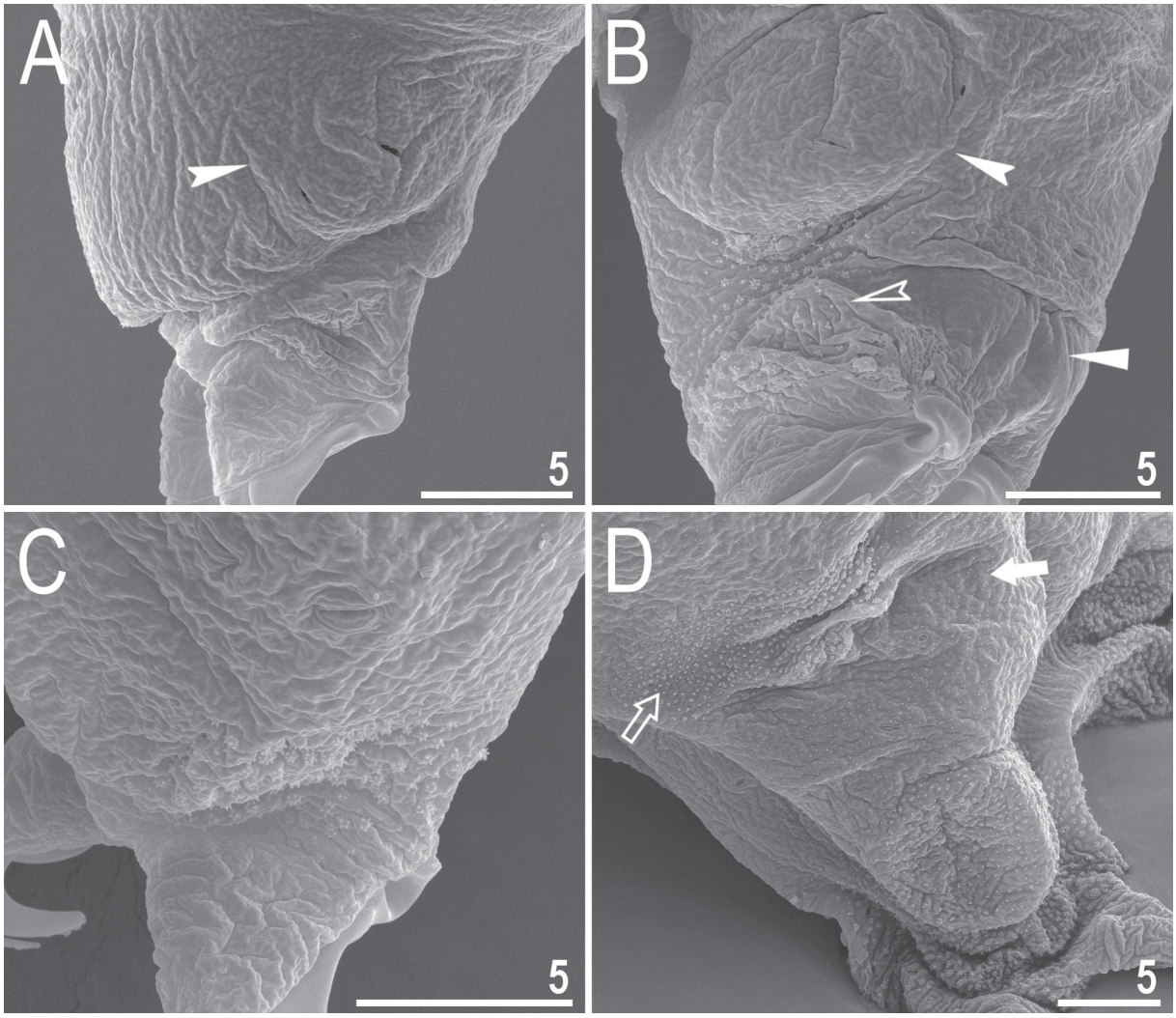

Fig. 25. *Macrobiotus hoianicus* sp. nov., paratypes (ISEA PAS), leg cuticle; SEM. **A**. Internal surface of leg I. **B**. Internal surface of leg III. **C**. Granulation on the external surface of leg II. **D**. Granulation on the hind leg. Filled arrow indicates regular body granulation faintly visible under PCM, empty arrow indicates dense granulation patches on the lateral sides of the caudal body region, filled indented arrowhead indicates a pulvinus-shaped cuticular bulge, empty indented arrowhead indicate a cuticular fold in the distal leg portion, and filled flat arrowhead indicates a divided cuticular bar. Scale bars in μm.

Table 9. Measurements [in μm] of selected morphological structures of the eggs of *Macrobiotus hoianicus* sp. nov.; eggs mounted in Hoyer's medium; process base/height ratio is expressed as percentage; N: number of eggs/structures measured; range: refers to the smallest and the largest structure among all measured specimens; SD: standard deviation.

Character	N	Range	Mean	SD
Egg bare diameter	30	57.0–72.3	65.0	4.1
Egg full diameter	30	64.7–84.2	74.5	4.6
Process height	90	3.1–5.8	4.4	0.6
Process base width	90	2.9–5.2	3.8	0.5
Process base/height ratio	90	63%–111%	88%	11%
Terminal disc width	90	2.1–4.3	3.3	0.5
Inter-process distance	90	1.8–4.5	3.0	0.6
Number of processes on the egg circumference	30	28–32	30.6	1.1

Fig. 26. *Macrobiotus hoianicus* sp. nov., paratypes (ISEA PAS), claws. **A**. Claws II (PCM). **B**. Claws IV (PCM). **C**. Claws I (SEM). **D**. Claws IV (SEM). Filled flat arrowhead indicates faintly visible cuticular bars. Scale bars in μm.

Differential diagnosis

By having (i) patches of dense cuticular granulation on the body in areas other than the legs, (ii) the first band of teeth in the OCA not visible in light microscopy, (iii) eggs with processes of inverted goblet shape bearing terminal discs lacking flexible filaments, and (iv) an egg surface between processes covered by a reticulum, the new species is most similar to only one species of *Macrobiotus*: *Macrobiotus kamilae* Coughlan & Stec, 2019, known so far only from India (Coughlan & Stec 2019). However, the new species differs from *M. kamilae* in several diagnostic characters: (i) the presence of only a single patch of granulation located on the dorso-lateral cuticle of the caudal body region (three distinct

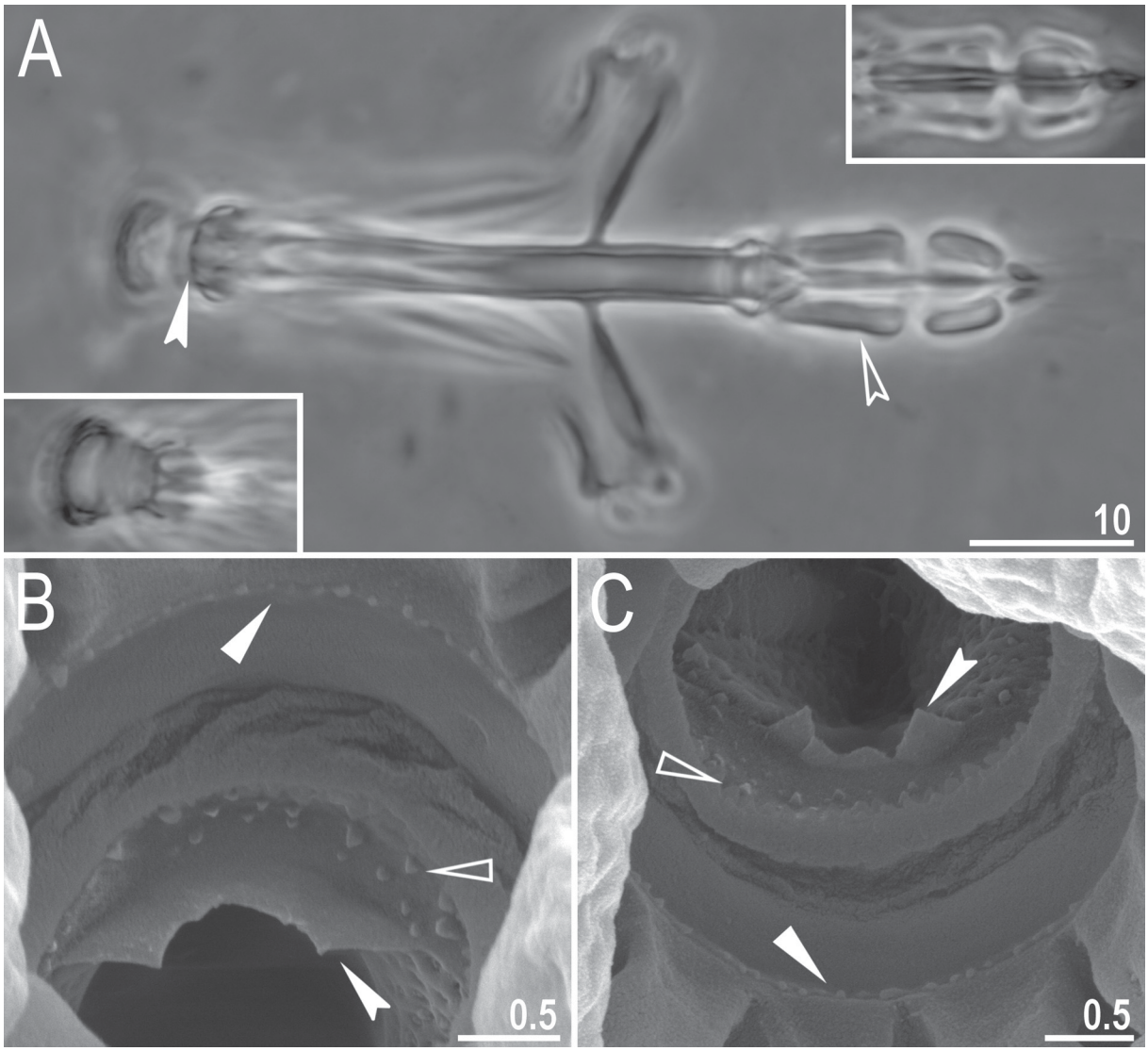

Fig. 27. *Macrobiotus hoianicus* sp. nov. **A**. Holotype (ISEA PAS), buccal apparatus and oral cavity armature; PCM; buccal apparatus in dorsal view. The lower left inset shows the ventral view of the OCA, and the upper right inset shows the placoids in ventral view (holotype, PCM). **B–C**. Paratypes (ISEA PAS), oral cavity armature observed under SEM from different angles, dorsal (B) and ventral (C) views, respectively. Filled flat arrowheads indicate the first band of teeth, empty flat arrowheads indicate the second band of teeth, filled indented arrowheads indicate the third band of teeth, and empty indented arrowhead indicates the central and subterminal constrictions in the first and second macroplacoids, respectively. Scale bars in μm.

granulation patches present on the dorso-lateral cuticle in *M. kamilae*); (ii) the absence of granulation on the internal surface of leg I (granulation present in *M. kamilae*); (iii) the presence of smooth lunulae on the hind legs (lunulae dentate in *M. kamilae*); (iv) a narrower buccal tube (external and internal widths 1.8–3.8 μm and 0.9–2.0 μm in the new species vs 4.1–6.0 μm and 2.4–4.3 μm in *M. kamilae*); (v) a shorter second macroplacoid (1.7–4.6 μm in the new species vs 4.8–8.0 μm in *M. kamilae*); and (vi) a shorter placoid row (7.9–16.8 μm in the new species vs 17.1–26.7 μm in *M. kamilae*).

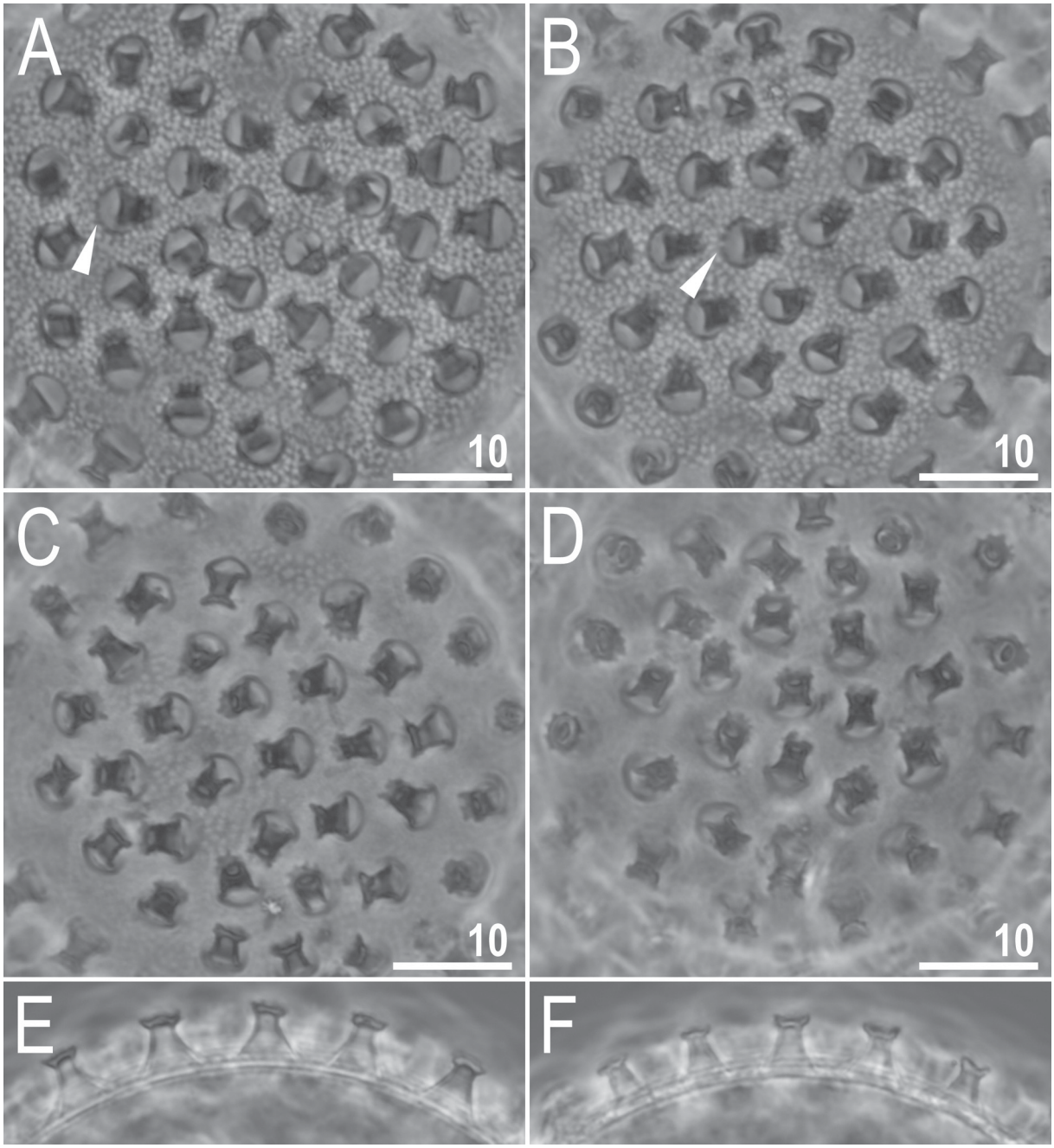

Fig. 28. *Macrobiotus hoianicus* sp. nov., PCM images of the egg at ×1000 magnification. **A–B**. Egg surface focused on the surface between processes. **C–D**. Egg surface focused on egg processes and terminal discs. **E–F**. Midsections of egg processes. Filled flat arrowheads indicate thickenings around the bases of the egg processes. Scale bars in μm; E–F same scale as in A–D.

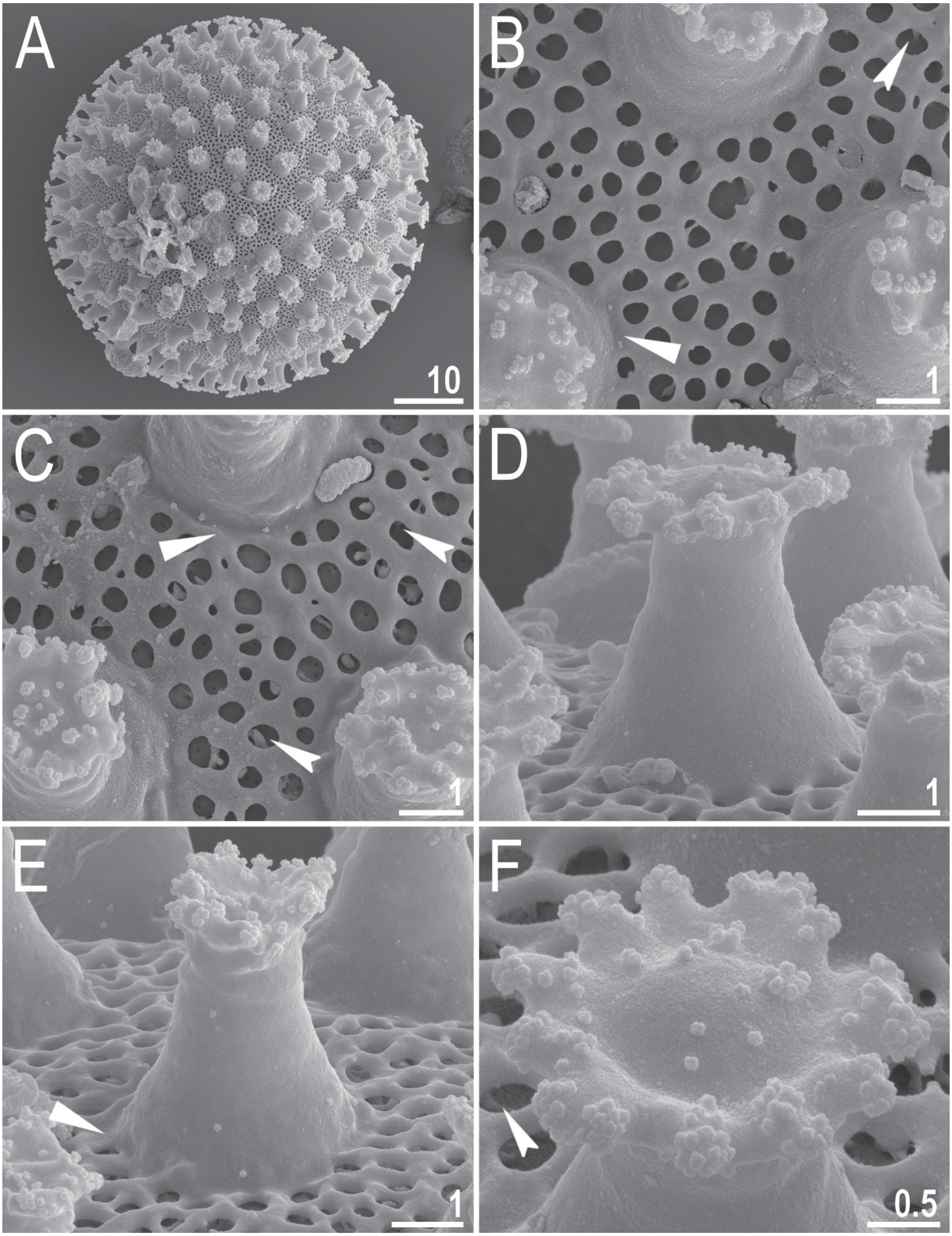

Fig. 29. *Macrobiotus hoianicus* sp. nov., SEM images of the eggs. **A**. Entire egg. **B–F**. Details of egg processes and the surface between them. Filled flat arrowheads indicate thickenings (corresponding to dark thickenings visible under PCM) around the bases of the egg processes, and filled indented arrowheads indicate pillar-like structures connecting the reticulum and egg processes to the egg surface. Scale bars in μm.

Phylogeny

Both Bayesian inference and maximum likelihood analyses produced trees with highly similar topologies and well-supported clades (Fig. 30), reflecting congruent relationships within Macrobiotidae clade I (sensu Stec *et al.* 2021a). All four new species described in this study were recovered within the genus *Macrobiotus* and were consistently placed within *Macrobiotus* clade C (sensu Stec *et al.* 2021a). Within clade C, *M. hoianicus* sp. nov. is recovered as sister to all remaining taxa in the clade. *Macrobiotus witalinskii* sp. nov. forms a clade with *Macrobiotus porifini* Kuzdrowska, Mioduchowska, Gawlak,

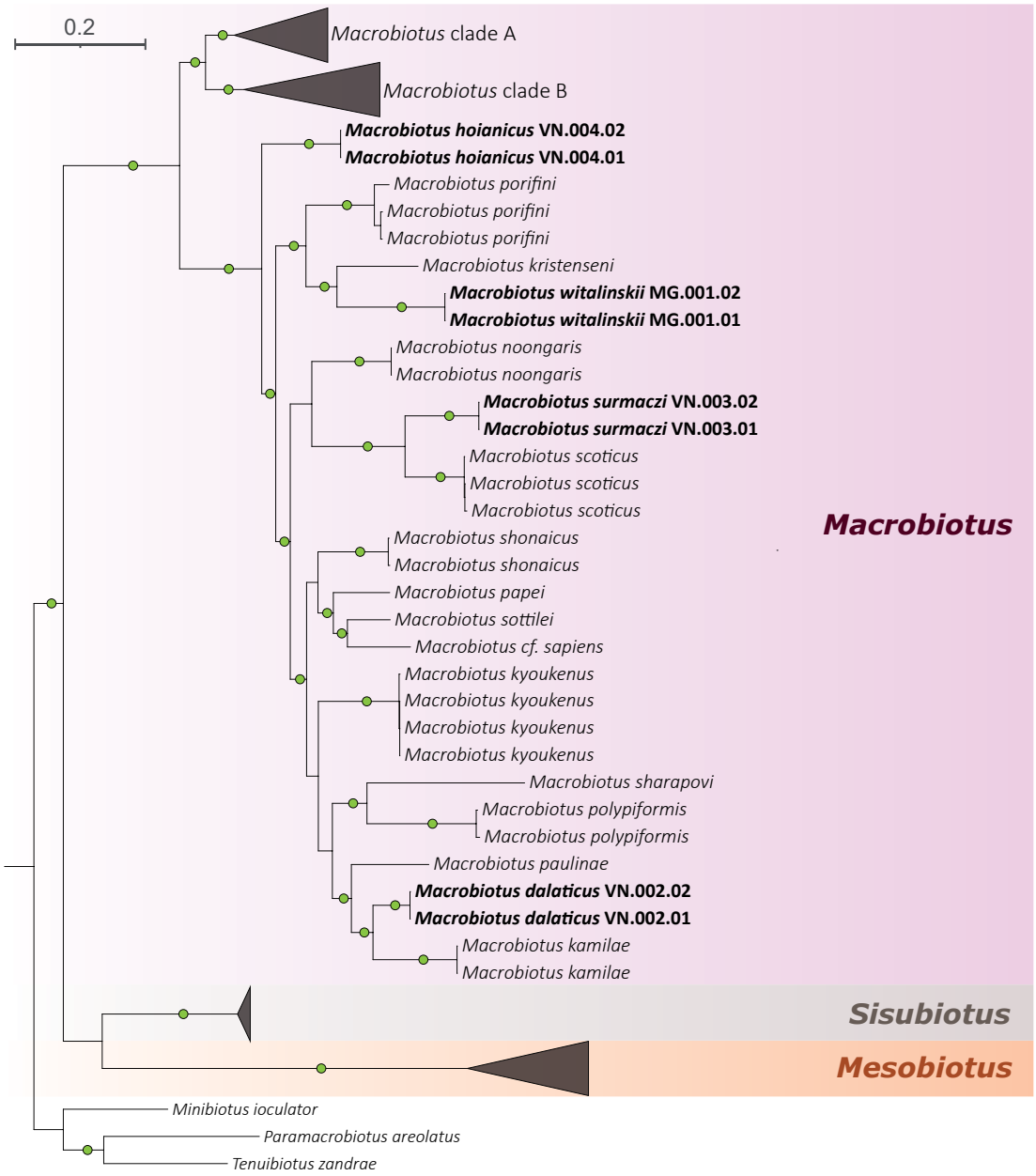

Fig. 30. Bayesian phylogenetic reconstruction of Superclade I within the family Macrobiotidae Thulin, 1928 with detailed between-species relationships showed in full for clade C of *Macrobiotus* C.A.S. Schultze, 1834. Values at nodes represent Bayesian inference posterior probabilities; nodes with support > 0.90 are indicated by green circles at the corresponding branches, whereas support values ≤ 0.90 are not indicated. Newly sequenced taxa are shown in bold. The scale bar represents substitutions per site.

Bartylak, A. Kepel, M. Kepel & Kaczmarek, 2021 and *M. kristenseni*, with *M. kristenseni* being its closest relative. *Macrobiotus surmaczi* sp. nov. clusters with *Macrobiotus noongaris* Coughlan & Stec, 2019 and *Macrobiotus scoticus* Stec, Morek, Gąsiorek, Blagden & Michalczyk, 2017, with *M. scoticus* recovered as its sister species. *Macrobiotus dalaticus* sp. nov. forms a clade with *Macrobiotus paulinae* Stec, Smolak, Kaczmarek & Michalczyk, 2015 and *M. kamilae*, with *M. kamilae* recovered as its sister species. In all analyses, each of the newly described species formed a well-supported, distinct monophyletic lineage, corroborating their delineation as separate species-level taxa (Fig. 30).

Discussion

The present study expands our knowledge of the genus *Macrobiotus* by documenting four novel species-level lineages. Each species is characterized by a detailed morphological and morphometric documentation and is supported by molecular data in the form of DNA sequences from four commonly used genetic markers. These data are therefore valuable not only for resolving the phylogenetic placement of the newly described taxa and understanding evolutionary relationships within the genus, but also for future faunistic and biodiversity inventories, including those employing high-throughput approaches such as DNA barcoding and metabarcoding (Topstad *et al.* 2021; He *et al.* 2024; Surmacz *et al.* 2026).

The phylogenetic analyses conducted herein recovered three well-defined, deeply divergent evolutionary lineages within *Macrobiotus*, a pattern congruent with multiple previous studies (e.g., Massa *et al.* 2021; Stec *et al.* 2021a, 2022; Vincenzi *et al.* 2024; Stec 2024). All taxa described in the present study belong to *Macrobiotus* clade C (sensu Stec *et al.* 2021a). When this group first emerged in earlier studies with limited taxon sampling, it was hypothesized to comprise predominantly yellowish representatives of the *Macrobiotus hufelandi* complex exhibiting modified egg processes, such as flexible filaments or flattened apices (Stec *et al.* 2018b). However, as taxon sampling increased, this pattern was no longer supported, as newly included taxa were often whitish and/or possessed typical inverted goblet-shaped egg processes (Coughlan & Stec 2019). The present study further contributes to this revised view, as *Macrobiotus hoianicus* sp. nov. is also whitish and bears typical inverted goblet-shaped egg processes without apparent modifications.

With respect to geographic distribution, *Macrobiotus* clade C appears to be widely distributed and effectively cosmopolitan, with representatives recorded from South America, Africa, Asia, and Europe (e.g., Roszkowska *et al.* 2017; Stec *et al.* 2018a; Coughlan & Stec 2019; Kiosya *et al.* 2021; Cesari *et al.* 2022). Nevertheless, the distribution ranges of individual species remain poorly understood, as most taxa are currently known only from their type localities (e.g., Roszkowska *et al.* 2017; Stec *et al.* 2018a; Coughlan & Stec 2019; Cesari *et al.* 2022). Notable exceptions include *M. scoticus*, which has been recorded from multiple localities in Denmark and Poland in addition to Scotland (Vecchi *et al.* 2022a; Gąsiorek *et al.* 2024; Surmacz *et al.* 2025b), *Macrobiotus shonaicus* Stec, Arakawa & Michalczyk, 2018, reported from several locations across Japan (Sugiura *et al.* 2020), and *Macrobiotus sottilei* Pilato, Kiosya, Lisi & Sabella, 2012, known from Belarus, Poland, Denmark, and Italy (Pilato *et al.* 2012; Kaczmarek *et al.* 2018a; Kiosya *et al.* 2021; Gąsiorek *et al.* 2024; Surmacz *et al.* 2025b). Importantly, many of these additional records were obtained through extensive DNA barcoding and metabarcoding efforts, highlighting the power of molecular approaches in high-throughput biodiversity assessments, particularly in taxonomically challenging groups of microinvertebrates such as tardigrades.

Acknowledgments

This study was supported by the European Commission's program *Transnational Access to Major Research Infrastructures* through the SYNTHESYS grant (grant no. DK-TAF TA4-005 to DS) and by the Institute of Systematics and Evolution of Animals, Polish Academy of Sciences.

References

Astrin J.J. & Stüben P.E. 2008. Phylogeny in cryptic weevils: molecules, morphology and new genera of western Palaearctic Cryptorhynchinae (Coleoptera : Curculionidae). *Invertebrate Systematics* 22 (5): 503–522. https://doi.org/10.1071/IS07057

Atherton S. 2025. A new species of *Sisubiotus* (Tardigrada: Macrobiotidae) from northern Sweden with a key to the genus. *Zootaxa* 5679 (3): 399–418. https://doi.org/10.11646/zootaxa.5679.3.5

Bertolani R., Rebecchi L., Giovannini I. & Cesari M. 2011. DNA barcoding and integrative taxonomy of *Macrobiotus hufelandi* C.A.S. Schultze 1834, the first tardigrade species to be described, and some related species. *Zootaxa* 2997 (1): 19–36. https://doi.org/10.11646/zootaxa.2997.1.2

Bertolani R., Guidetti R., Marchioro T., Altiero T., Rebecchi L. & Cesari M. 2014. Phylogeny of Eutardigrada: New molecular data and their morphological support lead to the identification of new evolutionary lineages. *Molecular Phylogenetics and Evolution* 76: 110–126. https://doi.org/10.1016/j.ympev.2014.03.006

Bertolani R., Cesari M., Giovannini I., Rebecchi L., Guidetti R., Kaczmarek Ł. & Pilato G. 2023. The *Macrobiotus persimilis–polonicus* complex (Eutardigrada, Macrobiotidae), another example of problematic species identification, with the description of four new species. *Organisms Diversity & Evolution* 23 (2): 329–368. https://doi.org/10.1007/s13127-022-00599-z

Casquet J., Thebaud C. & Gillespie R.G. 2012. Chelex without boiling, a rapid and easy technique to obtain stable amplifiable DNA from small amounts of ethanol-stored spiders. *Molecular Ecology Resources* 12 (1): 136–141. https://doi.org/10.1111/j.1755-0998.2011.03073.x

Castresana J. 2000. Selection of conserved blocks from multiple alignments for their use in phylogenetic analysis. *Molecular Biology and Evolution* 17 (4): 540–552. https://doi.org/10.1093/oxfordjournals.molbev.a026334

Cerretti P., Nania D., Di Marco M., Meier R., Ascenzi A., Evenhuis N. & Pape T. 2025. Declining rates of species description call for improved taxonomic strategies: Insights from a megadiverse insect order. *Systematic Entomology* n/a (n/a): e70019. https://doi.org/10.1111/syen.70019

Cesari M., Giovannini I., Altiero T., Guidetti R., Cornette R., Kikawada T. & Rebecchi L. 2022. Resistance to extreme stresses by a newly discovered Japanese tardigrade species, *Macrobiotus kyoukenus* (Eutardigrada, Macrobiotidae). *Insects* 13 (7): 634. https://doi.org/10.3390/insects13070634

Coughlan K. & Stec D. 2019. Two new species of the *Macrobiotus hufelandi* complex (Tardigrada: Eutardigrada: Macrobiotidae) from Australia and India, with notes on their phylogenetic position. *European Journal of Taxonomy* 573: 1–38. https://doi.org/10.5852/ejt.2019.573

Coughlan K., Michalczyk Ł. & Stec D. 2019. *Macrobiotus caelestis* sp. nov., a new tardigrade species (Macrobiotidae: *hufelandi* group) from the Tien Shan Mountains (Kyrgyzstan). *Annales Zoologici* 69 (3): 499–513. https://doi.org/10.3161/00034541ANZ2019.69.3.002

Cowie R.H., Bouchet P. & Fontaine B. 2022. The Sixth Mass Extinction: fact, fiction or speculation? *Biological Reviews* 97 (2): 640–663. https://doi.org/10.1111/brv.12816

Dastych H. 1993. A new genus and four new species of semiterrestrial water-bears from South Africa (Tardigrada). *Mitteilungen aus dem Hamburgischen Zoologischen Museum und Institut* 90: 175–186.

Degma P. & Guidetti R. 2025. Actual checklist of Tardigrada species. https://doi.org/10.25431/11380_1178608 [accessed 23 Mar. 2026].

Engel M.S., Ceríaco L.M.P., Daniel G.M., Dellapé P.M., Löbl I., Marinov M., Reis R.E., Young M.T., Dubois A., Agarwal I., Lehmann A. P., Alvarado M., Alvarez N., Andreone F., Araujo-Vieira K.,

Ascher J.S., Baêta D., Baldo D., Bandeira S.A., ... & Zacharie C.K. 2021. The taxonomic impediment: a shortage of taxonomists, not the lack of technical approaches. *Zoological Journal of the Linnean Society* 193 (2): 381–387. https://doi.org/10.1093/zoolinnean/zlab072

Erdmann W., Kosicki J.Z., Kayastha P., Mioduchowska M. & Kaczmarek Ł. 2024. An integrative description of *Mesobiotus mandalori* sp. nov. (Eutardigrada, Macrobiotoidea) from Poland. *The European Zoological Journal* 91 (1): 378–394. https://doi.org/10.1080/24750263.2024.2341884

Garey J.R., McInnes S.J. & Nichols P.B. 2008. Global diversity of tardigrades (Tardigrada) in freshwater. *Hydrobiologia* 595 (1): 101–106. https://doi.org/10.1007/s10750-007-9123-0

Gąsiorek P., Sørensen M.V., Lillemark M.R., Leerhøi F. & Tøttrup A.P. 2024. Massive citizen science sampling and integrated taxonomic approach unravel Danish cryptogam-dwelling tardigrade fauna. *Frontiers in Zoology* 21 (1): 27. https://doi.org/10.1186/s12983-024-00547-x

Guidetti R., Schill R.O., Bertolani R., Dandekar T. & Wolf M. 2009. New molecular data for tardigrade phylogeny, with the erection of *Paramacrobiotus* gen. nov. *Journal of Zoological Systematics and Evolutionary Research* 47 (4): 315–321. https://doi.org/10.1111/j.1439-0469.2009.00526.x

Guidetti R., Peluffo J.R., Rocha A.M., Cesari M. & de Peluffo M.C.M. 2013. The morphological and molecular analyses of a new South American urban tardigrade offer new insights on the biological meaning of the *Macrobiotus hufelandi* group of species (Tardigrada: Macrobiotidae). *Journal of Natural History* 47 (37–38): 2409–2426. https://doi.org/10.1080/00222933.2013.800610

Hall T.A. 1999. BioEdit: a user-friendly biological sequence alignment editor and analysis program for Windows 95/98/NT. *Nucleic Acids Symposium Series* 41 (41): 95–98.

Hatfield J.H., Allen B.J., Carroll T., Dean C.D., Deng S., Gordon J.D., Guillerme T., Hansford J.P., Hoyal Cuthill J.F., Mannion P.D., Martins I.S., Payne A.R.D., Shipley A., Thomas C.D., Thompson J.B., Woods L. & Davis K.E. 2025. The greatest extinction event in 66 million years? Contextualising anthropogenic extinctions. *Global Change Biology* 31 (9): e70476. https://doi.org/10.1111/gcb.70476

He Z.-Y., Hu H.-W., Thi Nguyen B.-A., Chen Q.-L., Weatherley A., Nash M., Bi L., Wu K. & He J.-Z. 2024. Distribution of soil tardigrades as revealed by molecular identification across a large-scale area of Australia. *Soil Biology and Biochemistry* 196: 109506. https://doi.org/10.1016/j.soilbio.2024.109506

Hoang D.T., Chernomor O., von Haeseler A., Minh B.Q. & Vinh L.S. 2018. UFBoot2: improving the ultrafast bootstrap approximation. *Molecular Biology and Evolution* 35 (2): 518–522. https://doi.org/10.1093/molbev/msx281

Hulterström J., Guidetti R., Jönsson K.I. & Atherton S. 2025. Integrative taxonomy supports the description of two new species of Macrobiotidae (Tardigrada, Eutardigrada) from Kristianstads Vattenrike Biosphere Reserve in Sweden. *European Journal of Taxonomy* 1030: 1–52. https://doi.org/10.5852/ejt.2025.1030.3135

Itang L.A.M., Stec D., Mapalo M.A., Mirano-Bascos D. & Michalczyk Ł. 2020. An integrative description of *Mesobiotus dilimanensis*, a new tardigrade species from the Philippines (Eutardigrada: Macrobiotidae: *furciger* group). *Raffles Bulletin of Zoology* 68: 19–31. https://doi.org/10.26107/RBZ-2020-0003

Kaczmarek Ł. & Michalczyk Ł. 2017. The *Macrobiotus hufelandi* group (Tardigrada) revisited. *Zootaxa* 4363 (1): 101–123. https://doi.org/10.11646/zootaxa.4363.1.4

Kaczmarek Ł., Cytan J., Zawierucha K., Diduszko D. & Michalczyk Ł. 2014. Tardigrades from Peru (South America), with descriptions of three new species of Parachela. *Zootaxa* 3790 (2): 357–379. https://doi.org/10.11646/zootaxa.3790.2.5

Kaczmarek Ł., Kosicki J.Z. & Roszkowska M. 2018a. Tardigrada of Bory Tucholskie National Park, Zaborski Landscape Park, and their surroundings (Pomerania Province, Poland). *Turkish Journal of Zoology* 42 (1): 6–17. https://doi.org/10.3906/zoo-1705-44

Kaczmarek Ł., Zawierucha K., Buda J., Stec D., Gawlak M., Michalczyk Ł. & Roszkowska M. 2018b. An integrative redescription of the nominal taxon for the *Mesobiotus harmsworthi* group (Tardigrada: Macrobiotidae) leads to descriptions of two new *Mesobiotus* species from Arctic. *PLoS ONE* 13 (10): e0204756. https://doi.org/10.1371/journal.pone.0204756

Kaczmarek Ł., Bartylak T., Stec D., Kulpa A., Kepel M., Kepel A. & Roszkowska M. 2020. Revisiting the genus *Mesobiotus* Vecchi et al., 2016 (Eutardigrada, Macrobiotidae) – remarks, updated dichotomous key and an integrative description of new species from Madagascar. *Zoologischer Anzeiger* 287: 121–146. https://doi.org/10.1016/j.jcz.2020.05.003

Kalyaanamoorthy S., Minh B.Q., Wong T.K.F., von Haeseler A. & Jermiin L.S. 2017. ModelFinder: fast model selection for accurate phylogenetic estimates. *Nature Methods* 14 (6): 587–589. https://doi.org/10.1038/nmeth.4285

Katoh K. & Toh H. 2008. Recent developments in the MAFFT multiple sequence alignment program. *Briefings in Bioinformatics* 9 (4): 286–298. https://doi.org/10.1093/bib/bbn013

Katoh K., Misawa K., Kuma K. & Miyata T. 2002. MAFFT: a novel method for rapid multiple sequence alignment based on fast Fourier transform. *Nucleic Acids Research* 30 (14): 3059–3066. https://doi.org/10.1093/nar/gkf436

Kayastha P., Berdi D., Mioduchowska M., Gawlak M., Łukasiewicz A., Gołdyn B. & Kaczmarek Ł. 2020. Some tardigrades from Nepal (Asia) with integrative description of *Macrobiotus wandae* sp. nov. (Macrobiotidae: *hufelandi* group). *Annales Zoologici* 70 (1): 121–142. https://doi.org/10.3161/00034541ANZ2020.70.1.007

Kayastha P., Roszkowska M., Mioduchowska M., Gawlak M. & Kaczmarek Ł. 2021. Integrative descriptions of two new tardigrade species along with the new record of *Mesobiotus skorackii* Kaczmarek et al., 2018 from Canada. *Diversity* 13 (8): 394. https://doi.org/10.3390/d13080394

Kayastha P., Mioduchowska M., Gawlak M., Sługocki Ł., Araújo R., Silva J.J.G. & Kaczmarek Ł. 2023. Integrative description of *Macrobiotus kosmali* sp. nov. (*hufelandi* group) from the Island of Madeira (Portugal). *The European Zoological Journal* 90 (1): 126–138. https://doi.org/10.1080/24750263.2022.2163312

Kayastha P., Mioduchowska M., Gawlak M., Rutkowski T., Redgate N., Sługocki Ł. & Kaczmarek Ł. 2025. Integrative description of *Macrobiotus anshui* sp. nov. from the Madeira Island and new record of *Macrobiotus dolosus* Bertolani, Cesari, Giovannini, Rebecchi, Guidetti, Kaczmarek and Pilato, 2022 (Macrobiotidae; *persimilis-polonicus* complex) from England. *The European Zoological Journal* 92 (1): 1084–1107. https://doi.org/10.1080/24750263.2025.2553672

Kiosya Y., Pogwizd J., Matsko Y., Vecchi M. & Stec D. 2021. Phylogenetic position of two *Macrobiotus* species with a revisional note on *Macrobiotus sottilei* Pilato, Kiosya, Lisi & Sabella, 2012 (Tardigrada: Eutardigrada: Macrobiotidae). *Zootaxa* 4933 (1): 113–135. https://doi.org/10.11646/zootaxa.4933.1.5

Kumar S., Stecher G., Suleski M., Sanderford M., Sharma S. & Tamura K. 2024. MEGA12: Molecular Evolutionary Genetic Analysis version 12 for adaptive and green computing. *Molecular Biology and Evolution* 41 (12): msae263. https://doi.org/10.1093/molbev/msae263

Kuzdrowska K.A., Mioduchowska M., Gawlak M., Bartylak T., Kepel A., Kepel M. & Kaczmarek Ł. 2021. Integrative description of *Macrobiotus porifini* sp. nov. (Macrobiotidae) from Madagascar and its phylogenetic position within the *hufelandi* group. *The European Zoological Journal* 88 (1): 375–389. https://doi.org/10.1080/24750263.2021.1883752

Lanfear R., Frandsen P.B., Wright A.M., Senfeld T. & Calcott B. 2017. PartitionFinder 2: new methods for selecting partitioned models of evolution for molecular and morphological phylogenetic analyses. *Molecular Biology and Evolution* 34 (3): 772–773. https://doi.org/10.1093/molbev/msw260

Li X., Yang D., Wang L. & Wiens J.J. 2025. The past and future of known biodiversity: Rates, patterns, and projections of new species over time. *Science Advances* 11 (49): eadz3071. https://doi.org/10.1126/sciadv.adz3071

Mapalo M.A., Stec D., Mirano-Bascos D. & Michalczyk Ł. 2016. *Mesobiotus philippinicus* sp. nov., the first limnoterrestrial tardigrade from the Philippines. *Zootaxa* 4126 (3): 411–426. https://doi.org/10.11646/zootaxa.4126.3.6

Mapalo M.A., Stec D., Mirano-Bascos D. & Michalczyk Ł. 2017. An integrative description of a limnoterrestrial tardigrade from the Philippines, *Mesobiotus insanis*, new species (Eutardigrada: Macrobiotidae: *harmsworthi* group). *Raffles Bulletin of Zoology* 65: 440–454.

Marnissi J.B., Cesari M., Rebecchi L. & Bertolani R. 2021. Integrative description of a new Tunisian tardigrade species, *Macrobiotus azzunae* sp. nov. (Eutardigrada, Macrobiotidae, *hufelandi* group). *European Journal of Taxonomy* 758: 122–146. https://doi.org/10.5852/ejt.2021.758.1429

Martínez A., Bonaglia S., Di Domenico M., Fonseca G., Ingels J., Jörger K.M., Laumer C., Leasi F., Zeppilli D., Baldrighi E., Bik H., Cepeda D., Curini-Galletti M., Cutter A.D., dos Santos G., Fattorini S., Frisch D., Gollner S., Jondelius U., ... & Fontaneto D. 2025. Fundamental questions in meiofauna research highlight how small but ubiquitous animals can improve our understanding of Nature. *Communications Biology* 8 (1): 1–17. https://doi.org/10.1038/s42003-025-07888-1

Massa E. & Vecchi M. 2024. Description of *Macrobiotus kathyae* sp. nov. (Parachela: Macrobiotidae) and first records of tardigrades from Indiana (USA). *Zootaxa* 5471 (3): 301–317. https://doi.org/10.11646/zootaxa.5471.3.1

Massa E., Guidetti R., Cesari M., Rebecchi L. & Jönsson K.I. 2021. Tardigrades of Kristianstads Vattenrike Biosphere Reserve with description of four new species from Sweden. *Scientific Reports* 11 (1): 4861. https://doi.org/10.1038/s41598-021-83627-w

McFatter M.M., Meyer H.A. & Hinton J.G. 2007. Nearctic freshwater tardigrades: a review. *Journal of Limnology* 66 (1s): 84. https://doi.org/10.4081/jlimnol.2007.s1.84

Michalczyk Ł. & Kaczmarek Ł. 2013. The Tardigrada Register: a comprehensive online data repository for tardigrade taxonomy. *Journal of Limnology* 72 (s1): e22–e22. https://doi.org/10.4081/jlimnol.2013.s1.e22

Mironov S.V., Dabert J. & Dabert M. 2012. A new feather mite species of the genus *Proctophyllodes* Robin, 1877 (Astigmata: Proctophyllodidae) from the Long-tailed Tit *Aegithalos caudatus* Passeriformes: Aegithalidae)—morphological description with DNA barcode data. *Zootaxa* 3253 (1): 54–61. https://doi.org/10.11646/zootaxa.3253.1.2

Morek W., Stec D., Gąsiorek P., Schill R.O., Kaczmarek Ł. & Michalczyk Ł. 2016. An experimental test of eutardigrade preparation methods for light microscopy. *Zoological Journal of the Linnean Society* 178 (4): 785–793. https://doi.org/10.1111/zoj.12457

Nelson D.R., Fletcher R.A., Guidetti R., Roszkowska M., Grobys D. & Kaczmarek Ł. 2020. Two new species of Tardigrada from moss cushions (*Grimmia* sp.) in a xerothermic habitat in northeast Tennessee (USA, North America), with the first identification of males in the genus *Viridiscus*. *PeerJ* 8: e10251. https://doi.org/10.7717/peerj.10251

Nguyen L.-T., Schmidt H.A., von Haeseler A. & Minh B.Q. 2015. IQ-TREE: a fast and effective stochastic algorithm for estimating maximum-likelihood phylogenies. *Molecular Biology and Evolution* 32 (1): 268–274. https://doi.org/10.1093/molbev/msu300

Nowak B. & Stec D. 2018. An integrative description of *Macrobiotus hannae* sp. nov. (Tardigrada: Eutardigrada: Macrobiotidae: *hufelandi* group) from Poland. *Turkish Journal of Zoology* 42 (3): 269–286. https://doi.org/10.3906/zoo-1712-31

Páll-Gergely B., Krell F.-T., Ábrahám L., Bajomi B., Balog L.E., Boda P., Csuzdi C., Dányi L., Fehér Z., Hornok S., Horváth A., Kóbor P., Koczor S., Kontschán J., Kovács P., Kovács T., Lukátsi M., Majoros G., Murányi D., ... & Móra A. 2024. Identification crisis: a fauna-wide estimate of biodiversity expertise shows massive decline in a Central European country. *Biodiversity and Conservation* 33 (13): 3871–3903. https://doi.org/10.1007/s10531-024-02934-6

Pilato G. 1981. Analisi di nuovi caratteri nello studio degli Eutardigradi. *Animalia* 8: 51–57.

Pilato G. & Binda M.G. 2010. Definition of families, subfamilies, genera and subgenera of the Eutardigrada, and keys to their identification. *Zootaxa* 2404 (1): 1–54. https://doi.org/10.11646/zootaxa.2404.1.1

Pilato G., Kiosya Y., Lisi O. & Sabella G. 2012. New records of Eutardigrada from Belarus with the description of three new species. *Zootaxa* 3179 (1): 39–60. https://doi.org/10.11646/zootaxa.3179.1.2

Polishchuk A., Kayastha P., Młodzianowska D., Michalska M., Gawlak M., Warguła J. & Kaczmarek Ł. 2025. Description of two new species and a new population of *Mesobiotus* cf. *coronatus* from Cotacachi-Cayapas National Park, Ecuador. *PLoS ONE* 20 (6): e0324518. https://doi.org/10.1371/journal.pone.0324518

Rambaut A., Drummond A.J., Xie D., Baele G. & Suchard M.A. 2018. Posterior summarization in bayesian phylogenetics using Tracer 1.7. *Systematic Biology* 67 (5): 901–904. https://doi.org/10.1093/sysbio/syy032

Raposo M.A., Kirwan G.M., Lourenço A.C.C., Sobral G., Bockmann F.A. & Stopiglia R. 2021. On the notions of taxonomic 'impediment', 'gap', 'inflation' and 'anarchy', and their effects on the field of conservation. *Systematics and Biodiversity* 19 (3): 296–311. https://doi.org/10.1080/14772000.2020.1829157

Rocha A., Camarda D., Doma I., Ostertag B., González-Reyes A., Pappalardo A.M. & Lisi O. 2025. *Macrobiotus olgae* sp. nov.: a new urban, limno-terrestrial eutardigrade (Tardigrada, Macrobiotidae) from Argentina. *Organisms Diversity & Evolution* 25 (1): 137–155. https://doi.org/10.1007/s13127-024-00663-w

Ronquist F. & Huelsenbeck J.P. 2003. MrBayes 3: Bayesian phylogenetic inference under mixed models. *Bioinformatics* 19 (12): 1572–1574. https://doi.org/10.1093/bioinformatics/btg180

Roszkowska M., Ostrowska M., Stec D., Janko K. & Kaczmarek Ł. 2017. *Macrobiotus polypiformis* sp. nov., a new tardigrade (Macrobiotidae; *hufelandi* group) from the Ecuadorian Pacific coast, with remarks on the claw abnormalities in eutardigrades. *European Journal of Taxonomy* 327: 1–19. https://doi.org/10.5852/ejt.2017.327

Roszkowska M., Stec D., Gawlak M. & Kaczmarek Ł. 2018. An integrative description of a new tardigrade species *Mesobiotus romani* sp. nov. (Macrobiotidae: *harmsworthi* group) from the Ecuadorian Pacific coast. *Zootaxa* 4450 (5): 550–564. https://doi.org/10.11646/zootaxa.4450.5.2

Saban K.E. & Wiens J.J. 2025. Unpacking the extinction crisis: rates, patterns and causes of recent extinctions in plants and animals. *Proceedings of the Royal Society B: Biological Sciences* 292 (2057): 20251717. https://doi.org/10.1098/rspb.2025.1717

Schill R.O. (ed.) 2018. *Water Bears: The Biology of Tardigrades*. Springer International Publishing, Cham.

Shi H.-T., Liu Y. & Lee T.M. 2025. Are we over-conserving charismatic species? *PLoS Biology* 23 (12): e3003494. https://doi.org/10.1371/journal.pbio.3003494

Short K.A., Sands C.J., McInnes S.J., Pisani D., Stevens M.I. & Convey P. 2022. An ancient, Antarctic-specific species complex: large divergences between multiple Antarctic lineages of the tardigrade genus *Mesobiotus*. *Molecular Phylogenetics and Evolution* 170: 107429. https://doi.org/10.1016/j.ympev.2022.107429

Stec D. 2019. *Mesobiotus datanlanicus* sp. nov., a new tardigrade species (Macrobiotidae: *Mesobiotus harmsworthi* group) from Lâm Đồng Province in Vietnam. *Zootaxa* 4679 (1): 164–180. https://doi.org/10.11646/zootaxa.4679.1.10

Stec D. 2021. Integrative descriptions of two new *Mesobiotus* species (Tardigrada, Eutardigrada, Macrobiotidae) from Vietnam. *Diversity* 13 (11): 605. https://doi.org/10.3390/d13110605

Stec D. 2022a. *Macrobiotus rebecchii* sp. nov.: a new limno-terrestrial and hermaphroditic tardigrade from Kyrgyzstan. *Animals* 12 (21): 2906. https://doi.org/10.3390/ani12212906

Stec D. 2022b. An integrative description of two new *Mesobiotus* species (Tardigrada: Eutardigrada: Macrobiotidae) with updated genus phylogeny. *Zoological Studies* 61: e85. https://doi.org/10.6620/ZS.2022.61-85

Stec D. 2024. Integrative taxonomy supports two new species of *Macrobiotus* (Tardigrada: Eutardigrada: Macrobiotidae) allowing further discussion on the genus phylogeny. *European Journal of Taxonomy* 930: 79–123. https://doi.org/10.5852/ejt.2024.930.2481

Stec D. & Kristensen R.M. 2017. An integrative description of *Mesobiotus ethiopicus* sp. nov. (Tardigrada: Eutardigrada: Parachela: Macrobiotidae: *harmsworthi* group) from the northern Afrotropic region. *Turkish Journal of Zoology* 41 (5): 800–811. https://doi.org/10.3906/zoo-1701-47

Stec D., Smolak R., Kaczmarek Ł. & Michalczyk Ł. 2015. An integrative description of *Macrobiotus paulinae* sp. nov. (Tardigrada: Eutardigrada: Macrobiotidae: *hufelandi* group) from Kenya. *Zootaxa* 4052 (5): 501–526. https://doi.org/10.11646/zootaxa.4052.5.1

Stec D., Gąsiorek P., Morek W., Kosztyła P., Zawierucha K., Michno K., Kaczmarek Ł., Prokop Z.M. & Michalczyk Ł. 2016. Estimating optimal sample size for tardigrade morphometry. *Zoological Journal of the Linnean Society* 178 (4): 776–784. https://doi.org/10.1111/zoj.12404

Stec D., Zawierucha K. & Michalczyk Ł. 2017a. An integrative description of *Ramazzottius subanomalus* (Biserov, 1985 (Tardigrada) from Poland. *Zootaxa* 4300 (3): 403–420. https://doi.org/10.11646/zootaxa.4300.3.4

Stec D., Morek W., Gąsiorek P., Blagden B. & Michalczyk Ł. 2017b. Description of *Macrobiotus scoticus* sp. nov. (Tardigrada: Macrobiotidae: *hufelandi* group) from Scotland by means of integrative taxonomy. *Annales Zoologici* 67 (2): 181–197. https://doi.org/10.3161/00034541ANZ2017.67.2.001

Stec D., Kristensen R.M. & Michalczyk Ł. 2018a. Integrative taxonomy identifies *Macrobiotus papei*, a new tardigrade species of the *Macrobiotus hufelandi* complex (Eutardigrada: Macrobiotidae) from the Udzungwa Mountains National Park (Tanzania). *Zootaxa* 4446 (2): 273–291. https://doi.org/10.11646/zootaxa.4446.2.7

Stec D., Arakawa K. & Michalczyk Ł. 2018b. An integrative description of *Macrobiotus shonaicus* sp. nov. (Tardigrada: Macrobiotidae) from Japan with notes on its phylogenetic position within the *hufelandi* group. *PLoS ONE* 13 (2): e0192210. https://doi.org/10.1371/journal.pone.0192210

Stec D., Morek W., Gąsiorek P. & Michalczyk Ł. 2018c. Unmasking hidden species diversity within the *Ramazzottius oberhaeuseri* complex, with an integrative redescription of the nominal species for the family Ramazzottiidae (Tardigrada: Eutardigrada: Parachela). *Systematics and Biodiversity* 16 (4): 357–376. https://doi.org/10.1080/14772000.2018.1424267

Stec D., Krzywański Ł. & Michalczyk Ł. 2018d. Integrative description of *Macrobiotus canaricus* sp. nov. with notes on *M. recens* (Eutardigrada: Macrobiotidae). *European Journal of Taxonomy* 452: 1–36. https://doi.org/10.5852/ejt.2018.452

Stec D., Roszkowska M., Kaczmarek Ł. & Michalczyk Ł. 2018e. An integrative description of a population of *Mesobiotus radiatus* (Pilato, Binda & Catanzaro, 1991) from Kenya. *Turkish Journal of Zoology* 42 (5): 523–540. https://doi.org/10.3906/zoo-1802-43

Stec D., Kristensen R.M. & Michalczyk Ł. 2020a. An integrative description of *Minibiotus ioculator* sp. nov. from the Republic of South Africa with notes on *Minibiotus pentannulatus* Londoño *et al*., 2017 (Tardigrada: Macrobiotidae). *Zoologischer Anzeiger* 286: 117–134. https://doi.org/10.1016/j.jcz.2020.03.007

Stec D., Krzywański Ł., Zawierucha K. & Michalczyk Ł. 2020b. Untangling systematics of the *Paramacrobiotus areolatus* species complex by an integrative redescription of the nominal species for the group, with multilocus phylogeny and species delineation in the genus *Paramacrobiotus*. *Zoological Journal of the Linnean Society* 188 (3): 694–716. https://doi.org/10.1093/zoolinnean/zlz163

Stec D., Tumanov D.T. & Kristensen R.M. 2020c. Integrative taxonomy identifies two new tardigrade species (Eutardigrada: Macrobiotidae) from Greenland. *European Journal of Taxonomy* (614): 1–40. https://doi.org/10.5852/ejt.2020.614

Stec D., Dudziak M. & Michalczyk Ł. 2020d. Integrative descriptions of two new Macrobiotidae species (Tardigrada: Eutardigrada: Macrobiotoidea) from French Guiana and Malaysian Borneo. *Zoological Studies* 59: e23. https://doi.org/10.6620/ZS.2020.59-23

Stec D., Vecchi M., Calhim S. & Michalczyk Ł. 2021a. New multilocus phylogeny reorganises the family Macrobiotidae (Eutardigrada) and unveils complex morphological evolution of the *Macrobiotus hufelandi* group. *Molecular Phylogenetics and Evolution* 160: 106987. https://doi.org/10.1016/j.ympev.2020.106987

Stec D., Vecchi M., Dudziak M., Bartels P.J., Calhim S. & Michalczyk Ł. 2021b. Integrative taxonomy resolves species identities within the *Macrobiotus pallarii* complex (Eutardigrada: Macrobiotidae). *Zoological Letters* 7 (1): 9. https://doi.org/10.1186/s40851-021-00176-w

Stec D., Vončina K., Møbjerg Kristensen R. & Michalczyk Ł. 2022. The *Macrobiotus ariekammensis* species complex provides evidence for parallel evolution of claw elongation in macrobiotid tardigrades. *Zoological Journal of the Linnean Society* 195 (4): 1067–1099. https://doi.org/10.1093/zoolinnean/zlab101

Sugiura K., Arakawa K. & Matsumoto M. 2020. Distribution of *Macrobiotus shonaicus* Stec, Arakawa & Michalczyk, 2018 (Tardigrada: Eutardigrada: Macrobiotidae) in Japan. *Zootaxa* 4767 (1): 56–70. https://doi.org/10.11646/zootaxa.4767.1.2

Surmacz B., Budzik K., Matsko Y. & Stec D. 2025a. Human impact on microinvertebrate diversity and distributions: questioning the resilience of tardigrades. *Global Ecology and Biogeography* 34 (12): e70167. https://doi.org/10.1111/geb.70167

Surmacz B., Fontaneto D., Vončina G. & Stec D. 2025b. Deciphering the patterns and drivers of tardigrade diversity along altitudinal gradients. *Molecular Ecology* 34 (24): e70196. https://doi.org/10.1111/mec.70196

Surmacz B., Vecchi M., Fontaneto D., Budzik K., Godziek J., Matsko Y. & Stec D. 2026. COI metabarcoding with a curated reference database and optimized protocol provides a reliable species-level diversity assessment of tardigrades. *Integrative Zoology* 21 (2): 275–290. https://doi.org/10.1111/1749-4877.12972

Topstad L., Guidetti R., Majaneva M. & Ekrem T. 2021. Multi-marker DNA metabarcoding reflects tardigrade diversity in different habitats. *Genome* 64 (3): 217–231. https://doi.org/10.1139/gen-2019-0218

Trifinopoulos J., Nguyen L.-T., von Haeseler A. & Minh B.Q. 2016. W-IQ-TREE: a fast online phylogenetic tool for maximum likelihood analysis. *Nucleic Acids Research* 44 (W1): W232–W235. https://doi.org/10.1093/nar/gkw256

Tumanov D.V. 2020. Integrative description of *Mesobiotus anastasiae* sp. nov. (Eutardigrada, Macrobiotoidea) and first record of *Lobohalacarus* (Chelicerata, Trombidiformes) from the Republic of South Africa. *European Journal of Taxonomy* 726: 102–131. https://doi.org/10.5852/ejt.2020.726.1179

Tumanov D.V., Androsova E.D., Gavrilenko M.D. & Kalimullin A.A. 2024. Integrative description of two new species of the genus *Mesobiotus* (Eutardigrada, Macrobiotoidea) from Russia, with an updated phylogeny of the genus. *European Journal of Taxonomy* 947: 20–52. https://doi.org/10.5852/ejt.2024.947.2619

Vaidya G., Lohman D.J. & Meier R. 2011. SequenceMatrix: concatenation software for the fast assembly of multi-gene datasets with character set and codon information. *Cladistics* 27 (2): 171–180. https://doi.org/10.1111/j.1096-0031.2010.00329.x

Vecchi M. & Stec D. 2021. Integrative descriptions of two new *Macrobiotus* species (Tardigrada, Eutardigrada, Macrobiotidae) from Mississippi (USA) and Crete (Greece). *Zoosystematics and Evolution* 97 (1): 281–306. https://doi.org/10.3897/zse.97.65280

Vecchi M., Cesari M., Bertolani R., Jönsson K.I., Rebecchi L. & Guidetti R. 2016. Integrative systematic studies on tardigrades from Antarctica identify new genera and new species within Macrobiotoidea and Echiniscoidea. *Invertebrate Systematics* 30 (4): 303–322. https://doi.org/10.1071/IS15033

Vecchi M., Stec D., Vuori T., Ryndov S., Chartrain J. & Calhim S. 2022a. *Macrobiotus naginae* sp. nov., a new xerophilous tardigrade species from Rokua sand dunes (Finland). *Zoological Studies* 61: e22. https://doi.org/10.6620/ZS.2022.61-22

Vecchi M., Choong H. & Calhim S. 2022b. *Sisubiotus hakaiensis* sp. nov. (Tardigrada, Macrobiotidae), a new tardigrade species from Calvert Island (British Columbia, Canada). *European Journal of Taxonomy* 823: 64–81. https://doi.org/10.5852/ejt.2022.823.1815

Vecchi M., McDaniel J.L., Chartrain J., Vuori T., Walsh E.J. & Calhim S. 2023. Morphology, phylogenetic position, and mating behaviour of a new *Mesobiotus* (Tardigrada) species from a rock pool in the Socorro Box Canyon (New Mexico, USA). *The European Zoological Journal* 90 (2): 708–725. https://doi.org/10.1080/24750263.2023.2263033

Vecchi M., Dykyy I., Khoyetskyy P., Vuori T., Calhim S. & Trokhymets V. 2024. The tardigrade *Mesobiotus aradasi* (Binda, Pilato & Lisi, 2005) is widely distributed along the Antarctic Peninsula. *Polar Biology* 47 (3): 227–238. https://doi.org/10.1007/s00300-023-03222-9

Vincenzi J., Cesari M., Kaczmarek Ł., Roszkowska M., Mioduchowska M., Rebecchi L., Kiosya Y. & Guidetti R. 2024. The xerophilic genera *Xerobiotus* and *Pseudohexapodibius* (Macrobiotidae; Tardigrada): biodiversity, biogeography and phylogeny. *Zoological Journal of the Linnean Society* 200 (1): 111–141. https://doi.org/10.1093/zoolinnean/zlad129

Yuan Z., Wang Y., Liu Q., Liu L. & Li X. 2022. *Macrobiotus hupingensis*, a new tardigrade species in the *Macrobiotus pallarii* complex from China. *Zoological Studies* 61: e86. https://doi.org/10.6620/ZS.2022.61-86

Printed versions of all papers are deposited in the libraries of two of the institutes that are members of the *EJT* consortium: Muséum national d'Histoire naturelle, Paris, France and Royal Museum for Central Africa, Tervuren, Belgium. The other members of the consortium are: Royal Belgian Institute of Natural Sciences, Brussels, Belgium; Meise Botanic Garden, Meise, Belgium; Natural History Museum of Denmark, Copenhagen, Denmark; Naturalis Biodiversity Center, Leiden, the Netherlands; Museo Nacional de Ciencias Naturales-CSIC, Madrid, Spain; Leibniz Institute for the Analysis of Biodiversity Change, Bonn – Hamburg, Germany; National Museum of the Czech Republic, Prague, Czech Republic; The Steinhardt Museum of Natural History, Tel Aviv, Israël.

Supplementary files

Supp. file 1. Raw morphometric data underling the description of *Macrobiotus witalinskii* sp. nov.
https://doi.org/10.5852/ejt.2026.1055.3277.14466

Supp. file 2. Raw morphometric data underling the description of *Macrobiotus dalaticus* sp. nov.
https://doi.org/10.5852/ejt.2026.1055.3277.14467

Supp. file 3. Raw morphometric data underling the description of *Macrobiotus surmaczi* sp. nov.
https://doi.org/10.5852/ejt.2026.1055.3277.14468

Supp. file 4. Raw morphometric data underling the description of *Macrobiotus hoianicus* sp. nov.
https://doi.org/10.5852/ejt.2026.1055.3277.14469

Supp. file 5. Model selections of sequence evolution for BI and ML analyses and raw trees.
https://doi.org/10.5852/ejt.2026.1055.3277.14470

Appendix 1 (continued on next five pages). Sequences used for phylogenetic analyses. Sequences obtained in this study are indicated in bold, and asterisks denotes *Macrobiotus* C.A.S. Schultze, 1834 sequences that was misidentified by previous authors, as noted by (Stec 2024). Shaded rows at the end of the table indicate outgroup taxa.

Species	18S	28S	ITS-2	COI	Source
***Macrobiotus witalinskii* MG.001.01**	**PX789912**	**PX789920**	**PX789928**	**PX794742**	**This study**
***Macrobiotus witalinskii* MG.001.02**	**PX789913**	**PX789921**	**PX789929**	**PX794743**	**This study**
***Macrobiotus hoianicus* VN.004.01**	**PX789914**	**PX789922**	**PX789930**	**PX794744**	**This study**
***Macrobiotus hoianicus* VN.004.02**	**PX789915**	**PX789923**	**PX789931**	**PX794745**	**This study**
***Macrobiotus surmaczi* VN.003.01**	**PX789916**	**PX789925**	**PX789932**	**PX794746**	**This study**
***Macrobiotus surmaczi* VN.003.02**	**PX789917**	**PX789924**	**PX789933**	**PX794747**	**This study**
***Macrobiotus dalaticus* VN.002.01**	**PX789918**	**PX789927**	**PX789934**	**PX794748**	**This study**
***Macrobiotus dalaticus* VN.002.02**	**PX789919**	**PX789926**	**PX789935**	**PX794749**	**This study**
Macrobiotus vattenrikense	PX093663		PX093644	PX093655	Hulterström *et al.* 2025
Macrobiotus anshui	OQ525805	OQ526003		OQ525803	Kayastha *et al.* 2025
Macrobiotus sharapovi	PV283176	PV283177	PV283179	PV282532	Polishchuk *et al.* 2025
Macrobiotus olgae 1			PQ461834	PQ276069	Rocha *et al.* 2025
Macrobiotus olgae 2			PQ461835	PQ276070	Rocha *et al.* 2025
Macrobiotus kathyae 1	PP391285	PP391287	PP391289	PP386934	Massa & Vecchi 2024
Macrobiotus kathyae 2	PP391286	PP391288	PP391290	PP386935	Massa & Vecchi 2024
Macrobiotus ovovittatus GL.001.01	OR543310	OR543318	OR543314	OR544395	Stec 2024
Macrobiotus ovovittatus GL.001.02	OR543311	OR543319	OR543315	OR544396	Stec 2024
Macrobiotus mileri IL.001.01	OR543312	OR543320	OR543316	OR544397	Stec 2024
Macrobiotus mileri IL.001.02	OR543313	OR543321	OR543317	OR544398	Stec 2024
Macrobiotus mileri IL.001.03				OR544399	Stec 2024
Macrobiotus mileri IL.001.04				OR544400	Stec 2024
Macrobiotus kosmali M8.1	OP142472	OP143765	OP153786	OP141639	Kayastha *et al.* 2023
Macrobiotus kosmali M8.2	OP142473	OP143766		OP141640	Kayastha *et al.* 2023
*Macrobiotus hupingensis**	MW183923	MZ470349	MZ474842	MW186952	Yuan *et al.* 2022
Macrobiotus dolosus C3209_2	OP596290			OP561772	Bertolani *et al.* 2023
Macrobiotus dolosus C3209_US2				OP561773	Bertolani *et al.* 2023
Macrobiotus dolosus C3209_4				OP561774	Bertolani *et al.* 2023
Macrobiotus dolosus C3581_V6	OP596292			OP561775	Bertolani *et al.* 2023
Macrobiotus dolosus C3209_1	OP596289				Bertolani *et al.* 2023
Macrobiotus dolosus C3581_V5	OP596291				Bertolani *et al.* 2023
Macrobiotus sidereus C2796_2	OP596293			OP561776	Bertolani *et al.* 2023
Macrobiotus sidereus C3282_UFK				OP561777	Bertolani *et al.* 2023

Appendix 1 (continued). Sequences used for phylogenetic analyses. Sequences obtained in this study are indicated in bold, and asterisks denotes *Macrobiotus* C.A.S. Schultze, 1834 sequences that was misidentified by previous authors, as noted by (Stec 2024). Shaded rows at the end of the table indicate outgroup taxa.

Species	18S	28S	ITS-2	COI	Source
Macrobiotus sidereus C3282_UFL				OP561778	Bertolani *et al.* 2023
Macrobiotus sidereus C3282_UFM				OP561779	Bertolani *et al.* 2023
Macrobiotus sidereus C3282_UFN	OP596294			OP561780	Bertolani *et al.* 2023
Macrobiotus sidereus C3282_UFO				OP561781	Bertolani *et al.* 2023
Macrobiotus sidereus C3282_UFP				OP561782	Bertolani *et al.* 2023
Macrobiotus fonturai C2861_5	OP596295			OP561783	Bertolani *et al.* 2023
Macrobiotus fonturai C2861_US1	OP596296			OP561784	Bertolani *et al.* 2023
Macrobiotus muralis C2861_FG	OP596297				Bertolani *et al.* 2023
Macrobiotus muralis C2861_6	OP596298				Bertolani *et al.* 2023
Macrobiotus cf. *muralis* C3251_2	OP596299			OP561785	Bertolani *et al.* 2023
Macrobiotus cf. *muralis* C3251_3	OP596300			OP561786	Bertolani *et al.* 2023
Macrobiotus cf. *muralis* C3251_FA	OP596301			OP561787	Bertolani *et al.* 2023
Macrobiotus cf. *muralis* C3251_4				OP561788	Bertolani *et al.* 2023
Macrobiotus cf. *muralis* C3251_5				OP561789	Bertolani *et al.* 2023
Macrobiotus hufelandi C2953_A02	OP596302			HQ876586	Bertolani *et al.* 2011, 2023
Macrobiotus cf. *hufelandi* C2959_A01	OP596303			HQ876590	Bertolani *et al.* 2011, 2023
Macrobiotus cf. *hufelandi* C2959_A02	OP596304			HQ876591	Bertolani *et al.* 2011, 2023
Macrobiotus vladimiri C2688_A02	OP596305			HM136932	Bertolani *et al.* 2011, 2023
Macrobiotus terminalis C2868_N02	OP596308			JN673959	Bertolani *et al.* 2011, 2023
Macrobiotus cf. *nelsonae* 1	HQ604965				Bertolani *et al.* 2014
Macrobiotus cf. *nelsonae* 2	HQ604966				Bertolani *et al.* 2014
Macrobiotus rebecchii 1	OP479887			OP477442	Stec 2022a
Macrobiotus rebecchii 2	OP479888			OP477443	Stec 2022a
Macrobiotus kyoukenus v3	ON818312		ON818300	ON809461	Cesari *et al.* 2022
Macrobiotus kyoukenus us3	ON818314		ON818301	ON809462	Cesari *et al.* 2022
Macrobiotus kyoukenus us4	ON818315		ON818302	ON809463	Cesari *et al.* 2022
Macrobiotus kyoukenus us5	ON818316		ON818303	ON809464	Cesari *et al.* 2022
Macrobiotus scoticus DK.056.01	OK663218	OK663207	OK662989	OK663228	Vecchi *et al.* 2022a

Appendix 1 (continued). Sequences used for phylogenetic analyses. Sequences obtained in this study are indicated in bold, and asterisks denotes *Macrobiotus* C.A.S. Schultze, 1834 sequences that was misidentified by previous authors, as noted by (Stec 2024). Shaded rows at the end of the table indicate outgroup taxa.

Species	18S	28S	ITS-2	COI	Source
Macrobiotus scoticus DK.056.02	OK663217	OK663206	OK662988	OK663229	Vecchi *et al.* 2022a
Macrobiotus naginae S226_1	OK663219	OK663230	OK663209	OK662990	Vecchi *et al.* 2022a
Macrobiotus naginae S226_2	OK663220	OK663231	OK663208	OK662991	Vecchi *et al.* 2022a
Macrobiotus naginae S605_1	OK663221	OK663232	OK663210	OK662992	Vecchi *et al.* 2022a
Macrobiotus naginae S605_2	OK663222	OK663233	OK663211	OK662993	Vecchi *et al.* 2022a
Macrobiotus sandrae S859_1	OK663223	OK663234	OK663212	OK662994	Vecchi *et al.* 2022a
Macrobiotus cf. *sapiens*	OK663226	OK663237	OK663215	OK662997	Vecchi *et al.* 2022a
Macrobiotus sandrae 1	MW695445			HQ876573	Bertolani *et al.* 2011; Marnissi *et al.* 2021
Macrobiotus sandrae 2	MW695446			HQ876577	Bertolani *et al.* 2011; Marnissi *et al.* 2021
Macrobiotus azzunae 1	MW695447		MW695454	MW698697	Marnissi *et al.* 2021
Macrobiotus azzunae 2	MW695448		MW695455	MW698698	Marnissi *et al.* 2021
Macrobiotus birendrai	MW680641	MW680644	MW680418	MW656266	Kayastha *et al.* 2021
Macrobiotus a. *groenlandicus* 1	MZ463664	MZ463679	MZ463654	MZ461006	Stec *et al.* 2022
Macrobiotus a. *groenlandicus* 2	MZ463663	MZ463678	MZ463655	MZ461007	Stec *et al.* 2022
Macrobiotus a. *groenlandicus* 3	MZ463662	MZ463677	MZ463653	MZ461005	Stec *et al.* 2022
Macrobiotus kirghizicus 1	MZ463666	MZ463672	MZ463659	MZ461002	Stec *et al.* 2022
Macrobiotus kirghizicus 2	MZ463665	MZ463671	MZ463660	MZ461003	Stec *et al.* 2022
Macrobiotus kirghizicus 3	MZ463667	MZ463673	MZ463661	MZ461004	Stec *et al.* 2022
Macrobiotus a. *ariekammensis* 1	MZ463668	MZ463674	MZ463656	MZ460999	Stec *et al.* 2022
Macrobiotus a. *ariekammensis* 2	MZ463669	MZ463675	MZ463657	MZ461000	Stec *et al.* 2022
Macrobiotus a. *ariekammensis* 3	MZ463670	MZ463676	MZ463658	MZ461001	Stec *et al.* 2022
Macrobiotus aff. *pseudohufelandi* PL	MN888373	MN888358	MN888345	MN888325	Stec *et al.* 2021a
Macrobiotus aff. *pseudohufelandi* ZA	MN888374	MN888359	MN888345	MN888326	Stec *et al.* 2021a
Macrobiotus annewintersae 1	MW588024	MW588030	MW588019	MW593927	Vecchi & Stec 2021
Macrobiotus annewintersae 2	MW588025	MW588031	MW588018	MW593928	Vecchi & Stec 2021
Macrobiotus basiatus	MT498094	MT488397	MT505165	MT502116	Nelson *et al.* 2020
Macrobiotus caelestis	MK737073	MK737071	MK737072	MK737922	Coughlan *et al.* 2019
Macrobiotus canaricus 1	MH063925	MH063934	MH063928	MH057765	Stec *et al.* 2018d
Macrobiotus canaricus 2			MH063929	MH057766	Stec *et al.* 2018d
Macrobiotus cf. *polonicus* 1	MW588026	MW588032	MW588021	MW593929	Vecchi & Stec 2021
Macrobiotus cf. *polonicus* 2	MW588027	MW588033	MW588020	MW593930	Vecchi & Stec 2021
Macrobiotus cf. *recens* 1	MH063927	MH063936	MH063932	MH057768	Stec *et al.* 2018d
Macrobiotus cf. *recens* 2			MH063933	MH057769	Stec *et al.* 2018d
Macrobiotus crustulus	MT261912	MT261903	MT261907	MT260371	Stec *et al.* 2020d
Macrobiotus engbergi 1	MN443039	MN443034	MN443036	MN444824	Stec *et al.* 2020c
Macrobiotus engbergi 2			MN443037	MN444825	Stec *et al.* 2020c
Macrobiotus engbergi 3				MN444826	Stec *et al.* 2020c

Appendix 1 (continued). Sequences used for phylogenetic analyses. Sequences obtained in this study are indicated in bold, and asterisks denotes *Macrobiotus* C.A.S. Schultze, 1834 sequences that was misidentified by previous authors, as noted by (Stec 2024). Shaded rows at the end of the table indicate outgroup taxa.

Species	18S	28S	ITS-2	COI	Source
Macrobiotus glebkai	MW247177	MW247176	MW247180	MW246134	Kiosya *et al.* 2021
Macrobiotus hannae	MH063922	MH063924	MH063923	MH057764	Nowak & Stec 2018
Macrobiotus kamilae 1	MK737070	MK737064	MK737067	MK737920	Coughlan & Stec 2019
Macrobiotus kamilae 2				MK737921	Coughlan & Stec 2019
Macrobiotus kristenseni	KC193577			KC193573	Guidetti *et al.* 2013
Macrobiotus macrocalix	MH063926	MH063935	MH063931	MH057767	Stec *et al.* 2018d
Macrobiotus noongaris 1	MK737069	MK737063	MK737065	MK737919	Coughlan & Stec 2019
Macrobiotus noongaris 2			MK737066		Coughlan & Stec 2019
Macrobiotus papei	MH063881	MH063880	MH063921	MH057763	Stec *et al.* 2018a
Macrobiotus paulinae	KT935502	KT935501	KT935500	KT951668	Stec *et al.* 2015
Macrobiotus polonicus AT 1	MN888369	MN888355	MN888337	MN888317	Stec *et al.* 2021a
Macrobiotus polonicus AT 2			MN888338	MN888318	Stec *et al.* 2021a
Macrobiotus polonicus AT 3				MN888319	Stec *et al.* 2021a
Macrobiotus polonicus SK 1	MN888370	MN888356	MN888332	MN888320	Stec *et al.* 2021a
Macrobiotus polonicus SK 2			MN888333	MN888321	Stec *et al.* 2021a
Macrobiotus polonicus SK 3			MN888334		Stec *et al.* 2021a
Macrobiotus porifini 1	MT241900	MT241897		MT246659	Kuzdrowska *et al.* 2021
Macrobiotus porifini 2		MT241898		MT246660	Kuzdrowska *et al.* 2021
Macrobiotus porifini 3		MT241899		MT246661	Kuzdrowska *et al.* 2021
Macrobiotus polypiformis 1	KX810008	KX810009	KX810010	KX810011	Roszkowska *et al.* 2017
Macrobiotus polypiformis 2				KX810012	Roszkowska *et al.* 2017
Macrobiotus pseudohufelandi 1	HQ604989			AY598776	Bertolani *et al.* 2014
Macrobiotus pseudohufelandi 2	HQ604990			AY598777	Bertolani *et al.* 2014
Macrobiotus rybaki 1	MW588029	MW588034	MW588022	MW593931	Vecchi & Stec 2021
Macrobiotus rybaki 2	MW588028	MW588035	MW588023	MW593932	Vecchi & Stec 2021
Macrobiotus scoticus	KY797265	KY797266	KY797268	KY797267	Stec *et al.* 2017b
Macrobiotus shonaicus 1	MG757132	MG757133	MG757134	MG757136	Stec *et al.* 2018b
Macrobiotus shonaicus 2			MG757135	MG757137	Stec *et al.* 2018b
Macrobiotus sottilei	MW247178	MW247175	MW247179	MW246133	Kiosya *et al.* 2021
Macrobiotus vladimiri FI	MN888375	MN888360	MN888347	MN888327	Stec *et al.* 2021a
Macrobiotus wandae	MN435112	MN435116	MN435120	MN482684	Kayastha *et al.* 2020
Macrobiotus pallarii 1	MT809069	MT809081	MT809094	MT807924	Stec *et al.* 2021b
Macrobiotus pallarii 2	MT809070	MT809082	MT809095	MT807925	Stec *et al.* 2021b
Macrobiotus pallarii 3	MT809071	MT809083	MT809096	MT807926	Stec *et al.* 2021b
Macrobiotus pseudopallarii 1	MT809067	MT809079	MT809091	MT807921	Stec *et al.* 2021b
Macrobiotus pseudopallarii 2	MT809068	MT809080	MT809092	MT807922	Stec *et al.* 2021b
Macrobiotus ripperi FI	MT809076	MT809089	MT809103	MT807930	Stec *et al.* 2021b
Macrobiotus ripperi PL	MT809074	MT809086	MT809100	MT807933	Stec *et al.* 2021b
Macrobiotus margoae US	MT809072	MT809084	MT809098	MT807927	Stec *et al.* 2021b
Macrobiotus gretae 1	MW588434		MW588431	MW581665	Massa *et al.* 2021

Appendix 1 (continued). Sequences used for phylogenetic analyses. Sequences obtained in this study are indicated in bold, and asterisks denotes *Macrobiotus* C.A.S. Schultze, 1834 sequences that was misidentified by previous authors, as noted by (Stec 2024). Shaded rows at the end of the table indicate outgroup taxa.

Species	18S	28S	ITS-2	COI	Source
Macrobiotus gretae 2	MW588437		MW588433	MW581668	Massa *et al.* 2021
Macrobiotus gretae 3	MW588435		MW588432	MW581666	Massa *et al.* 2021
Macrobiotus gretae 4	MW588436			MW581667	Massa *et al.* 2021
Sisubiotus hakaiensis 1	OM523054	OM523059	OM523057	OM523181	Vecchi *et al.* 2022b
Sisubiotus hakaiensis 2	OM523055	OM523060	OM523058	OM523182	Vecchi *et al.* 2022b
Sisubiotus spectabilis FI 1	MN888371	MN888357	MN888331	MN888322	Stec *et al.* 2021a
Sisubiotus spectabilis FI 2				MN888323	Stec *et al.* 2021a
Sisubiotus spectabilis NO	MN888372	MN888364	MN888344	MN888324	Ste *et al.* 2021a
Sisubiotus splendidus	PV744336	PV744341	PV746802		Atherton 2025
Mesobiotus efa 1	OR804457	OR805135	OR805169	OR803035	Tumanov *et al.* 2024
Mesobiotus efa 2	OR804458	OR805136	OR805170	OR803036	Tumanov *et al.* 2024
Mesobiotus efa 3	OR804459	OR805137	OR805171	OR803037	Tumanov *et al.* 2024
Mesobiotus vulpinus 1	OR804461	OR805140	OR805172	OR803040	Tumanov *et al.* 2024
Mesobiotus vulpinus 2	OR804462	OR805141	OR805173	OR803041	Tumanov *et al.* 2024
Mesobiotus occultatus DT97	OR794157	OR794158	OR803042	OR805249	Tumanov *et al.* 2024
Mesobiotus aradasi	OQ933000	OQ932999	OQ940183	OQ928739	Vecchi *et al.* 2024
Mesobiotus huecoensis S2027.1	OQ756249			OQ756246	Vecchi *et al.* 2023
Mesobiotus huecoensis S2027.4	OQ756248			OQ756247	Vecchi *et al.* 2023
Mesobiotus mandalori 1	OP829143	OP829056	OP829058	OP825090	Erdmann *et al.* 2024
Mesobiotus mandalori 2	OP829144	OP829057		OP825091	Erdmann *et al.* 2024
Mesobiotus anastasiae	MT903468	MT903612	MT903470	MT904513	Tumanov 2020
Mesobiotus hilariae	KT226070			KT226108	Vecchi *et al.* 2016
Mesobiotus cf. *barabanovi*	MN310392	MN310388	MN310390	MN313170	Kaczmarek *et al.* 2020
Mesobiotus datanlanicus	MK584659	MK584658	MK584657	MK578905	Stec 2019
Mesobiotus dilimanensis	MN257048	MN257049	MN257050	MN257047	Itang *et al.* 2020
Mesobiotus ethiopicus	MF678793	MF678792	MN122776	MF678794	Stec & Kristensen 2017
Mesobiotus fiedleri	MH681585	MH681693	MH681724	MH676056	Kaczmarek *et al.* 2020
Mesobiotus harmsworthi	MH197146	MH197264	MH197154	MH195150	Kaczmarek *et al.* 2018b
Mesobiotus insanis	MF441488	MF441489	MF441490	MF441491	Mapalo *et al.* 2017
Mesobiotus occultatus	MH197147		MH197155	MH195152	Kaczmarek *et al.* 2018b
Mesobiotus philippinicus	KX129793	KX129794	KX129795	KX129796	Mapalo *et al.* 2016
Mesobiotus radiatus 1	MH197153	MH197152	MH197267	MH195147	Stec *et al.* 2018e
Mesobiotus radiatus 2			MH197268	MH195148	Stec *et al.* 2018e
Mesobiotus romani	MH197158	MH197151	MH197150	MH195149	Roszkowska *et al.* 2018
Mesobiotus imperialis 1	OL257854	OL257866		OL311514	Stec 2021
Mesobiotus imperialis 2	OL257855	OL257867		OL311515	Stec 2021
Mesobiotus marmoreus 1	OL257856	OL257868	OL257861	OL311516	Stec 2021
Mesobiotus marmoreus 2	OL257857	OL257869	OL257862	OL311517	Stec 2021
Mesobiotus marmoreus 3	OL257858	OL257870	OL257863	OL311518	Stec 2021
Mesobiotus skorackii		MW680636		MW656257	Kayastha *et al.* 2021

Appendix 1 (continued). Sequences used for phylogenetic analyses. Sequences obtained in this study are indicated in bold, and asterisks denotes *Macrobiotus* C.A.S. Schultze, 1834 sequences that was misidentified by previous authors, as noted by (Stec 2024). Shaded rows at the end of the table indicate outgroup taxa.

Species	18S	28S	ITS-2	COI	Source
Mesobiotus sp. Macro07_042	MW751942			MW727957	Short *et al.* 2022
Mesobiotus cf. *furciger* Macro06_296	MW751936			MW727958	Short *et al.* 2022
Mesobiotus cf. *furciger* Macro06_310	MW751937			MW727961	Short *et al.* 2022
Mesobiotus cf. *furciger* Macro06_313	MW751939			MW727960	Short *et al.* 2022
Mesobiotus cf. *furciger* CC_MF_4	MW751949			MW727933	Short *et al.* 2022
Mesobiotus cf. *furciger* ABDC_MF_3	MW751944			MW727932	Short *et al.* 2022
Mesobiotus cf. *furciger* KPRI_MF_1	MW751962			MW727934	Short *et al.* 2022
Mesobiotus cf. *furciger* HMI_MF_1	MW751957			MW727941	Short *et al.* 2022
Mesobiotus cf. *furciger* EBNI_MF_2	MW751952			MW727937	Short *et al.* 2022
Mesobiotus cf. *furciger* EBNI_MF_4	MW751954			MW727938	Short *et al.* 2022
Mesobiotus cf. *furciger* PSAI_MF_2	MW751967			MW727939	Short *et al.* 2022
Mesobiotus cf. *furciger* Macro06_162	MW751934			MW727955	Short *et al.* 2022
Mesobiotus cf. *furciger* Macro06_171	MW751935			MW727956	Short *et al.* 2022
Mesobiotus cf. *furciger* JN07_MF_1	MW751959			MW727951	Short *et al.* 2022
Mesobiotus cf. *furciger* JN07_MF_4	MW751960			MW727953	Short *et al.* 2022
Mesobiotus cf. *furciger* JN07_MF_8	MW751961			MW727947	Short *et al.* 2022
Mesobiotus cf. *furciger* FN01_MF_6	MW751955			MW727945	Short *et al.* 2022
Mesobiotus diegoi 1	OP142527	OP142520	OP142514	OP143858	Stec 2022b
Mesobiotus diegoi 2	OP142526	OP142521	OP142515	OP143857	Stec 2022b
Mesobiotus maklowiczi 1	OP142525	OP142518		OP143855	Stec 2022b
Mesobiotus maklowiczi 2	OP142524	OP142519		OP143856	Stec 2022b
Mesobiotus peterseni 1	OP142528	OP142522	OP142516	OP143859	Stec 2022b
Mesobiotus peterseni 2	OP142529	OP142523	OP142517	OP143860	Stec 2022b
Minibiotus ioculator	MT023998	MT024041	MT024000	MT023412	Stec *et al.* 2020b
Paramacrobiotus areolatus	MH664931	MH664948	MH666080	MH675998	Stec *et al.* 2020b
Tenuibiotus zandrae	MN443040	MN443035	MN443038	MN444827	Stec *et al.* 2020c